2013

Thermal and hydrological conditions of the Goethe rock glacier, Central Sierra Nevada, California

Jezra Beaulieu
Western Washington University

Thermal and Hydrological Conditions of the Goethe Rock Glacier, Central Sierra Nevada, California

By
Jezra Beaulieu
Accepted in Partial Completion
of the Requirements for Degree
Master of Science

Kathleen Kitto, Dean of the Graduate School

ADVISORY COMMITTEE:

Chair, Dr. Douglas Clark

Dr. Robert Mitchell

Dr. Andy Bunn

Master's Thesis

In presenting this thesis in partial fulfillment of the requirements for a master's degree at Western Washington University, I grant to Western Washington University the non-exclusive royalty-free right to archive, reproduce, distribute, and display the thesis in any and all forms, including electronic format, via any digital library mechanisms maintained by WWU.

I represent and warrant this is my original work, and does not infringe or violate any rights of others. I warrant that I have obtained written permissions from the owner of any third party copyrighted material included in these files.

I acknowledge that I retain ownership rights to the copyright of this work, including but not limited to the right to use all or part of this work in future works, such as articles or books.

Library users are granted permission for individual, research and non-commercial reproduction of this work for educational purposes only. Any further digital posting of this document requires specific permission from the author.

Any copying or publication of this thesis for commercial purposes, or for financial gain, is not allowed without my written permission.

Jezra Beaulieu

November 15, 2013

Thermal and Hydrological Conditions of the Goethe Rock Glacier, Central Sierra Nevada, California

A Thesis
Presented to
The Faculty of
Western Washington University

In Partial Fulfillment
Of the Requirements for the Degree
Master of Science:

By Jezra Beaulieu

November, 2013

Abstract

The potential of rock glaciers in the Sierra Nevada to provide critical hydrological reservoirs and ecological habitats in a changing climate remains largely untested. In an effort to constrain the microclimatic contributions of buried ice, continuous temperatures were recorded in the near-surface debris of a variety of ice-cored and associated landforms in the Goethe cirque from August 2011 and July 2012 (Goethe rock glacier=GRG, valley-wall rock glaciers=VRG, Recess Peak debris=RPD, talus=TAL, ranging from most ice to least ice). In addition, continuous meteorological conditions on the rock glacier and stage of the main meltwater outwash stream were recorded to assess temporal and spatial responses of hydrologic inputs and outputs to the rock glacier. The mean annual surface temperature (MAST) of the GRG is -2°C and the mean annual temperature at depth (MADT) is -2.5°C. The GRG has the steepest average annual temperature gradient of all the landforms with 0.44°C/m, indicating the presence of a large ice core. The MAST for RPD, VRG, and TAL are -0.5°C, -2°C, and -2.5°C, respectively, and their MADTs are -1°C, -3°C, and -3°C respectively. The mean annual air temperature (MAAT) from the on-site weather station in the cirque was -1.5°C, and the total cumulative precipitation was 552 mm. The modeled discharge varies from 0-1.6 cms, averaging 0.35 cms, and the stream temperatures vary from 0-3.85°C, averaging 0.53°C. According to Tritium signatures of stream water samples, the percent of ice-core melt versus snowmelt in the stream was 0% for the mid-summer of 2011, 5% for fall of 2011, and 13% for the early summer of 2012.

The thermal and hydrological conditions in the Goethe cirque indicate a large sensitivity to meteorological conditions that is seasonally moderated by cold internal temperatures within the ice and debris of the landforms. The two contrasting summers during the yearlong study period exhibited different characteristics, particularly in discharge, stream temperature, and relative contribution of runoff source. The summer of 2011 was largely affected by exceptional snowpack from the previous winter, which was

expressed by lower mean debris matrix temperatures, strong correlations between discharge and air temperature, and tritium signals that indicate a nearly pure snow-melt source for the outlet stream. The summer of 2012 was characterized by an exceptionally low snowpack compared to the winter of 2010-2011, which was expressed by higher mean matrix temperatures, strong correlations between stream temperature and matrix temperatures, and a tritium signal that indicated a modest amount of ice melt contribution to discharge in the outlet stream. Projected decreases in snow-cover and earlier onset of spring snowmelt for the region will likely change the timing of peak runoff in alpine basins, as well as increase the duration that rock glacier debris matrix is open to warm air temperatures, thereby inducing more melt of internal ice and greater contribution of ice melt to stream runoff. With continued warming, even these insulated ice bodies will degrade unless the climate returns to cooler and wetter conditions.

Table of Contents

List of Figures

List of Tables

List of Acronyms

GRG	Goethe Rock Glacier
RPD	Recess Peak Debris
VRG	Valley-wall Rock Glacier
TAL	Talus
MAAT	Mean annual air temperature
MAST	Mean annual surface temperature
MADT	Mean annual depth temperature
DST	Daily surface temperature
DDT	Daily depth temperature
DMAT	Daily mean air temperature
Q	Discharge
ST	Stream temperature
PPT	Precipitation

1.0 Introduction

Rock glaciers are dynamic landforms containing a core of ice beneath a regolith of angular boulders sourced from the cirque headwall. They are abundant in semi-arid and arid mountain ranges, and their extensive distribution may play an important role with continued climate change. Because of the insulation provided by their surface regolith, rock glaciers may act as thermal and hydrological "buffers" to the widespread loss of clean-ice glaciers in mountainous regions (Clark et al., 1994; Millar et al., 2007). They can also be valuable records of past climate, as the preserved ice under the regolith serves as a climatological archive (Potter, 1972; Clark et al., 1996). Despite their wide distribution, however, uncertainties remain about their origins and connection to alpine environments. Their relationship to air temperature and snow cover has been assessed in mountain ranges in Europe and Greenland (Berger et al., 2003; Hanson and Holzle, 2004; Gonzalez et al., 2009; Humlum, 1997), and their hydrological significance has been evaluated in South America (Brenning, 2005; Azocar and Brenning, 2010) and the Rocky Mountains of Colorado (Williams et al., 2006; Clow et al., 2003), but similar research is sparse in the Sierra Nevada. Furthermore, rock glaciers in the Sierra Nevada have been largely overlooked as critical hydrological reservoirs and ecological habitat (Millar and Westfall, 2007; Millar and Westfall, 2010). Rock glaciers may provide important habitat refuges for nearby alpine communities as these regions experience accelerated warming predicted by many climate forecasts for the Sierra Nevada (Stewart et al., 2004; Dettinger et al., 2004; Maurer, 2007).

The purpose of my study is to establish a baseline of the thermal and hydrological conditions at the Goethe rock glacier in the central Sierra Nevada, and to identify the morphological and meteorological controls on temperatures within the debris and streamflow in its outlet stream in order to assess its importance as a frozen reservoir of water. To characterize the rock glacier catchment, I 1) established a spatially distributed

network of recording thermistors across the rock glacier to record ground thermal regimes, 2) collected continuous meteorological data from near the center of the rock glacier, 3) measured discharge and temperature of the primary outwash stream below the rock glacier, and 4) analyzed the isotopic components of stream runoff to test its source. Temperature profiles were also collected at adjoining talus, active valley wall rock glaciers, and relict surface debris in order to investigate the range of orographic and geomorphologic constraints (i.e., aspect, elevation, subsurface ice content) on ground thermal regimes for a spectrum of related landforms. In combination, these records allowed me to investigate the relationships between the modern microclimatic conditions and outlet stream discharge responses and to assess the relative proportion of streamflow that is generated by ice-melt or precipitation. By combining my instrumental data with the Parameter-elevation Regressions on Independent Slopes Model (PRISM) for the region (Daly et al., 1994), I evaluated my short-term (11 months) results relative to the longer (~100-year) averages.

2.0 Previous Research

Rock glaciers are common in high-altitude continental mountain ranges and in dry Polar Regions, but also occur in the dryer portions of more maritime ranges such as the Sierra Nevada and Cascade Mountains (e.g., Clark et al., 1994; Goshorn-Maroney, 2012). Although substantial debate has surrounded the origins of rock glaciers (e.g., Potter, 1972; Clark et al., 1998; Burger et al., 1999), most workers accept that active rock glaciers preserve a core of mostly ice underlying an insulating debris mantle (e.g., Clark et al., 1994; Konrad and Clark, 1998; Brenning, 2005). Because of the insulation provided by the surface debris, rock glaciers continue to persist and can even advance during warmer climatic periods while nearby clean-ice glaciers thin and retreat (Clark et al., 1994). Rock glaciers may represent an end-member in the spectrum of glacial

landforms, and may provide valuable information on the future of alpine glaciers and permafrost.

Steenstrup (1883) was the first to describe an active rock glacier in the late 19th century in northern Greenland. Rock glaciers were originally described as creeping talus formations (Spencer, 1900; Rohn, 1900) until Chamberlain and Salisbury (1906) explicitly compared rock glaciers with true clean-ice glaciers. Jackli (1957) and Wahrhaftig and Cox (1959) were the first to rigorously investigate rock glaciers in the central Alaska Range as expressions of creeping permafrost, where interstitial ice was necessary for movement down-slope. Rock glaciers have since been extensively studied and mapped in the Swiss Alps (Haeberli and Muhll, 1990; Jong and Kwaduk, 1988; Ikeda et al. 2003; Kerschner, 1978), Scandinavia (Martin and Whalley, 1987; Humlum, 1996, 1997, 1998), the Alaska Range (Foster and Holmes, 1965; Calkin et al. 1987), the Rocky Mountains (Vick 1981, Jackson 1980, Potter 1972, Potter et al. 1998, Johnson et al. 2007), the Cascade Mountains (Thompson, 1967; Goshorn-Maroney, 2010), and the Sierra Nevada (Clark et al. 1994; Konrad and Clark, 1998; Millar and Westfall, 2007). Their extensive global distribution reflects the diverse array of environments and climatic conditions in which rock glaciers can exist.

2.1 Definition of Rock Glaciers

Rock glaciers have been defined based on both their genesis and their morphology. It has been disputed whether the ice in rock glaciers is of a glacial or periglacial origin, yet many researchers currently agree that rock glacier development can be of either origin (Potter, 1972; Potter et al., 1998; Clark et al., 1998; Konrad and Clark, 1998). Some have postulated that there exists a spectrum of dynamics involved in rock glacier development (Burger et al., 1999; Berthling, 2011). Fundamentally, rock glaciers comprise a morphologically distinct class of dynamic landforms characterized by some form of internal ice and surficial regolith. Although many workers have attempted to

describe the characteristics of rock glaciers, Potter (1972) provides arguably the best broadly inclusive definition:

> A rock glacier is a tongue-like or lobate body usually of angular boulders that resembles a small glacier, generally occurs in high mountainous terrain and usually has ridges and furrows and lobes on its surface, and has a steep front at the angle of repose.

Subsequent to Potter, other workers have attempted to include the genesis of rock glaciers in their definition. In particular, Barsch (1992) and Haeberli (1985) have been strong advocates of the idea that all rock glaciers are manifestations of creeping periglacial ice and therefore can only form under permafrost conditions. The definition provided by Haeberli (1985) is:

> Active rock glaciers are the visible expression of steady-state creep of supersaturated mountain permafrost bodies in unconsolidated materials. They display the whole spectrum of forms created by cohesive flows.

Previous research has strived to present evidence of glacial ice in the cores of rock glaciers (e.g. Cecil et al., 1998; Monnier et al., 2012; Clark et al., 1998), but remote access has proven that to be difficult. Ice cores were extracted from the Galena Creek rock glacier in the Absaroka Mountains of Wyoming (Potter et al., 1998), thereby validating the glaciogenic model. There are generally very few boreholes and exposed ice outcrops on many rock glaciers, therefore ground penetrating radar (GPR), DC resistivity tomography, and seismic studies could be useful tools for imaging the internal structure of rock glaciers (Monnier et al., 2012). Some rock glaciers have areas of exposed sedimentary ice where annual layers are present, indicating glacial conditions prior to rock glacier genesis (Cecil et al., 1998; Konrad et al, 1999). Exposures of sub-surface, bubbly, layered (glacial) ice have been recorded and photographed at the

Goethe rock glacier (letters from Mike Loughman to Clyde Wahrhaftig, 1959), and were observed during the 2012 field season for this project.

2.1.1 Rock Glacier Activity

An important aspect of my study is the dynamic condition of rock glaciers, because I am investigating and comparing the thermal regimes of a spectrum of debris-types from actively ice-cored to non-ice-cored talus. Rock glaciers can be categorized as active, inactive, or relict, depending on the state of the ice within the rock glacier (Martin and Whalley, 1987). Active rock glaciers contain a core of mostly ice that is still flowing by internal deformation. Inactive rock glaciers still contain ice but are not flowing and are distinguished by the presence of undisturbed vegetation, stable rock debris, and moderate surface weathering on the rock debris. Relict rock glaciers no longer contain ice and therefore do not flow, and may have a deflated appearance due to loss of ice in the core (Martin and Whalley, 1987). The focus of my study, the Goethe rock glacier, fits the definition of an active rock glacier, with abundant evidence that it is still moving (e.g., Clark et al., 1994). In contrast, the smaller adjoining valley-wall rock glaciers appear to be stabilizing into inactive rock glaciers, while the stable oxidized boulders of late-Pleistocene Recess Peak deposits in the area fit the definition of relict debris.

2.2 Rock Glaciers and Climate

Rock glaciers respond slowly to climate because of the insulation provided by the thick surficial layer of rock debris; some studies suggest a lagtime of 100 to 1000 years and an ablation rate that is estimated as two orders of magnitude less than clean ice (Potter, 1972). While most clean-ice glaciers have receded substantially in the last century, many rock glaciers continue to advance in disequilibrium with the current climate (Clark et al., 1994; Brenning, 2005). Regardless of their origin, however, the internal ice in rock glaciers will eventually respond to changes in the regional climate. Previous research

has constrained temperature and precipitation parameters that are specific to rock glacier development in permafrost regions (Barsch, 1996; Humlum, 1998). The mean annual air temperature (MAAT) is the open-air temperature that is just above the surface of the rock glacier and the mean annual precipitation (MAP) is the annual precipitation received at the rock glacier averaged over the period of record. According to the permafrost model, the MAAT must be less than -2^{o} C to sustain rock glacier development (Barsch, 1996). Humlum (1998) found that a vast majority of mid-latitude rock glaciers occur at MAATs below -6.5^{o} C and MAPs less than 800 mm. Based on Parameter-elevation Regressions on Independent Slopes Model (PRISM) 100-year climate data (Daly et al., 1994) the mean annual air temperature (MAAT) of modern and relict rock glaciers in the central Sierra Nevada varies from 0.3˚C to 2.2˚C and the mean annual precipitation varies from 1346 to 1513 millimeters (Millar and Westfall, 2007). These values are somewhat higher than those in other regions, most likely because the Sierra Nevada is at lower latitude than most regions with rock glaciers.

A common metric for rock glacier development is the average winter temperature at the base of the snowpack (BTS) that is useful for quantifying the thermal regime within the rubble when the void space network is disconnected from the atmosphere. The BTS reflects the MAAT, which is ultimately important for assessing the thermal equilibrium of a rock glacier. Similar to the MAAT, Barsch (1996) states that the BTS must be less than -2 ^{o}C, for rock glacier subsistence. When the snowcover is continuous and thick enough (~0.6 m) to isolate the ground from the atmosphere (Hansen and Hoelzle, 2004), the temperature gradient inverts such that warmer, less dense air is trapped within the rubble and cold dense air exists above the snowcover (Berger et al., 2004; Millar and Westfall, 2007; Goshorn-Maroney, 2011). If snowcover is discontinuous, cold dense air can sink into the void spaces and displace the warmer air, instigating convection (a process termed *Balch ventilation* (Thompson, 1962). Similarly, warm air can rise through relatively small gaps in the snowcover, creating a “chimney effect” in morphologically distinct locations (Barsch, 1996).

2.2.1 Movement Responses to Climate

The increased temperature trend detected in many permafrost environments has caused dynamic responses in some rock glaciers. Kaab et al. (2007) and Bondin et al. (2009) monitored and modeled the rock glacier response to warming temperatures and found a correlation with increased flow velocities. MAATs that are near 0^{o} C corresponded to flow rates greater than 1.5 m/year and temperatures that were less than -2^{o} C corresponded to flow rates that were generally less than 1 m/year (Kaab et al., 2007). Bondin et al. (2009) found that in addition to direct temperature effects, conditions that allow early snow accumulation insulated warmer temperatures in the rock debris, resulting in overall greater water content in the debris that promoted basal sliding and faster flow rates.

2.3 Ground Thermal Regime

The ground-thermal regime in the overlying debris of rock glaciers is crucial for assessing temperature gradients and relationships with atmospheric air temperature. Ground-thermal regimes have been investigated in various studies using miniature temperature loggers (MTLs), which are inexpensive and durable devices that easily allow long-term field investigation of temperature. Humlum (1997) first used MTLs to measure thermal conditions on rock glaciers in Greenland. Later studies used MTLs to map permafrost in alpine regions of the Alps, Japan, Norway and Spain (Hoelzle et al., 1999, Ishikawa and Hirakawa, 2000; Santo-Gonzalez et al., 2009; Juliussen and Humlum, 2008). These studies indicate that temperature profiles vary with sediment size of debris that is overlying the rock glacier or permafrost feature. Temperatures in coarse blocky material respond more quickly than in finer sediment because of the presence of large void spaces that more-readily allow air exchange with surface temperatures (Harris and Pedersen, 1998). In such situations, cold, dense air sinks into the void spaces and displaces warm air in a process known as *Balch ventiliation,* or the *Balch effect* (Balch, 1990). This mechanism, in essence, sustains the ice core in the rock glacier. Harris and

Pedersen (1998) describe multiple mechanisms for thermal flux in the pore spaces of rock glaciers:

1. *The Balch effect:* cold air, which is denser than warm air, tends to displace warm air in the pore space.
2. *The chimney effect:* during the winter, cold air enters into the pore space through holes in the snow cover. Warmer air, displaced by cold air, travels upslope eventually escaping through other holes in the snow cover. This process can cause the upper part of a talus slope to be warmer than the lower part.
3. *Summer time evaporation/sublimation of water/ice in the blocky deposit:* latent heat is absorbed by these phase changes, significantly reducing diurnal heating.
4. *Continuous air exchange with the atmosphere:* nearly instantaneous cooling/warming of air in the pore space, via convective and conductive processes.

The two most basic physical processes that affect which type of mechanism is occurring in the debris matrix are (Juliussen and Humlum, 2008):

- **Convection:** the physical displacement of air due to differing densities, i.e. the Balch Effect or wind pumping. This mechanism may dominate during transitional seasons or when snow cover is discontinuous.
- **Conduction:** the warming of adjacent air or rock bodies due to radiative properties. This mechanism may dominate the summer temperatures at depth.

Previous studies on the ground thermal regime of rock glaciers in Europe and Greenland have shown distinct seasonal responses to climate (Humlum, 1997; Hoelzle et al., 1999). In the summer, there is a lag of several hours between high and low surface temperatures and those at depth within the rock debris, where larger void spaces have quicker responses than smaller void spaces. Once continuous snow cover isolates the rock debris from the atmosphere, temperatures in the surface debris establish a stable

temperature inversion. As the snow begins to melt in the spring, the repeated freeze-thaw of meltwater and subsequent release and absorption of latent heat warms the rubble until it reaches the freezing point of water (0^{o} C), whereupon temperatures stabilize until the melting is complete. This 0^{o} C interval is described as the "zero-curtain effect" (Muller, 1947).

Millar and others (2012) were the first to deploy MTLs in rock glaciers and other periglacial landforms in the Sierra Nevada. They selected rock glaciers and talus with north-facing slopes and established strings of two MTLs: one at the surface of the rubble and one at a meter of depth within the debris matrix. Their findings indicate that the MAAT of matrix temperatures for all rock glacier locations and years of monitoring (-0.8 ^{o}C) were significantly different (p <0.05) than the MAAT of surface temperatures, which varied by location. Matrix temperatures generally warmed at a slower rate than the surface in the summer, and had lower daily variance. The temperatures in the matrix were 1-4 ^{o}C lower than surface temperatures in the summer, and 0-1 ^{o}C higher in the winter. Both matrix and surface temperatures stabilize at 0 ^{o}C in the late spring/early summer during the "zero-curtain" interval. Statistical modeling of the relationship between surface and matrix temperatures yielded third-order polynomial best-fit regressions, whereas talus features yielded second-order polynomial functions. The models suggest resistance (hysteresis) in the matrix to warming and cooling of surface temperatures for specific ranges of thermal conditions, particularly during late summer and autumn (Millar et al., 2012).

2.4 Hydrology of Rock Glaciers

Rock glaciers are likely to become increasingly critical alpine water reservoirs. Clean-ice glaciers have been a primary source of dry season water storage and runoff in the Sierra Nevada, yet projections suggest their contributions will continue to decline through the next century (Maurer, 2007; Basagic, 2008). The hydrological importance of rock

glaciers and permafrost in the region has often gone unnoticed because of remote access and superficial similarities to ice-free talus, rockfalls, and scree slopes (Schrott, 1996; Burger et al., 1999). More research is necessary to estimate rock glacier distribution and extent in order to quantify their total contribution to alpine streamflow under warming climates. Similar to clean-ice glaciers and mountain permafrost, rock glaciers are energy-controlled as opposed to precipitation-controlled, making them critically important for stream runoff during the dry summer season of arid and semi-arid mountain ranges where rock glaciers are common (Azocar and Brenning, 2010).

Weather stations in the central Sierra Nevada have shown trends toward warmer winters and significant changes in snowmelt and streamflow timing since the 1940s (Dettinger and Cayan, 1994; Stewart et al., 2004; Knowles and Cayan, 2005). Snowmelt and streamflow have peaked increasingly early (1-4 weeks) in many watersheds of California, mostly in moderate-altitude basins that are more sensitive to warming winter temperatures (Stewart et al., 2004). Higher-altitude basins have not responded as significantly to these warming trends because they are strongly snow-dominated and are not as sensitive to modest changes in winter temperatures and precipitation timing (Dettinger and Cayan, 1994). However, with further warming, even at these altitudes more precipitation will likely fall as rain rather than snow, thereby reducing snowpack at high elevations and ultimately affecting the seasonal distribution of runoff (Stewart et al., 2005). With less snow contributing to runoff, rock glacier ice-melt may be a significant source of runoff in future climates. One goal of this study is to constrain the contribution of rock-glacier ice melt relative to snow precipitation in the Goethe cirque and to asses its relationships with air temperatures and ground temperatures.

2.4.1. Source Waters of Outflow

Water in the outlet stream of a rock glacier is derived from snowmelt, rainfall, melting of the ice core, and groundwater, and the relative proportion of each source is heavily

dependent on both seasonal and diurnal variations in meteorological conditions. Generally, spring/early summer runoff is dominated by intense snowmelt on warm days, summer runoff is dominated by rainfall, and late summer/early fall runoff is dominated by ice core meltwater and groundwater (Krainer and Mostler, 2002; Berger et al., 2004). Studies in Greenland, Wyoming and Colorado have successfully analyzed the meltwater components of rock glaciers with oxygen isotopes and geochemical concentrations (Cecil et al., 1998; Humlum, 1999; Williams et al., 2006). Williams and others (2006) found that melted snow comprised 30% of rock glacier outflow in Colorado, soil water from alpine organic matter comprised 32%, and baseflow (including ice-core melt) comprised 38% annually. Their ^{18}O results suggested that the majority of baseflow was melt of internal ice that had undergone multiple freeze/thaw episodes.

There has been little research on the isotopic components of outflow as a proxy for ice-melt contribution in the Sierra Nevada because the internal ice of the rock glaciers is too young to utilize oxygen isotopes for age determination of outflow. Instead, tritium (^{3}H) could serve as a substitute. Tritium is commonly used for dating groundwater, but has also been used for dating rock glacier meltwater (Cecil et al., 1998). It has proven to be a valuable tracer for young water because of the spike of ^{3}H in atmospheric fallout from bomb testing in the 1950s (Plummer et al., 2003). The ^{3}H from precipitation decays to ^{3}He with a half-life of 12.4 years, such that precipitation before the 1950s will contain less than 0.1 Tritium units (TU), whereas precipitation that fell during the decade of 1950-1960 will now contain approximately 70 TU (Plummer et al., 2003). The tritium content of modern precipitation varies by region and proximity to the ocean, but ranges from 4-5 TU. Although useful for constraining relative ages of water sources, tritium analysis is a quantitative method with qualitative results. Modern ^{3}H concentrations in precipitation can be quite variable between regions and even precipitation events, requiring calibration for a specific field site (Plummer et al., 2003). Tritium concentrations in precipitation over the past 25 years has also decreased at the same rate as ^{3}H decay, making it difficult to determine unique ages of mixed meltwater

streams (Plummer et al, 2003). However, the method should still provide constraints on the relative contributions of old ice versus more recent precipitation in the outlet stream of a rock glacier.

Cecil et al. (1998) used the tritium method at the Galena Creek rock glacier in Wyoming and determined that the ice, independently dated to contain ice that is at least 2000 years old, had very low ^{3}H values that varied from -1.3±1.3 to 0.2±1.0 TU. Tritium concentrations in the outlet stream below the rock glacier were 9.2±0.6 to 13.2±0.8 TU, equivalent to values of precipitation from the five years prior to their study. They concluded that such a low apparent contribution from melting of "old" ice in the stream suggests slow melt rates for the ice core, providing further evidence for an insulating debris mantle (Cecil et al., 1998).

2.4.2. Water Discharge Variation

Rock glaciers are complex water reservoirs because of the matrix of debris, ice and sediment that causes them to respond slowly to seasonal and daily variations in temperature and precipitation (Burger et al., 1997; Berger et al., 2004; Azocar and Brenning, 2010). Seasonal and daily variations in water discharge from active rock glaciers is primarily controlled by weather conditions, thermal properties of the debris matrix and other physical properties, such as surficial lakes and meltwater channels in the ice (Krainer and Mostler, 2002; Berger et al., 2004). Discharge that is derived from snowmelt and rain events is quickly released, whereas melting of internal ice is slowly released (Berger et al., 2004). Compared to clean-ice glaciers, rock glacier runoff contains less suspended sediment and more dissolved oxygen, making their outlet streams more desirable for biota (Giardino et al., 1992; Millar et al 2011).

The most detailed hydrologic studies of rock glaciers are in the Austrian Alps (Krainer and Mostler, 2002; Berger et al., 2004), one of which is located at an east-west trending

composite rock glacier consisting of two lobes (total area 0.22 km^2) at 2380 m in elevation (Berger et al., 2004). They found that peak runoff occurred during warm weather periods and immediately after thunderstorm events (0.3-1.0 cms) with a delay of 3-12 hours from the time of maximum melting of snow and ice until runoff in the outlet stream. When most snow had melted in the summer, baseflow from the rock glacier was 0.15-0.2 cms, indicating that meltwater from the internal ice was not a significant part of yearly runoff. Late summer discharge, was characterized by a general decrease in discharge with small peaks during rainfall events up to 0.25 cms (Berger et al., 2004). Once air temperatures were below freezing, diurnal variations ceased and runoff reduced rapidly to 0.02 cms (Berger et al., 2004).

Three different rock glaciers in the Austrian Alps display similar seasonal and daily water-discharge variations as observed by Berger et al. 2004 (Krainer and Mostler, 2002). In addition, the lack of correlation between water discharge and air temperature after snow melted from the cirque suggests that ablation of internal ice under the debris is of minor importance. As long as the rock glacier has sufficient snow cover, the predominant source of discharge is snowmelt (Krainer and Mostler, 2002). When comparing water discharge from rock glaciers to clean ice glaciers of similar size, Krainer and Mostler (2002) found that mean annual discharge from rock glaciers (0.3-0.37 cms per km^2) was significantly lower than clean-ice glaciers (0.6-0.8 cms per km^2), but that their seasonal and daily discharge variations were very similar. They concluded that although the amount of discharge is less, their geographic spatial distribution is greater, making rock glaciers' overall water equivalent more significant.

2.4.3. Stream Temperature

Water temperature fluctuations in the outlet streams of rock glaciers are attenuated relative to air temperature, but exhibit similar daily variations as air temperature from late summer to early fall after snowmelt diminishes (Millar et al., 2012). The mean

annual temperature of the outlet streams of rock glaciers in the Sierra Nevada is -0.2° C, with a standard deviation of 1.2°C. Summer stream temperatures averaged less than 0.6° C compared to the summer air temperature of 6.7°C, suggesting that internal ice is supplying substantial meltwater to the outlet streams (Millar et al., 2011). Similarly, water temperatures in the outlet streams at the termini of rock glaciers in the Austrian Alps were constantly near freezing, below 1 ^{o}C during the whole melt season, suggesting that meltwater flows in direct contact with an ice core (Haeberli, 1973; Krainer and Mostler, 2002; Berger et al., 2004). In autumn and winter, stream temperatures dropped below 0°C, interpreted to be ice. Temperatures then increased to and stabilized at 0°C, interpreted to be caused by snowmelt, after which diurnal variance increased and the summer regime resumed (Millar et al., 2012).

2.5 Ecological Significance of Rock Glaciers in a Changing Climate

There has been much research on the paleoclimatic conditions of rock glacier development, but more recently rock glaciers have been more widely recognized for their hydrological and ecological significance in a warming climate, particularly in arid alpine environments where rock glaciers are common (Millar and Westfall, 2007; Azocar and Brenning, 2010; Millar and Westfall, 2010). Because most rock glaciers are in disequilibrium with rapidly changing climates, they are likely to have relatively stable hydrological responses and become critical water reservoirs in alpine environments (Schrott, 1996).

Millar and Westfall (2007; 2010) first recognized the potential for rock glaciers to support climatically sensitive alpine wetland environments in the Sierra Nevada that might otherwise perish without a persistent ice body nearby. Their mapping indicates that rock glaciers in the Sierra Nevada extend from ~4000 to 2225 meters in elevation within NNW to NNE facing cirques (Millar and Westfall, 2007; Millar and Westfall, 2010). They found that at-risk ecosystems near these sites are of particular interest because of

many species' sensitivities to specific climatic conditions. Meltwater streams of these rock glaciers flow year-round and have mean summer temperatures that vary from -2˚C to 2˚C, well suited for biota to survive through summer conditions that are otherwise too warm (Millar and Westfall, 2007; Millar et al., 2010). If not for the presence of these thermal and hydrological reservoirs, some plant and animal species would be forced to migrate up-elevation to cooler and wetter climates. Because migration to higher elevations is generally not an option in the highest terrain of the Sierra Nevada, many species will have to adapt or will likely diminish.

Former ecological studies indicate a general global movement of species upward in elevation towards cooler temperatures and greater precipitation (Parmesan, 2006). The upward movement of alpine flora has been observed across Switzerland (Pauli et al., 1996), and the upward movement of treelines has been observed in Siberia (Moiseev and Shiyatov, 2003) and the Canadian Rocky Mountains, where air temperatures have increased in the past 100 years (Luckman and Kavanagh, 2000). In the Western United States, pikas are particularly compromised because their original habitat is high-elevation talus (>2000 m), with a preference for northern aspects (commonly expressed as rock glaciers). Rock-ice features (RIF) and rock glaciers accounted for 83% of observed pika sites in California, Nevada, and Oregon (Millar and Westfall, 2010). Climate modeling and temperature surveys of pika habitats suggest that a large-scale and climate-dependent collapse of the pika population is underway (Beever et al., 2003; Millar and Westfall, 2010). Consequently, rock glaciers may play a pivotal role in the persistence of the pika population.

My study should contribute detailed constraints to reconnaissance studies on the potential for the Goethe rock glacier to provide persistent water and cooler air temperatures in the face of continued warming and drying predicted for the region.
This study provides in-situ hourly measurements of stream stage and temperature, meteorological conditions, and temperature within the debris of a spectrum of ice-

cored landforms in a single cirque valley. Such detailed results enable comparison between a range of alpine landforms (active, relict, and non-ice cored debris), as well as provide a baseline of mean summer temperatures in the cirque that could potentially serve as thermal niche for adapting alpine species. Not only was I able to compare thermal gradients between the landforms, I was also able to compare their thermal regimes from two contrasting climate years.

3.0 Study Area

The Goethe rock glacier occupies a NNW facing cirque in the headwaters of the San Joaquin River, central Sierra Nevada, and is one of the larger active rock glaciers in the High Sierra, with an area of approximately 1 km^2 (Figure 1). The Goethe cirque lies above a series of paternoster lakes near the eastern end of the Glacier Divide, which runs eastward off the main Sierra Nevada crest. The rock glacier itself is approximately 1000 meters wide and 650 meters long, ranging in elevation from 3700 meters at the cirque headwall to 3500 meters at the toe of the rock glacier. It feeds an outlet stream and contains two thermokarst ponds on its surface, indicating that ice is actively melting beneath the surface regolith of the rock glacier. The Goethe cirque also contains other periglacial landforms such as active and relict valley-wall rock glaciers and taluses that were included in this project in order to compare temperature profiles in these comparable but ice-free landforms at different elevations and aspects. The Goethe cirque was ideal for this study because it is representative of many other rock glacier cirques in the region, it contains a variety of ice-cored and non-cored landforms, its outlet stream was well defined, and it is relatively easy to access.

The main Goethe rock glacier (GRG) consists of two lobes that are separated by a medial longitudinal “moraine;” each lobe supports at least one thermokarst lake. The active valley-wall rock glaciers are categorized as one landform (VRG) and reside to the east of

the main rock glacier (Figure 1). The easternmost active rock glacier varies in elevation from 3660-3550 meters and is about 100 meters wide and 220 meters long. The western active rock glacier ranges in elevation from 3620-3560 meters and is about 150 meters wide and 120 meters long. They have characteristics similar to the main rock glacier such as a steep terminus at the angle of repose, unstable surficial boulders, and ridge-and-furrow morphology, indicating that they are active rock glaciers as well. Their surface debris, however, appears less disturbed than that on GRG, displaying greater clast weathering and incipient soil and vegetation in areas with fine sediment. The Recess Peak-aged debris (RPD) on the west side of the cirque is immediately north from the western-most lobe of the main rock glacier (Figure 1). This deposit is remnant of surficial or lateral debris along the west side of the Recess Peak glacier that occupied the Goethe cirque in the Pleistocene (~13,100±85 cal years BP) (Clark and Gillespie, 1997). There are two distinct accumulations, one deposit lying immediately upslope of the other by about 60 meters; the upper deposit is at 3680 meters in elevation and the lower is at 3620 meters in elevation. Their extents are roughly similar but their margins are not well defined. An additional deposit I investigated is a talus field (TAL) that lies east of the active valley-wall rock glaciers and north of Alpine Col, a mountain pass to the other side of Glacier Divide. This deposit varies in elevation from 3760-3660 meters and its dimensions are 120 meters wide and 170 meters long.

3.1. Climate of the Sierra Nevada

The Sierra Nevada has a Mediterranean climate that is usually characterized by peak precipitation in the winter as snowfall and peak stream runoff in the spring that diminishes by late summer. Millar and Westfall (2007) extracted MAP and MAAT for a range of alpine valleys (2225 - 3932 m) on the eastern slopes of the central Sierra Nevada utilizing the PRISM climate model. The PRISM model combines information from a distributed network of weather stations and standard lapse rates to output 30 arcsec climate data (Daly et al., 1994). The MAP for this region is between 1346 and

1513 mm and MAAT ranges from 0.3 to 2.2°C (Millar and Westfall, 2007). Although climate estimates from PRISM are quite good, the resolution limits of the data preclude accurate modeling of localized lapse rates or aspect, most likely causing overestimates of MAAT for specific sites.

4.0 Methods

The purpose of my study is to establish a baseline of the thermal and hydrological conditions at the Goethe rock glacier in the central Sierra Nevada, and to identify the morphological and meteorological controls on temperatures within the debris and streamflow in its outlet stream in order to assess its importance as a frozen reservoir of water. This required collecting substantial in-situ instrumental data consisting of meteorological conditions, ground temperatures, and meltwater temperature and discharge. Datalogging instruments were established at the field site in August 2011 and will continue to log until October 2013, but for the purpose of this project data was collected in July 2012.

4.1 Ground Thermal Regime

The microclimate of alpine valleys is complex, reflecting effects of aspect, elevation, regional and global weather systems, and even rock type (Barsch, 1996). Because macro-scale temperature profiles of these alpine valleys are poorly understood, I chose to compare temperature profiles of multiple landforms within one cirque to investigate the macroclimatic significance of a large rock glacier in a basin. I deployed a total of 38 DS1921G Thermochron iButtons (thermistors) and distributed 18 strings at varying elevations across the rock glacier and adjoining landforms: 11 on the GRG, two on the RPD, two on the VW1, one on VW2, and two on TAL (Figure 1). Because GRG is more morphologically diverse than the other landforms, I designated locations according to morphology, placing thermistors on ridges, furrows, and frontal slopes, or at the center and sides to record conditions on all major morphologic components of the rock glacier.

The other landforms were much smaller so elevation was the major characteristic for designating thermistor locations. On the GRG, thermistors were placed on the two main lobes at varying elevations, at the top of the steep frontal slope of the lobes, near the thermokarst lakes, and on the medial moraine between the two lobes. On the VW1 and VW2, thermistors were placed immediately above the steep frontal slope and at the spoon-shaped depression that occurs between the rock debris and cirque headwall (Figure 1). On the RPD and TAL, thermistors were placed at two different elevations to compare the thermal regime of a non-ice cored landform at the same elevation and aspect as the main rock glacier. Though the RPD and TAL are at different aspects and elevations relative to each other, I can compare their lapse rates to that of the rock glacier directly adjacent to each respective landform.

4.1.1 Thermistor Deployment

Two thermistors were installed at each location, one at the surface of the debris and one at a depth of 1-3 meters. The depth of the subsurface logger at each site depended on how deep I could place the sensor tether through the void spaces of the rubble; 16 subsurface loggers were at 1-2 meters depth, and two were greater than 3 meters below their respective surface loggers. The loggers at the surface were secured between boulders to record the temperature of the surface of the debris in the summer, and the base of the snow cover (BTS) in the winter. Only two sensors were used on each string to allow a greater spatial coverage of the rock glacier and adjacent landforms. This geometry represented a trade-off of spatial coverage over more detailed depth profiles because it only constrains two points in each depth profile. As a result, I needed to interpolate the temperature profile between the two thermistors, and then extrapolate the profile to depth to predict the depth of permanently frozen ground. Based on previous work on other rock glaciers (e.g., Goshorn-Maroney, 2012), I used a simple linear regression function to construct each profile and infer the average

ground temperature and potential depth of ice at each location (discussed in detail below).

The thermistor strings were located using a handheld Garmin GPS (nominal X-Y accuracy ~2-m). The sensors were contained in wire mesh pockets for protection from small animals. The wire mesh pockets were then secured in PVC T-tubes (2 cm diameter) that were connected to the tether in order to protect the sensors from water and direct solar radiation while allowing airflow to the instrument (Figure 2). Some loggers were unfortunately placed in direct sun when installed on the rock glacier, resulting in unreasonable daily peaks in temperature during summer months. Unfortunately, in these cases, shielding by the PVC tubing proved insufficient to prevent excess heating from direct solar radiative heating. To correct for this, I visually inspected the data from loggers that were affected by direct solar heating and altered the outlying measurements (Appendix A). I modified specific data points for those loggers by calculating lapse rates between the weather station air temperature and the logger temperature during times that were not affected by solar heating, and then subtracted the appropriate amount from the original dataset (Appendix A). I could then assess temperature trends during the summer with more confidence.

The Thermochron iButtons (model DS1921G) have an effective recording range of -30° to 70° C, measured at 0.5° C increments, and a nominal accuracy of ±1° C. Each sensor can store up to 2100 data points: in my study, I set them to record approximately 6 points per day for 11 months. The sensors recorded every 255 minutes in order to preserve the most memory, however that interval proved to be difficult to manage when analyzing the data. I interpolated hourly data from the 255-minute time series for every logger at every location in order to directly assess relationships with hourly meteorological and hydrological data (Appendix B). The datasets were re-sampled using the “its” (Portfolio & Risk Advisory Group and Commerzbank Securities, 2009) and “zoo”

(Zeileis and Grothendieck, 2005) time series packages in R (R Core Team, 2012), which extracted data points every hour.

4.1.2 Modeled Temperature Conditions

Temperature data were downloaded in the field using 1-Wire Viewer (version 3.15.50, Maxim). During collection and download, some loggers were inaccessible due to shifting of rocks in the matrix and other loggers were unable to download, due to either loss of battery life or effects of melting snow. Data were then investigated with descriptive statistics and regression analysis to constrain the relationship between air temperature, surface temperatures, and subsurface temperatures within the debris of the landforms. Because each logger string had a different distance between surface and subsurface loggers, I calculated gradients by subtracting subsurface temperatures from surface temperatures then dividing by each respective depth in order to normalize all locations. To test the relationships between matrix temperatures and air temperature for each landform, I fit regression models to find the best statistical fits and Pearson correlation coefficients. When comparing temperature means of the landforms, I averaged all surface temperatures and subsurface temperatures of each respective landform separately, which were then input to the regression models. Because sample density is different for each landform, significance of correlations (p-values) was not calculated. I also fit regression models to the matrix temperatures to address how aspect and elevation affect ground temperatures in the landforms of ice content.

4.2 Meteorological Conditions

To constrain local weather in the cirque, I established an automated Campbell Scientific weather station on a large stable flat-topped boulder near the middle of the rock glacier along the longitudinal moraine separating the two main lobes at 3663 meters in elevation (Figure 2). The weather station recorded solar radiation (W/m^2), wind speed and direction (m/s, degrees), total precipitation (mm), and temperature (° C) and

humidity (%) at hourly intervals (list of sensors in Appendix or Tables?). These parameters are crucial to establish the response-times of alpine landforms in the Goethe cirque to short-term weather events and to longer-term seasonal fluctuations. By assessing response times of the thermal and hydrological conditions of the rock glacier to meteorological conditions, my study attempts to evaluate the rock glacier's equilibrium with and response to the modern climate as well as the effect of the insulating debris mantle. The data I present here spans August 19, 2011 to July 12, 2012.

Because the weather station I installed at Goethe cirque was not capable of measuring actual snow precipitation in the Goethe cirque, I used snow water equivalent (SWE) and snow depth data from Bishop Pass Snow Telemetry Station (SNOTEL). This station is 18 km to the southeast of the Goethe cirque at an elevation of 3482 and has hourly data dating back to 2002 (NOHRSC, 2013). One major assumption in this study is that snow depth and SWE are equivalent to that of Bishop Pass because of its close proximity. It is likely that the Bishop Pass record is a minimum threshold for snowfall that occurred at Goethe, due to its lower elevation (~200 m) and different surrounding topography; Bishop Pass is in an open valley, as opposed to Goethe rock glacier, which is in an enclosed cirque valley. Wind patterns may also differ which would cause drifting of snow and thicker snow depths at certain locations as opposed to others.

To test how representative the climate years of 2011 and 2012 were compared to the average climate of the past century, I compared annual, winter (October-April), and summer (May-September) averages from my weather station to those generated using PRISM (Daily et al., 1994). To test the validity of the PRISM model, I correlated monthly data from my weather station to the PRISM monthly data with a simple linear regression, which resulted in positive correlations with a good fit and R^2 values of 0.98 for temperature.

4.3 Streamflow Gauging

Stream discharge and water temperature measurements at the outlet stream of the rock glacier test the origin of the water (rock-glacier ice core or annual snow-melt and rainfall) and if runoff is more or less persistent than runoff from other non-rock glacier sources. Downvalley, two melt-water streams emanate from the toe of the rock glacier, and multiple subsurface melt-water streams flow beneath the debris layer within the rock glacier. The smaller surficial outlet stream on the east side of the main rock glacier was dominated by sheet flow and too shallow to collect discharge measurements. In most locations of the main outlet stream, the outflow was distributed across a shallow and complex creek system. To minimize local effects as much as possible, I established a discharge gauging profile below the rock glacier based on two main factors: a relatively simple channel morphology with only a few boulders in the channel, and a location in which most of the flow was constrained by a few large boulders. Instrumentation was installed right at the toe of the rock glacier and about 50 meters upstream from the delta into Goethe Lake (Figure 1).

I collected flow velocity measurements with a Marsh McBirney Flo-Mate and top-setting wading rod (HACH, 2011) in the main outlet stream of the rock glacier at various stages from August 17, 2011 to July, 2012 to create a rating curve for the stream based on U.S. Geological Survey midsection method (USGS, 2007). Measurements were taken daily at mid-morning when water depth was low and late afternoon or evening when water depth was high from the daily snowmelt (Table 1). A Solinst Levelogger Junior pressure transducer (Solinst, www.solinst.com) was placed in a stilling well at this site where barometric pressure and temperature were continuously recorded at intervals of 20 minutes (Figure 2). The levelogger has an accuracy of 0.1% FS and 0.1° C.

In order to achieve the “true” stage height in the outlet stream, atmospheric pressure was modeled in order to calibrate the pressure transducer (Appendix C). Because the

on-site weather station did not have a barometric pressure recorder, I modeled this factor based on data from the nearby but lower Bishop Airport (1263 m elevation), and used the temperature lapse rate to more closely constrain the true air pressure at the rock glacier by incorporating it into the barometric formula based on derivations in the U.S. Standard Atmosphere guidelines (NASA, 1976). I then compared relative humidity (RH) data between the Goethe weather station and the Bishop Airport to perform sensitivity analysis of air pressure to moisture content in the air. Because humid air is less dense than dry air, the molar mass (M) of air will slightly vary with water content, ultimately affecting modeled air pressure and apparent stream level (for every 0.01 change in M, there is an effective 0.07 m change in stream level). Once the air pressure at Goethe was calculated, I subtracted these results from the pressure transducer level data to calculate the actual changes in water depth in the outlet stream .

A rating curve was developed from the stream velocity measurements made in the field for the summers 2011 and 2012. Although, I only collected 11 total velocity measurements, the rating curve fit quite well. The best-fit regression line through the observed discharge measurements is a second-order polynomial with an R^2 equal to 0.97 (Figure 3). There is a lot of compounded error of the modeled discharge values, which includes instrumental error (0.1% FS), human error from field measurements, and calibration error from modeled barometric pressure (mbar). Therefore, many interpretations were made on general trends of streamflow and not absolute amounts of discharge. To assess the percentage to which I can be confident with modeled discharge, I calculated the percent of stage values per interval that were under the maximum observed stage in the field (0.53 m). Only 48% of the stream stage values in the summer of 2011 (Interval 1) were under 0.53 m, whereas 37% of the stage values in the spring and summer of 2012 (Intervals 4 and 5) were under 0.53 m. Although these are relatively low confidence intervals, discharge values above this threshold are within reason given the channel morphology of the stream.

4.4 Isotopic Signatures of Runoff

The goal of the Tritium isotopic analysis is to assess variation in meltwater contribution to total discharge over the course of the summer. Tritium radiometric analysis of the samples will help constrain the relative age of the ice, snow and melt-water and furthermore the total contribution of melt water from the ice core versus seasonal precipitation to the total discharge from the rock glacier. Although the absolute age of the Goethe rock glacier ice core is undetermined, it should vary between a few hundred to a few thousand years (e.g., Conrad et al. 1996). Such pre-industrial ice should have negligible amounts of post-bomb (~1950) levels of Tritium in it. In contrast, recent snow should have small (but significant) amounts of Tritium (<5 TU) that are remnants of the spike in the 1950s related to aboveground nuclear testing (USGS, 2004). Some post-bomb snow and snowmelt may have adhered to the ice core as congelation ice; thereby creating a buffer zone around the ice core that has a pre-bomb signature. If actual melting of the ice core occurs, the tritium signature may appear to be higher than it would be without the buffer of congelation ice. Therefore the calculated percentages of ice melt to snowmelt in the stream would be minimum values for the actual percentages.

I collected water samples from the outlet stream at the gauging site to evaluate the influence of melting of an (older) ice-core to the influence of shorter-term (annual) precipitation in the total discharge of the outlet stream. I collected three late-summer stream samples during the project: August 2011, October 2011, and July 2012. I also collected a snow sample from 2011 as a control for the modern precipitation. All samples were analyzed at the Tritium Laboratory at Rosenstiel School of Marine and Atmospheric Sciences at the University of Miami, Miami, FL. Because the tritium content of the samples was expected to be low (<10 TU), they were analyzed by low-level gas proportional counting by electrolytic enrichment in order to attain greater accuracy. This process lowers the detection limit to about 1 TU. Percentages of each

respective stream TU content to snow TU content served as a proxy for percentages of ice melt to snowmelt for each respective discharge point measurement (at the time of sample collection).

5.0 Results

5.1 Climate

5.1.1 Weather Conditions for the 2012 Water Year

Although my study spans August 2011-July 2012, I investigated the weather conditions of winter 2010-2011 to provide context for my dataset. Weather during water years 2011 (October 1, 2010-September 30, 2011) and 2012 (October 1, 2011-September 30, 2012) was starkly different. The 2011 water year was an unusually wet year, considering it was a La Nina phase of ENSO, which generally indicates dry weather for the Sierra Nevada. The region received approximately 120% of its 1000 mm average precipitation in the 2011 water year, with a total of 450 cm of snow (125 cm SWE) as recorded by the Bishop Pass SNOTEL station (NOHRSC, 2013). Snow depth and SWE reached similar levels in 2006, but levels in the 2012 water year were the lowest since the beginning of monitoring in 2002. In contrast, water year 2012 received half of average precipitation, with approximately 100 cm of snow corresponding to 50 cm of SWE (NOHRSC, 2013).

The mean annual air temperature (MAAT) at the Goethe cirque from August 2011 to July 2012 was -1.5°C. Average summer air temperature for 2011 (August and September) is 6.5° C, average winter temperature (DJF) is -7.1° C, and average summer temperature for 2012 (June and July) is 7.7° C. Precipitation closely corresponds with large decreases in air temperature (Figure 4). Bishop Pass records indicate that total precipitation (snow and non-snow) from August 2011 to July 2012 is 610 mm. The Goethe weather station rain gage only recorded a total of 553 mm, but totals are misleading during winter months when snow most likely melted into the rain bucket,

thereby recording precipitation when there may not have been. When calculating precipitation at Goethe during months when air temperature is above freezing, the total summer precipitation that was recorded at Goethe weather station was 15 mm from August 12-October 1, 2011 and 23 mm from April 22-July12, 2012, however these totals do not reflect an entire summer's precipitation. The non-snow precipitation record at Bishop Pass during the same time periods indicates 52 mm and 50 mm of precipitation, respectively.

5.1.2 PRISM

Records at the Goethe cirque were compared to PRISM monthly totals for precipitation and averages for temperature in order to validate and provide a climatic context for the in-situ data. Modeled temperature and precipitation from PRISM for the Goethe cirque compare reasonably well to data recorded at the Goethe weather station from August 2011 to July 2012. The fit of the observed temperature to the modeled temperature was very good ($R^2 > 0.98$), but on average, PRISM's monthly minimum temperature was approximately 2° C colder and the monthly maximum temperature was approximately 2° C warmer than that of Goethe, varying by month. Summer precipitation at Goethe was not as good a fit with PRISM as temperature with R^2 of 0.51. Although the monthly totals did not match that of Goethe, the total precipitation modeled by PRISM for the study period was 550 mm, which is very comparable to the 552 mm recorded at Goethe from August 2011 to July 2012.

To evaluate the validity of the Bishop Pass SNOTEL winter precipitation as a proxy for the Goethe cirque, I compared the monthly total precipitation for the study period from Goethe, PRISM and Bishop Pass (Table 2). Bishop Pass snow precipitation and PRISM's winter snow precipitation for Goethe was a better fit than the Goethe weather station record with an R^2 of 0.71. According to PRISM's 1980-2010 climate normals, Bishop Pass receives 10.6 mm (7.5%) more precipitation in the winter (Oct-Feb), 12.4 mm (13%) more in the spring (Mar-May), and 1.5 mm (3 %) less in the summer (June-Aug) than the

Goethe cirque. Over the study period from August 2011- July 2012, Bishop Pass received a total of 57 mm more precipitation (snow and non-snow) than Goethe cirque.

According to PRISM climate normals for the Goethe cirque, average minimum temperature is -5.68°C and average maximum temperature is 5.11°C for the 1981 to 2010 period. Average annual minimum and maximum temperatures show a slightly decreasing trend from 1895 to 2012, where maximum temperatures decreased 0.023°C/year and minimum temperatures decreased 0.003°C/year since 1895 (Figure 5a). However, since 1981, maximum temperatures increased 0.03°C/year and minimum temperature increased 0.12°C/year (Figure 5b).

PRISM's MAP for the Goethe cirque averages at 832 mm for the entire 1895-2012 period and 845 mm (climate normals say 1088 mm) over the 1981-2010 period. Average winter precipitation from October to April increased 0.54 mm/year from 1895 to 2012 (Figure 6). The average winter precipitation is 735 mm since 1895, but this has increased to 743 mm in the last 30 years (1981-2010). Bishop Pass received a total of 1250 mm SWE during the winter of 2011-2012, which is 120% of the 30-year average. Average summer precipitation from May to September has decreased 0.009 mm/year since 1895 (Figure 6), though in the last 30 years, the average has increased from 96 mm to 99 mm.

5.2 Temperature Conditions

To assess the temperature data, the time series were categorized into roughly five seasonal intervals that were defined based on similar temperature trends between the loggers such as the presence or absence of diurnal variance, or dominant positive or negative gradients (Appendix D). The seasonal intervals are somewhat different than the intervals used to correct for direct solar radiation spikes in Appendix A. Therefore the beginning and ending dates for each interval may vary from logger to logger; dates

shown in the results for each interval are approximate bounds. Although the lengths of each interval may vary, the temperature trends of the rock glacier and surrounding landforms exhibit distinct means and variance during each interval (Figures 7-8). Summer conditions exhibit large diurnal variance at the surface, and smaller diurnal variance at depth that also lags behind surface temperatures. Surface and subsurface temperatures have a positive gradient where temperature cools with depth. Winter conditions generally lack diurnal variance, and surface and subsurface temperatures have a negative gradient with temperature warming with depth. Transitional seasons are characterized by both positive and negative gradients with some periods lacking diurnal variance (Figures 9-20). Temperature gradients are generally low throughout the year and most often within 1 degree of instrument error, resulting in error overlap and uncertain interpretation.

5.2.1 Annual Observations

The mean annual air temperature (MAAT) at the Goethe weather station from August 2010 to July 2011 is -1.5°C. The mean annual surface temperature (MAST) of the GRG is -2°C and the mean annual temperature at depth (MADT) is -2.5°C. The GRG has the largest average annual temperature gradient of all the landforms with 0.44°C/m. The MAST for RPD, VRG, and TAL are -0.5°C, -2°C, and -2.5°C respectively, and their MADTs are -1, -3, and -3 respectively (Table 3). The average annual temperature gradient for the RPD is 0.09°C/m, which is the lowest of all landforms. The average annual gradient for the VRG is 0.37°C/m, and that of the TAL is 0.13°C/m.

Overall, the GRG and TAL have the lowest annual median surface temperatures (Figure 20), however, GRG has greater variance due to a larger sample size. The VRG and GRG have similar annual distributions and variance, though the VRG has a higher median surface temperature of about 1°C. The RPD's annual surface temperature signature is statistically similar to annual air temperature (notches overlap), which is also statistically different than the other landforms (Figure 21; Chambers et al., 1983). The annual

gradients among the landforms have very similar distributions, variances, and medians (Figure 22). Although only a fraction of a degree smaller, both the RPD and TAL have smaller annual median gradients, but because annual gradients are within the nominal instrument error, comparative interpretation is ambiguous.

5.2.2 Seasonal Observations

The seasonal intervals for each logger somewhat varied depending on elevation, aspect and local shading (Appendix D). Each interval has unique temperature trends, exhibiting different medians and variances (Figures 7-8). Surface temperature distributions were very similar among the landforms with the highest medians during Intervals 1 and 5 and the lowest medians during interval 3. The greatest variance is during Intervals 2 and 5, and the least variance is during Intervals 3 and 4. The gradients (°C/m) between surface and subsurface temperatures were also different for each interval, displaying the least variance during Interval 3 and greatest variance during Interval 4 (Figure 8). The highest median gradients occurred during Intervals 1 and 5, however gradients are higher during Interval 5 for all landforms (Tables 5-6).

Interval 1

Interval 1 (8/12/11 ~ 10/1/11) is generally characterized by above freezing temperatures at the surface and subsurface of the rubble, large diurnal variance, and positive gradients between surface and subsurface temperatures. The GRG surface temperatures and gradients display the greatest variability of all the landforms. The VRG and TAL have very similar distributions and variances, and RPD has the highest median surface temperature and lowest gradient of all the landforms (Figures 21-22). Peak surface temperatures are generally concurrent with peak air temperature, though most peak subsurface temperatures lag by one to two hours. This interval has a daily mean air temperature (DMAT) of 6.5°C (Table 3), with total precipitation of 23 mm that mostly fell during afternoon thunderstorms.

GRG

The average daily mean surface temperature (DST) on the GRG is 8°C, varying from -1°C to 19°C with an average diurnal variance of 5°C (Figures 9-15). Hourly data indicate that maximum surface temperatures most often occur at 15:00, one hour after peak air temperature, though peak times are variable for each logger due to differences in aspect and shading. Subsurface temperatures are moderated relative to surface temperatures and lag at least one hour behind maximum surface temperatures. The average daily subsurface temperature (DDT) for Interval 1 is 6°C, varying from 1°C to 13°C, with an average diurnal variance of 1°C. The average gradient between the surface and subsurface is 1.23°C/m.

RPD

Average DST is 8.4°C, varying from 0.5°C to 16°C, which is the highest average for Interval 1 (Figure 16). Maximum surface temperatures most often occurred at 15:00 for surface loggers, with subsurface temperatures most often peaking one hour before surface temperatures. The RPD 2 was the only location on this landform with both surface and subsurface datasets, as the subsurface logger of the RPD 1 was not found. The average DDT temperature is 6°C, varying from 1°C to 12.5°C. The gradient between the surface and subsurface loggers of the RPD 1 was 0.36°C/m, which is the lowest gradient of all the landforms during Interval 1.

VRG

The daily mean surface temperature was 7.4°C, varying from -1.5 to 16.5°C, and the daily mean subsurface temperature is 4°C, varying from 1°C to 9°C (Figures 17-18). The average diurnal variance of surface loggers is approximately 8°C, whereas the average diurnal variance of subsurface loggers is 0.5°C to 1°C. Peak surface temperatures occurred at 15:00, with subsurface loggers lagging behind by one hour. Subsurface temperatures for the VRG 3b logger were the coldest of all subsurface loggers in the cirque during this interval (Figure 18). Although this location was at one of the lowest

elevations, the subsurface logger was the deepest of any of the loggers in the cirque. The average gradient for the two locations with both surface and subsurface loggers was 1.14°C/m.

TAL

The TAL is at the highest elevation of any of the landforms, and therefore exhibits some of the coldest temperatures. It is also shaded for most of the day and adjacent to Alpine Col, a mountain pass between the north and south sides of Glacier Divide. Average DST is 6°C for the two surface loggers, varying from 0.5°C to 11.5°C over the entire interval, whereas the DDT for the two subsurface loggers is 3°C, varying from 1 to 6°C (Figures 19-20). Diurnal variance is 2°C to 5°C, and the average gradient is 1.5°C/m. Peak surface and subsurface temperatures both occurred at 16:00, lagging behind air temperature by two hours.

Interval 2

Interval 2 (10/2/11 ~ 1/21/12) is characterized by the period between the first major snow fall in early October to when most loggers are decoupled from atmospheric temperatures likely due to extensive snow cover. Daily mean temperatures are increasingly more negative and gradients between surface and subsurface loggers occasionally switch from positive (temperatures cool with depth) to negative (temperatures warm with depth). DMAT at Goethe is -4.3°C, and mean surface and subsurface temperatures are negative (Table 4). The GRG, VRG, and TAL have statistically similar distributions, medians and variances, whereas the RPD and air temperature have statistically similar medians and distributions (Figure 21). All landforms have similar gradient medians during Interval 2, however the TAL has the lowest median (Figure 22).

GRG

Average DST is -6°C, varying from -18°C to 14°C, and DDT is -6°C varying from -14°C to 4°C (Figures 9-15). The average gradient between the surface and subsurface is 0.02°C/m, and switches from positive to negative from day to night. The gradient is consistently negative after the first snowstorm, then returns to a diurnally changing gradient when that snow presumably melts. Surface temperatures generally peak at 14:00, concurrently with air temperature. When the gradient is positive (presumably when the loggers are not snow-covered), subsurface peak temperatures lag behind surface temperatures from 5-7 hours.

RPD

Average DST is -5°C varying from -15°C to 4°C, and average DDT is -4°C varying from -9°C to 3°C (Figure 16). Surface temperatures peak around 16:00, whereas subsurface temperatures generally stabilize throughout the day without peaking. Surface temperatures closely correspond to air temperature trends relative to the other landforms during this interval. Diurnal variance is about 3°C for surface temperatures and 0.5°C for subsurface temperatures, and the gradient between surface and subsurface is -0.3°C/m.

VRG

Average DST is -6°C varying from -17°C to 11°C, and average DDT is -6°C varying from -12°C to 11°C (Figures 17-18). Subsurface temperatures stabilize throughout the day with only small diurnal variance, whereas surface temperatures have large diurnal variance when the gradient is positive. Peak surface temperatures occur at 15:00, one hour after peak air temperatures, and the average gradient is -0.1°C/m.

TAL

Average DST is -5°C varying from -15°C to 6.5°C, and average DDT is -4°C varying from -9.5°C to 1.5°C (Figures 19-20). Both surface and subsurface temperatures are

attenuated relative to air temperature with an average diurnal variance of 2°C. The average gradient between surface and subsurface temperatures is -0.9°C/m, which is the most negative gradient of all landforms during this interval. When surface temperatures exhibit diurnal fluctuations, peak temperatures occur at 15:00, synchronously with air temperature.

Interval 3

Interval 3 (1/22/12 ~ 4/17/12) is characterized by stable surface and subsurface temperatures, little to no diurnal variance, and dominantly negative gradients throughout the cirque (Tables 3-6). The beginning of Interval 3 begins with the first major snowfall (from 11 cm to 143 cm of snow in one day), when surface loggers become decoupled with the atmosphere. DMAT is -6.8°C ranging from -18°C to 0.2°C. Bishop Pass snow depth peaks at 155 cm in the middle of April, which corresponds to a SWE of 37 cm. The snow depth is deep enough to decouple matrix temperatures from the atmosphere (>100 cm); therefore the DST is referred to as the basal temperature of the snowpack (BTS) during this Interval 3. There are few periods during this interval where the gradient becomes positive at some locations, most likely because the surface loggers were in contact with the air when overlying snow-cover temporarily melted. The GRG, VRG, and TAL have statistically similar temperature trends, as their median notches overlap, whereas the RPD has the highest median surface temperature that does not coincide with any other landform (Figure 21). Gradients during Interval 3 are very similar among the landforms, with GRG having the greatest variance (Figure 22).

GRG

The average BTS is -7°C with temperatures varying from -10°C to 3°C, and the average DDT is -6°C with temperatures varying from -9°C to -4.5°C (Figures 9-15). Air temperature reaches above 0°C in mid-March, which is coincident with some surface loggers regaining small daily fluctuations. The GRG 11a logger nearest to the weather station, very closely corresponds to air temperature more than any other logger during

this interval (Rubble void space is largest at this location, most likely causing logger to reflect true air temp rather than BTS). The gradient during Interval 3 is -0.45°C/m, the only negative gradient for the year.

RPD

Both the average BTS and DDT is -4°C, varying from -5.5°C to -2°C and -4.5°C to -1.5°C, respectively. The gradient during this interval is -0.4°C/m, but switches to a positive gradient on two occasions, when air temperature is above 0°C (Figure 16). The RPD 1b logger is on average 2°C colder than the RPD 2b logger, over an elevation difference of 25 m.

VRG

Surface temperatures on VRG generally have the largest diurnal variance of any loggers during Interval 3, with the exception of G11a (Figures 17-18). In particular V3a has diurnal fluctuation in surface temperature during February and March, presumably because snow cover has melted at this location, which is the lowest elevation logger site in the cirque. Over this period, peak surface temperatures occur at 16:00, whereas peak air temperatures occur between 13:00-14:00. Average BTS is -7°C varying from -12.5°C to 0°C, and average DDT is -6.5°C varying from -7.5°C to -5°C. The average gradient is -0.3°C/m, the smallest of all landforms during Interval 3.

TAL

Average BTS is -8°C varying from -17°C to -4.5°C, and average DDT is -6°C varying from -7°C to -3.5°C (Figures 19-20). The average gradient is the largest of all landforms during this interval at -0.6°C/m. Logger location T2 consistently had a negative gradient throughout the interval, whereas T1 had a positive gradient in the first half of January.

Interval 4

Interval 4 (4/18/12 ~ 5/20/12) can be inferred as the "zero-curtain" where abundant melting of winter snow releases latent heat causing surface and subsurface temperatures to stabilize at 0°C. This process results in gradients of 0±1°C/m and lack of diurnal variance in the logger temperatures. All loggers begin Interval 4 between April 17 and April 22 when the DMAT is positive (2.4°C) and snow depth decreases from 155 cm to 72 cm. Some logger locations may emerge from the snow cover (regain positive mean temperatures and diurnal variance) before others depending on aspect, elevation, and local shading, resulting in different bounds for Interval 4 for some loggers compared to others. Similarly, surface loggers regain positive mean temperatures and diurnal variance during Interval 4 before subsurface loggers, so that one logger site may have two separate lengths of this interval. Gradients were calculated between surface and subsurface loggers from when both enter Interval 4 to when the subsurface logger exits Interval 4. Two storm events caused both surface and subsurface temperatures to drop from the 0°C plateau in the middle of Interval 4. All landforms generally have similar median surface temperatures that are a few degrees below air temperature, with GRG having the lowest and RPD having the highest (Figure 21). Gradient medians are also similar among the landforms at approximately 0^{o}C/m (Figure 22).

GRG

The average DST is -1.5°C varying from -11°C to 1°C, and average DDT is -1.3°C varying from -5.5°C to 0.5°C (Figures 9-15). The average gradient for GRG is 0.95°C. Gradients for individual loggers do not seem to have a relationship with aspect or elevation. Rather they are most likely dependent on localized melting of snow that causes surface loggers to reconnect with air temperature before subsurface loggers. Lower elevation loggers (i.e., G1 and G6) do however have shorter lengths for Interval 4 relative to higher elevation loggers (Figures 9-15).

RPD

Average DST is -0.24 varying from -3°C to 0.5°C, and average DDT is -0.5°C varying from -4.5°C to 0°C (Figure 16). The average gradient is 0.43°C/m, the lowest and least variable of all landforms during Interval 4 (Figure 22). Location R2 has one of the longer Interval 4 periods, where both surface and subsurface loggers remain at 0°C for the majority of the interval.

VRG

Average DST is -1.26 ranging from -7.5°C to 14.5°C and average DDT is -0.87°C ranging from -5.5°C to 1°C (Figures 17-18). The average gradient is 1.1°C/m, however there is an anomalous relationship between the individual logger gradients and elevation. Logger site V3 (3597 m) displays a larger gradient than V1 (3630 m) by 0.4°C, although it is nearly 40 meters lower in elevation.

TAL

Average DST is -1.4°C ranging from -6°C to 10°C, and average DDT is -0.9°C ranging from -5.5°C to 0°C (Figures 19-20). The average gradient is 1.43°C/m, which is the largest of all loggers for this interval. TAL subsurface loggers remain in Interval 4 for much longer than any of the other subsurface loggers. Site T2 in particular remains in Interval 4 for approximately 2 months, as opposed to a few weeks like many other sites (Figure 19). Site T1 begins Interval 4 in the beginning of May, which is much later than the other sites (Figure 20).

Interval 5

During Interval 5 (5/21/12 ~ 7/12/112), all loggers have largely positive averages and gradients (temperatures cool with depth) and exhibit large diurnal fluctuations, particularly at the surface. Surface temperatures closely correspond to air temperatures, and subsurface temperatures are dampened and generally lag relative to surface temperatures. Lower elevation loggers, especially surface loggers, have a longer

Interval 5 than those at higher elevations, regardless of which landform it is located. DMAT is 8.9°C, ranging from -2.7°C to 13°C, and total precipitation is 15 mm (Table 4). TAL is the most unique of the landforms during Interval 5 because it has the lowest median surface temperature and the greatest gradient (Figure 21). The median TAL gradient is statistically different than any of the landforms, however it has the smallest sample size of only 5 days of data during this interval. GRG and VRG gradient boxplot notches overlap indicating they are statistically similar populations, whereas RPD has the smallest gradient and is statistically different from the rest (Figure 22).

GRG

The average DST is 6.3°C ranging from -9°C to 19°C (5.5°C to 11°C on the average). The average DDT is 5°C, ranging from -7.5°C to 16°C (4.1°C to 7.2°C on the average) (Figures 9-15). The average gradient is 2.6°C/m, which is over twice that of Interval 1. Loggers with the largest gradients are at higher elevations, and loggers with the lowest gradients are at the lowest elevations. Peak surface temperatures as well as peak air temperature occur at 16:00, and peak subsurface temperatures tend to occur one hour before surface temperatures at most locations.

RPD

The average DST is 7°C ranging from -8°C to 16°C and the average DDT is 6.5°C ranging from 0°C to 12.5°C (Figure 16). The gradient is 1.5°C/m and is the lowest of all the landforms. Surface temperatures occur synchronously with air temperature at 16:00, with subsurface temperatures occurring one hour before.

VRG

The average DST is 8°C ranging from -4°C to 18.5°C, and the average DDT is 4°C ranging from 0°C to 11°C (Figures 17-18). Location VRG 3b has the most subdued temperatures of all subsurface loggers in the cirque, barely exceeding 4°C, however, VRG 3a has some of the highest temperatures of all surface loggers. This location is at the lowest

elevation of all loggers, and also has the largest depth between the surface and subsurface loggers. The average gradient is 2.4°C/m.

TAL

The average DST is 6.4°C ranging from -9.5°C to 17°C and the average DDT is 3°C ranging from 0°C to 6°C (Figures 19-20). The average gradient is 4.8°C, which is the largest gradient of all the loggers. Surface temperatures on TAL become positive one month before subsurface temperatures emerge from the zero-curtain, resulting in a very large gradient for this interval. The average gradient is 4.8°C, which is the largest gradient of all the loggers during any interval. Daily maximum surface temperatures occur at 14:00, preceding air temperature by two hours, whereas subsurface temperatures do not peak at the same time everyday and generally stabilize throughout the day.

5.2.3 Ground Temperature Profiles

Ground thermal profiles were constructed for each logger location with both summer and winter profiles (Figures 23-24). Trendlines were drawn between the surface and subsurface average summer and winter temperatures that were then projected to depth to infer the average ground temperature and potential depth of ice at each location. Where the summer profile intersects the 0°C isotherm is a proxy for the possible depth to ice, and where the summer and winter profiles intersect each other is a proxy for the average ground temperature (Goshorn-Maroney, 2012). Average summer temperatures were calculated using the average temperatures between Intervals 1 and 5, and Interval 3 was considered the average winter temperature for each logger. Because I only deployed one subsurface logger at each location, the exact trajectory of temperature at depth is uncertain. The change in temperatures with depth is very likely non-linear and asymptotic as they approach 0 °C. These profiles only provide the likely maximum values for the average ground temperature and likely minimum values for the potential depth of ice.

The mean ground temperature at GRG is -3 °C and the average depth to ice is 6.4 m. Locations G3, G8, and G9 have the lowest average ground temperatures and smallest depths to the surface of underlying ice. These loggers are also the three loggers at the highest elevations on GRG (Figure 23). Locations G1, G6, G7, and G11 have the highest ground temperatures and greatest depth to ice on GRG (Figures 23-24). Loggers G1, G6, and G7 are the lowest elevation loggers also located at the toe of the rock glacier, whereas logger G11 is at high elevation, but placed in an area of large boulders.

The mean ground temperature at RPD is 4°C and the average depth to ice is 46 m (Figure 24). The R2 logger is at a comparable elevation and aspect to loggers G8 and G9, however, the average ground temperature is 7°C higher and depth to potential ice is nearly 40 meters lower. The mean ground temperature at VRG is -1.75°C, with an average 7.6 m of depth to ice, and the mean ground temperature at TAL is -2.25°C with an average 3.9 m of depth to ice (Figure 24).

5.2.4 Geographical Constraints on Temperature

Surface temperatures exhibit a negative trend with elevation during summer months, where temperatures decrease with increasing elevation. Linear regressions of elevation and average summer surface and subsurface temperatures for all landforms result in R^2 values that are very low (0.02-0.07) indicating that elevation is not a major component controlling temperature in the rubble of the cirque. Surface temperatures have slightly stronger relationships with elevation than subsurface temperatures overall (Figure 25). Summer subsurface temperatures exhibit a slightly positive trend with elevation (nearly horizontal regression line), indicating a very weak relationship with elevation.

When assessing relationships between individual landforms and elevation, the GRG and VRG have lower correlations with elevation relative to the RPD and TAL, yet this is

biased due to differences in sample size. Logger site V3 has the lowest annual temperatures, and is at the lowest elevation of all loggers in the cirque. This logger is located at the toe of the rock glacier right below the headwall, so cold air could be funneling down the toe of rock glacier into the rubble. When analyzing VRG and TAL temperatures together with elevation (since they are adjacent to each other), surface temperatures closely correlate to elevation with an R^2 of 0.95 for Interval 1, and R^2 of 0.5 for Interval 5. Subsurface temperatures of the VRG and TAL, however, do not display a strong relationship with elevation, with an R^2 of 0.015. Sample size for the VRG and TAL combined is smaller (5 loggers) than GRG (7 surface loggers), potentially creating biased correlations relative to that of GRG.

5.3 Discharge and Stream Temperature

5.3.1 Seasonal Observations

Intervals for stream discharge (Q) and stream temperature (ST) are slightly different than the seasonal intervals for the temperature loggers (Figure 26). Interval 1 spans August 17, 2011 to October 5, 2011 and is considered the first summer period ST is above zero and both Q and ST display diurnal variance. Interval 1 terminates after the first snow storm occurs, causing Q to significantly decrease and ST to hover near 0^o C. Interval 2 spans October 6, 2011 to November 3, 2011, and is defined by the period when ST is near zero, occasionally dropping to -2°C. By late October, Q is near 0 cms and ST remains below 0°C, suggesting that the sensor was either recording air temperatures or frozen ice at that time. Interval 3 spans November 4, 2011 to April 17, 2012 when Q is near 0 cms, with small diurnal fluctuations that may be reflecting changes in air pressure and instrument resolution rather than actual flow. Stream temperature is consistently below 0^o C during this interval. Interval 4 spans April 18, 2012 to May 28, 2012 and is coincident with the "zero-curtain" of the temperature loggers. This period is defined by increasing Q of up to 1.6 cms, and ST that remains at 0°C for the entire interval. Interval 5 spans May 29, 2012 to July 11, 2012 and is defined

by Q and ST that display summertime diurnal variance after the major snow melt-off period.

Mean annual discharge (Q) and stream temperature (ST) were calculated with weighted averages of each interval that did not include Interval 3 (winter). The annual weighted averages of Q and ST are 0.35 cms and 0.53°C respectively. The average daily minimum Q is 0.28 cms and average daily maximum Q is 0.55 cms. The annual average minimum ST was -0.5^{o} C and the annual average maximum was 1.5°C. The maximum Q of the year was 1.6 cms, and the maximum ST of the year was 3.85^{o} C. Absolute minimum values of Q and ST are not reliable measures due to sensor accuracy, error overlap with modeled air pressure, and possible freezing of the stream around the sensor. Trends in Q and ST closely correspond to changes in air temperature and precipitation, where discharge generally increases and stream temperature decreases during a precipitation event (Figure 27).

Although I cannot accurately interpolate discharge for 27% of the stage heights on record, I am fairly confident interpreting discharge for the majority of stage heights, because the annual weighted average discharge for the entire study period (0.35 cms) is only 0.05 cms more than the greatest discharge observed in the field. In addition, the main objective of this study is to interpret post-snowmelt flows, which are generally within the range of observed stage heights and discharges. In order to quantify uncertainty in modeled discharge, I assessed the range of stage heights recorded in each runoff interval separately. Interval 4, the snowmelt interval, has the greatest amount (60%) of stage heights below the maximum observed stage height (0.53 m), however the 40% of stages above that are up to 0.64 m greater (0.23 m on average). Although only 13% of stage heights in Interval 5 are within rating curve confidence, the majority of stage heights are within 0.27 m (0.11 m on average) of the maximum observed stage height. Interval 1 overall has the greatest confidence because 48% of stage heights are under 0.53 m, and the majority of stage heights above this value are within 0.21 meters

(0.08 m on average) of the maximum observed stage heights. In the future, it would be useful to measure the cross-sectional area of the floodplain in order to develop a range of probable stage heights and discharges during high flows.

Interval 1

Mean Q is 0.38 cms varying between 0.11 and 0.63 cms with average diurnal variance of about 0.10 cms (Figure 28). The average daily minimum Q is 0.34 cms and most often occurs at 6:00 and average daily maximum Q is 0.43 and most often occurs at 17:00. Daily runoff trends closely correspond to daily air temperature trends, though daily peaks in Q are about 3-4 hours lagged behind air temperature. During extreme warm or cold periods, peak discharge lags behind air temperature by 24-48 hours. Daily peaks in discharge occur almost immediately or up to one hour after precipitation events. Most rain events during Interval 1 are too small (up to 1.5 mm) to cause a pronounced change in flow.

Mean ST is 1.0°C, varying from 0°C to 3.8°C with an average diurnal variance of 2°C. The average daily minimum ST is 0.30°C and most often occurs at 7:00, and average daily maximum ST is 2.4°C and most often occurs at 14:00. Maximum and minimum ST occur synchronously with maximum and minimum air temperature (Figure 28). The stream shows slight increases in temperature during and directly following precipitation events, though very small (0.1°C), and usually occurs one hour after peak precipitation. In late September, precipitation events are coincident with near freezing air temperature, resulting in decreased ST that is concurrent with the peak precipitation for that day. Stream temperature generally increases again after the precipitation event, resulting in two peaks in ST for days with precipitation.

Mean Q and ST have a negative correlation during Interval 1 (r=-0.52) where ST decreases as Q increases (Table 10). Similarly max AT and minimum ST have a slightly negative correlation, although very weak (r=0.15). Mean ST and AT, however, have a

stronger, slightly positive correlation (r=0.18). Mean Q and mean AT have the strongest correlation for this interval, with a correlation coefficient of 0.75. Mean Q and ST have a correlation coefficient of -0.52, however, Q and AT have a stronger correlation with a coefficient of 0.75. Similarly, mean Q and surface and subsurface temperatures in the GRG debris both have correlation coefficients of 0.74. ST has a stronger, yet negative, correlation with surface temperatures than subsurface temperatures with a correlation coefficient of -0.46.

Interval 2

Mean Q is 0.06 cms and varies between 0 and 0.19 cms, with average diurnal variance of 0.03 cms. The average minimum Q is 0.05 cms and most often occurs at 6:00 and the average maximum Q is 0.08 cms and occurs at 15:00. Diurnal lagtimes with air temperature were approximately eight hours for minimum Q and only one hour for maximum Q. The first winter storm from October 4-7 brought 50 cm of snow, equal to about 6 cm of SWE (Figure 26), resulting in a lagtime of about 3 days between minimum air temperature and minimum Q for this period. Discharge then increased as air temperature increased to above freezing, although discharge from October 20th to November 3rd may not be reflecting actual discharge due to possible freezing of the stream, as indicated by stream temperatures that were down to -2.5°C (Figures 26-27). However, fieldwork on October 13, 2011 confirmed that the stream was flowing under approximately a foot of snow.

Mean ST is -0.25°C and varies between -2.7 and 1.6°C, with an average diurnal variance of 0.5°C. Average minimum ST is -0.95°C and occurs at 10:00, and the average maximum ST is 0.50°C and occurs at 15:00. Minimum ST lags nearly 10 hours behind minimum air temperature, but only one hour behind maximum air temperature. Stream temperature trends from October 20th to November 3rd closely mimic air temperature, reaching nearly -3°C at night and 1°C during the day, suggesting the stream possibly experienced a period of diurnal freeze/thaw cycles. Similar to Q

measurements for this interval, ST may be recording air or ice temperature from October 20th to November 3rd, which is indicated by water temperatures below 0°C.

Interval 3

Discharge and stream temperatures records for this period were not analyzed because the stream was most likely frozen, as indicated by Q near 0 cms and ST remaining below 0^{o} C (Figures 26). Neither discharge or stream temperature seem to respond to air temperature or precipitation during this time (Figure 27). Interpretations were not made from measurements during this interval.

Interval 4

Mean Q is 0.4 cms and varies from 0.02 cms to 1.62 cms with a daily variance of 0.2-0.3 cms. The average daily minimum Q is 0.30 cms and most often occurs at 5:00, which is one hour before minimum air temperature. The average daily maximum Q is 0.58 cms and occurs between 20:00 and 0:00, which lags behind maximum air temperature by four to eight hours. Mean ST increases from -0.6°C to 0°C on April 17 and remains at 0°C for the duration of Interval 4 (Figures 26 and 29).

Two snow events on April 26 and May 26 were recorded at the Bishop Pass weather station that was recorded as rain at the Goethe weather station (Figure 26). Because air temperature at Goethe was below 0°C during these events, I have inferred that the rain being recorded at Goethe was snow that then melted into the rain gauge. Total Q on these days decreases to near 0 cms, and diurnal variance decreases from 0.3 cms to 0.01 cms (Figure 29). Air temperature stabilizes to above freezing from May 8-23, resulting in a large increase in total Q from 0.2 cms to 1.6 cms, and an increase in average diurnal variance from 0.3 cms to 0.5 cms. This 15-day period represents the highest discharge observations of the entire record for this study.

Interval 5

Mean Q for Interval 5 is 0.44 cms and varies from 0.19 to 0.89 cms, with average diurnal variance of 0.1 cms (Figure 29). The average daily minimum Q is 0.21 cms and most often occurs at 5:00, and the average daily maximum is 0.32 cms and occurs at 18:00. Daily minimum Q occurs one hour before minimum air temperature on average, and daily maximum Q lags behind maximum air temperature by two hours on average. However, discharge responds to extreme cold or warm days approximately 24 hours later, similar to trends found in Interval 1.

Mean ST is 0.97°C and varies from 0 to 3.5°C, with an average diurnal variance of 2.3°C. The average daily minimum ST is 0.1°C and most often occurs at 6:00, concurrently with minimum daily air temperature and one hour behind minimum daily discharge. The average daily maximum ST is 2.4°C and most often occurs at 14:00, which is two hours prior to maximum daily air temperature and four hours prior to maximum daily discharge. Stream temperature generally increases one hour following peak precipitation. Although the magnitude of change in ST most likely depends on the temperature of the precipitation, colder days show a greater decrease in ST in response to precipitation (Figure 29). Rain precipitation was recorded on two days at the Goethe weather station, but was recorded on 10 days at the Bishop Pass station during Interval 5. All precipitation events occurred in the afternoon between 13:00 and 19:00, generally concurrent with maximum daily air temperature.

A few noteworthy events are June 5th and July 5th, when peak snowmelt discharge has completed, and runoff trends reflect the rock glaciers relationship to summer air temperature and precipitation. On June 5 (day 294), air temperature decreased from 5°C to -10°C and ST remained at 0°C until temperature reached above 0°C at 12:00, during which 0.5 mm of precipitation was recorded at the Goethe weather station (Figure 29). The precipitation recorded was most likely snow that then melted in the rain gauge after air temperature was above freezing. Stream temperature then rose to

0.5°C at 18:00, nearly 6 hours after above-freezing conditions. On July 5th (day 324), the daily maximum ST decreased from 3°C to 1°C and the daily maximum Q increased from 0.4 to 0.9 cms in 2 days (Figure 29). Daily maximum stream temperature lagged one hour behind peak rainfall, whereas Q continued to increase for the 13 hours following peak rainfall for that day. Discharge then rapidly decreased from 0.9 to 0.5 cms over the course of 3 hours. Rainfall on this day was not recorded at Goethe but was recorded at Bishop Pass (<5 mm).

Overall, correlation coefficients between AT, ST, and Q are between 0.4 and 0.8, indicating strong correlations during Interval 5 (Table 10). Maximum ST is more correlated with AT than minimum ST. Mean Q and mean ST have a positive correlation with r=0.42, though maximum Q and minimum ST have a stronger correlation with r=0.54. Similar to Interval 1, Q and AT have the strongest correlation of all (r=0.78), with maximum values having a stronger relationship than minimum values. Maximum AT and minimum ST show a strong positive correlation (r=0.64). Similarly, mean ST and surface and subsurface temperatures in the GRG rubble exhibit strong positive correlations with coefficients of 0.7 and 0.67, respectively. When a 2nd order polynomial is fit to the regression between ST and surface and subsurface temperatures, ST is more correlated to subsurface temperatures with a correlation coefficient of 0.8. There is a positive relationship between ST and subsurface temperatures until the subsurface reaches 4°C, then there is a prominent negative relationship. Q has a slightly lower correlation with rubble temperatures than it does in Interval 1, with correlation coefficients of 0.57 for surface temperatures, and 0.66 for subsurface temperatures.

5.4 Tritium Signatures of Runoff

Tritium signatures in the outlet stream were analyzed for August (mid-summer) and October (fall) of 2011 and July (early summer) of 2012 (Table 11). The control sample of snow, which was collected in August of 2011, contained 3.91 TU. Mid-summer stream

water contained 4.03±0.14 TU, fall stream water contained 3.72±0.14 TU, and early-summer stream water contained 3.41±0.11 TU. The errors in TU are one standard deviation (1 sigma) including all conceivable contributions during analysis. When related to discharge at the time of sampling and considering all confidence intervals, the possible percentage ranges of discharge that is ice melt versus snowmelt is 0-4% for mid-summer, 0-13% for fall, and 7-19% for early summer. When calculating with just the averages, percentages are 0%, 5%, and 13% respectively.

6.0 Discussion

The results of this study quantitatively and qualitatively characterize the thermal, meteorological and hydrological conditions at the Goethe rock glacier in an effort to evaluate its importance as a frozen reservoir of water. In order to assess the response of the rock glacier to modern climate, I constrained the morphological and meteorological controls on temperatures within the debris of the Goethe rock glacier and streamflow in its outlet stream. In order to assess the glacier-melt contribution to streamflow, I investigated the relationships between microclimatic conditions and outlet stream discharge responses, and assessed the relative proportion of streamflow that is generated by ice-melt or precipitation with Tritium signatures of runoff. Furthermore, I compared weather conditions at Goethe to the extended centurial record in order to provide climatic context to my year of data.

6.1 Climate and Meteorological Conditions

The winter of 2010 (prior to this study) was one of the heaviest snow years in the region's history with nearly 120% of normal snowpack, which lingered until the following winter. In contrast, winter was very short during 2011-2012 where snowcover

(~50% of normal) only spanned from January to mid April. Many subsurface temperature loggers were open to the air, as indicated by their diurnal variance and occasional positive gradients during Interval 2, which spanned from the first snowstorm in early October to January.

The meteorological conditions at the Goethe rock glacier are consistent with those defined by Barsch (1996) and Humlum (1998) for rock glacier development and persistence (-1° C to -2° C). The MAAT as recorded by the Goethe weather station is -1.5° C, the MAST as recorded by surface loggers on the landforms ranged from -2.5° C to -0.5° C, and the MADT ranged from -3° C to -1° C. Ground thermal profiles reveal a mean ground temperature of -3° C, consistent with Ikeda et al. (2003) and Barsch (1996). Total precipitation recorded by Goethe (552 mm) was also close to that modeled by PRISM for the same period (566 mm), which is nearly half of the annual mean precipitation for the 1981-2010 period (~1088 mm).

Because the weather station does not have remote sensing software, I was only able to work with manually downloaded data for this project that does not include the second half of the summer of 2012. Therefore, it is difficult to make direct comparisons between the two summers of the study period. During the summers of 2011 and 2012, the greater amount of runoff, higher water temperatures, and overall higher gradients between surface and subsurface temperatures indicate a consistent open-network of debris allowing air temperatures to inundate void spaces. Data to be collected (summer 2013) from the rest of summer of 2012 will provide a more detailed assessment of comparisons between a typical “wet” and “dry” year.

6.2 Temperature Conditions

Surface and subsurface temperatures within the debris of all landforms considered in my study exhibit similar seasonal trends, yet there are specific differences in

temperature variations and means between the landforms that appear to largely reflect the presence or absence of internal ice that attenuates these temperatures relative to true air temperature. Several mechanisms have been proposed to drive temperature at depth, including convection, chimney ventilation, evaporation-sublimation, and conduction (Harris and Pedersen, 1998; Juliussen and Humlum, 2008; Goshorn-Maroney, 2012), all of which are evident in the temperature logger data at Goethe. These processes likely contribute to temperature attenuation in the matrix, and lagged response times to changes in air temperature, as well as persistence of internal ice within the ice-cored landforms. Summer regimes (Interval 1 and 5) are dominated by conduction, where warm air temperatures conduct heat through the overlying debris to the subsurface, resulting in overall positive gradients. Fall regimes (Interval 2) are dominated by convection and occasionally chimney ventilation when snow cover is discontinuous, as expressed by transitioning positive and negative gradients. Winter regimes are dominated by consistent gradient inversions when snow cover is continuous, with localized chimney ventilation. Spring regimes are dominated by evaporation-sublimation and snowmelt, resulting in consistent 0° C temperatures in the debris.

The RPD landform not containing ice has similar daily and seasonal trends to those that are ice-cored, however it has higher mean temperatures and an overall lower gradient to depth. Because the field area had extensive snowcover resulting from the winter 2010, it was not apparent whether there was a potentially ice-cored landform nearby from original reconnaissance mapping and field investigation of TAL. However, when inspected during a dry year, there is evidence that the talus just to the north and west of the TAL loggers has an overly steepened front, suggesting flow related to possible presence of deforming subsurface ice. Although the TAL loggers are not directly on this landform, their temperature trends could be expressing the cold temperatures emitted from an ice-cored landform. Logger string T2 is 30 meters directly below the steepened front of the possibly ice-cored debris, whereas T1 is approximately 100 meters to the

West of the oversteepend debris. Cold air from subsurface ice could be draining towards T2, which could be causing its relatively lower mean temperatures, whereas T1 is likely reflecting mean temperatures of a non-ice-cored landform, or true talus.

6.2.1 Summer Regimes

As expected during the summer, subsurface temperatures are attenuated relative to surface temperatures and lagged in time by 1-4 hours, regardless of landform. Conductive processes govern surface temperatures via radiative heat from the surrounding boulders. This heat is then transferred slowly to the subsurface air. The daily average surface temperature was nearly always warmer than the subsurface, resulting in positive stable density gradients. A precipitation event in early September resulted in temporarily negative gradients for most logger locations, where surface temperatures dropped suddenly with air temperature and ground temperatures did not equilibrate fast enough to maintain a positive gradient (Figures 9-20). The gradients quickly returned to positive after the precipitation event. RPD also exhibited negative gradients during other precipitation events that were not experienced by the other landforms (Figure 16), indicating a faster response time of ground temperatures to air temperatures, and thus a lack of internal buffering from cold circulating air or ice body in RPD.

Higher elevation loggers exhibit larger gradients than lower elevation loggers, and ice-cored landforms (GRG and VRG) exhibit significantly larger gradients than non-ice-cored (RPD) (Figure 22). TAL is anomalous in that it was originally examined as a non-ice cored landform, yet it has the lowest surface and subsurface temperatures in the cirque, as well as the largest gradients during the summertime. Its isolated location, higher elevation, and greater local shading throughout the day could cause these trends. It is also adjacent to Alpine Col, a mountain pass to the South side of the Glacier Divide, which may affect wind patterns and funneling of air over the mountain crest.

The summer of 2011 (Interval 1) is notably different than the summer of 2012 (Interval 5). Although each respective interval spans a different portion of summer, and cannot be directly related, I have interpreted their temperature trends in relation to their respective meteorological conditions. Interval 5 has a higher DMAT by nearly 2° C than Interval 1, however temperatures in the debris of the landforms are similar (within 1° C) to that of Interval 1, with some locations exhibiting cooler temperatures means than interval 1 (Table 5). Gradients of the landforms during Interval 1 are overall 1-3° C smaller than Interval 5 (Tables 6-7), most likely because residual snow cover was substantially greater during Interval 1 throughout the cirque, attenuating both surface and subsurface temperatures. Interval 1 surface temperatures overall exhibit a stronger relationship with elevation than Interval 5. Conversely, Interval 5 subsurface temperatures exhibit a stronger relationship with elevation than Interval 1, yet both Intervals have very weak correlations. Because snow depth was considerably less during Interval 5 than Interval 1, the void space in the matrix during the low-snow summer (interval 5) is relatively more coupled to the atmospheric temperature regime, and therefore more coupled to the large-scale lapse in temperature relative to elevation

6.2.2 Fall Regimes

The defining characteristic of the fall regime is the progressive transition in gradients from positive to negative. During this interval, repeated shifts in gradients cause inverted density gradients and natural convection to occur. During the summer, less dense warm air is on top of denser cold air, whereas in the fall, surface temperatures become denser and colder and subsurface temperatures are relatively less dense and warmer. This causes expulsion of warm matrix air through the pore spaces in the debris. Due to sporadic snowfall during Interval 2, snow cover was likely discontinuous, as suggested by the Bishop Pass record (Figures 8-20). When snow cover is discontinuous, cold dense air can sink into the void spaces and displace warmer air,

known as the *Balch Effect* (Thompson, 1962). In the same vein, warm air that may be temporarily trapped under the snowcover after a storm can rise and escape through gaps in the snow cover causing the *chimney effect* to occur. The combination of these two convective processes causes gradients in the debris to switch periodically during this Interval (Figures 8-20).

The temperature trends during Interval 2 persisted for much longer than indicated by other studies in the Sierra Nevada (Millar et al., 2011) and the Cascade Mountains (Goshorn-Maroney, 2012). I attribute this to a late and light snow year during fall 2011; all loggers were not completely decoupled from the atmosphere until late January when a large storm brought over 150 cm of snow. Air temperature was consistently near or below freezing, but the lack of continuous snow cover caused surface and subsurface temperatures to maintain some daily variation, as well as exhibit the coldest temperatures of the study period. Extensive ground cooling occurred during this time, as subsurface air was exposed to surface air.

The ice-cored landforms (GRG and VRG) had similar average matrix temperatures that were more than 1° C colder than the RPD or TAL landforms, as well as the average air temperature for Interval 2. All landforms had very similar gradients, with TAL having the largest and most negative gradient. Subsurface temperatures show a slightly positive correlation with elevation, although weak (r=0.3), suggesting that some higher elevation loggers are experiencing warmer temperatures, possibly due to warmer air funneling upslope during convection in the matrix (i.e. chimney effect (Harris and Pedersen, 1998)). Surface temperatures show an expected decreasing trend with higher elevation, opposite to that of subsurface temperatures.

6.2.3 Winter Regimes

The consistently inversed gradients that characterize Interval 3 are a result of consistent and continuous snowcover in the cirque. Previous work has tested the effect of snowcover on the thermal regime of blocky debris in various geographic locations, and concluded that a continuous snow depth greater than ~0.6 m thick decouples matrix temperatures from air temperature (Hanson and Hoezle, 2002; Goshorn-Maroney, 2012). The snow is thick enough so that air cannot transfer through the pore spaces, causing both surface and subsurface temperatures to exhibit similar temperatures and lack of daily variation (Figures 8-19). According to Bishop Pass snow depth records, snow depth remained greater than 1 m for the duration of Interval 3, and it is likely that this is a maximum estimate for snow depth in the Goethe cirque.

The BTS is fairly consistent between landforms, regardless of relative locations or depths in the matrix (-7 to -8 °C), suggesting that snow depth was fairly consistent on all landforms. However, the BTS is nearly 2° C higher in RPD than the other landforms, although it has one of the highest elevations (Table 4). The TAL also exhibits a slightly warmer BTS than the others, although it too has one of the highest elevations and generally exhibits colder temperatures throughout the year relative to other landforms. Warmer basal temperatures at these high elevations could be either due to aspect or internal circulation of warm air in the subsurface (i.e. chimney ventilation). The RPD has a southeast aspect, so could be experiencing relatively more surficial snowmelt, whereas, TAL has a northern aspect and receives the least direct sun in the cirque. The RPD is the only landform to have warmer mean surface temperature than subsurface temperature, suggesting that the temperature trends are likely a result of aspect and thus greater snow melt at the surface. Less snow depth at that site would result in overall higher temperatures and greater correlation to air temperature, which has been observed in the data (Table 8-9). In contrast, the TAL (T2) has the coldest surface temperatures during Interval 3, suggesting that relatively warm subsurface temperatures are a result of warm air rising in the matrix, rather than surface warming

from direct sun. Similarly, the BTS at GRG displays a positive trend with elevation, where temperatures are slightly warmer at higher elevations. This variation is within the nominal uncertainty of the instrument error, so may not be significant.

During the winter, logger sites with the largest relative rubble size occasionally displayed positive gradients (e.g. G11, G4, G7), presumably because snow fell or melted between void spaces, allowing loggers to be connected to air temperatures. This relationship is reflected in surface temperature correlations with air temperature (Table 8). In particular, the weather station surface logger (G11) has a statistically significant correlation with air temperature during Interval 3 (r=0.95), whereas all other loggers have very low correlations with air temperature (Table 8).

6.2.4 The Zero-Curtain

Interval 4 has been interpreted as the "zero-curtain", where the melting of snow and ice cause stabilized temperatures in the matrix at 0° C (Outcalt et al., 1990). This is usually onset at the same time mean air temperature reaches above freezing (Figures 8-19). The values of surface temperatures and gradients do not exhibit a strong relationship with aspect or elevation during Interval 4, however, the length and onset of Interval 4 is different for each logger string depending on the amount of snow, aspect, local shading, and elevation. Generally, lower elevation loggers (e.g. G1 and G6) have the shortest zero-curtain, suggesting that they melted out before higher elevation loggers (Figures 8 and 10). In contrast, higher elevation loggers (e.g. G3, and G9) generally have the longest zero-curtains (Figures 9 and 13). Similarly, aspect, which is a proxy for the amount of direct sun, affects the local snow depth and melting rates of snow. TAL receives the least direct sun and experienced the longest zero-curtain that began and ended relatively later than the other landforms.

6.2.5 Ground Thermal Regimes

Thermal profiles projected to depth are useful for interpreting the mean annual ground temperature, the 0° C isotherm, and how temperatures change with depth in the rubble (Figures 23-24). There is great uncertainty associated with my thermal profiles because I only installed two loggers at each site, and therefore can only project linearly to depth. Other studies have used more than two loggers on each string (e.g. Goshorn-Maroney, 2012) and found that thermal profiles can exhibit cubic trends in the rubble (increasingly smaller temperature gradients with increasing depth), however, most thermal profiles that were constructed in Goshorn-Maroney (2012) exhibited linear gradation with depth, which lends more confidence to my projected linear thermal profiles. The greatest depth reached in my study was nearly 3.5 meters, which is likely only approximately one-third of the depth to frozen ground according to estimates of debris thickness in previous work (Barsch, 1996). Although my study cannot extract the exact projection of temperature in the matrix, temperature gradients likely decrease to near zero at the ice core or frozen ground.

Thermal profiles have a distinct relationship with relative elevation and type of landform. Logger strings G3, G8, G9 are the highest elevation logger strings on GRG and have the lowest mean ground temperature and smallest projected depths to the 0° C isotherm (Figures 23-24). Conversely, logger strings G1, G7, G6 are the lowest elevation logger strings on GRG, have the highest mean ground temperature and greatest projected depths to ice (Figures 23-24). This suggests that the higher elevation portions of the main rock glacier have less debris mantling the ice core, which is to be expected, as the accumulation zone is predominantly snow and ice. The toe, or lower elevation portions of the rock glacier, has thicker debris from movement and collection down-slope. Logger string G11 is somewhat of an anomaly because it is placed in the middle of the two rock glacier lobes where there is likely buildup of large boulders and sediment. This site also had the largest grain-size of sediment of any other logger site. The RPD has the highest ground temperature (4°C) and greatest projected depths to possible

ground ice (46 m) of all the landforms, both of which make the existence of any significant ground ice unlikely. VRG has a comparable ground temperature profile to that of GRG, yet with a slightly higher ground temperature and greater possible depth to the 0° C isotherm. These values for VRG are reasonable relative to GRG considering it has lower mean elevation. Thermal profiles of TAL are anomalous because they exhibit higher ground temperatures than GRG, but the smallest depths to the 0° C isotherm. As previously mentioned, logger string T2 is directly down slope of a potentially ice-cored landform, possibly causing the attenuated subsurface temperatures relative to any other landform and resulting in smaller projected depths to the 0° C isotherm. TAL also has the steepest topography of any landform and is surrounded by bedrock outcrops, so if any ground ice is present; it should be fairly close to the surface of the debris.

6.2.6 Geographical and Morphological Constraints

Regressions of all landforms' summer temperatures together with elevation indicate that surface temperatures have an expected negative relationship with elevation whereas subsurface temperatures have a slightly positive change with elevation (Figure 25). Relationships are weak, however, making any cirque-scale trends anecdotal. When observing trends of only GRG with elevation during summer months, Interval 1 temperatures have a stronger relationship with elevation than Interval 5, with correlation coefficients of 0.5 for subsurface temperatures and 0.6 for surface temperatures. Interval 5 correlation coefficients are 0.26 and 0.09, respectively. Although the regression fit is poor, Interval 5 surface temperatures show an increasing temperature trend with elevation, which is not exhibited in the other landforms.

Strings V1 and V2 and T1 and T2 have the strongest correlations with elevations, as expressed by linear regression fits with R^2 greater than 0.95. Logger string V3 is anomalous in that subsurface temperatures are some of the lowest in the cirque

although it also has the lowest elevation of any logger. This suggests that this logger string may be very close to a body of ice or snow packed into the rubble. This logger is located right above the toe of the easterly valley-wall rock glaciers (VRG2), where debris cover may be thin, or cold dense air could be draining down-slope. Omitting this outlier from the regression, all surface and subsurface temperatures of TAL and VRG show a strong correlation with elevation, suggesting there is not a strong buffering of a large ice body affecting temperature in the rubble. RPD also has an observed negative relationship with elevation; however, there are too few data points to make a meaningful interpretation.

When assessing all landforms' temperatures with elevation, the general cirque-scale (and in particular GRG's) weakness in relationship with elevation implies that temperatures in the debris are strongly affected by elements other than standard lapse rates in atmospheric temperatures. A study by Lundquist and others (2007) states that a simple lapse rate is a poor description of surface temperature trends in complex terrain, which could be due to localized temperature inversions, cold air drainage, and large-scale weather patterns. Although their study has a greater geographical and altitudinal scope than mine (loggers in this study only span 200 meters in elevation), the temperatures at Goethe cirque support their conclusions in a single valley. Because elevation is not the apparent control on temperatures in the cirque, temperature trends could be due to the morphological environment, local convection processes, or the presence or absence of ground ice. This might suggest that subsurface temperatures are moderated by other environmental factors like aspect, shading, or ice content in the rubble. Local shading, whether from a large headwall or a nearby boulder, has proven to be a major factor affecting matrix temperatures, especially at high elevations where solar radiation is so strong.

6.3 Discharge and Stream Temperature Variations

The Goethe rock glacier outlet stream exhibits characteristic daily and seasonal variations in discharge and stream temperature that are consistent with previous work in other locations (Krainer and Mostler, 2002; Berger et al., 2004; Millar et al, 2011). Diurnal variation is highest during the heavy snowmelt season (Interval 4), when air temperature is consistently above freezing thereby melting the residual winter snowpack and causing the largest annual peaks in flow. Diurnal variation is lowest during the fall and winter (Intervals 2 and 3), when the air temperature is consistently below freezing and has been interpreted as a period when the stream is frozen or dry. The summer season (Intervals 1 and 5) exhibits modest daily variations in stream flow and temperature, when snow cover has largely melted away and peaks in flow and temperature are a result of baseflows from lingering pockets of melted snow and ice, groundwater, and precipitation. Lag times between daily peak flow and daily peak air temperature during the summer months suggest that the rock glacier is a complex water reservoir, with subsurface channels and cavities that may store water temporarily throughout the day. Lag times are also likely related to the time needed to conduct heat through the rubble to reach the subsurface.

6.3.1 Spring Runoff Regime

The outlet stream is heavily snowmelt-dominated during the spring, and exhibits the highest annual peaks in discharge. The uncertainty in discharge is high because the rating curve was developed with flows that were only half that of Interval 4, making projections ambiguous. Although 60% of Interval 4 is below the maximum observed stage height (0.53 m), stage heights higher than that are on average 0.27 m greater, making their respective discharges exponentially uncertain. Stream temperature, however, is well constrained throughout the study period and exhibits similar trends to that of Millar et al. (2011). Mass melting of snow in the cirque causes a “flat-line” of stream temperature at 0° C, similar to the “zero-curtain” described in the matrix temperatures of the landforms during Interval 4 (Section 6.2.4). Discharge is highly

sensitive to air temperature during this time; when air temperature is consistently above or within a few degrees of freezing for more than a week, the highest peaks and daily variation in flow occur (Figure 29).

6.3.2 Summer Runoff Regime

During Interval 1, the amount of discharge has the strongest correlation with air temperature from the weather station and temperatures within the debris of the rock glacier (Table 10). Conversely, stream temperature has a very weak positive correlation with air temperature, and negative correlation with temperatures in the debris. This relationship implies that snowmelt was the dominant process affecting both discharge and stream temperature in the outlet stream, especially considering that snow was extensive into late summer and fall of 2011. Any warming trends in ST are likely due to water that came in contact with heated rock debris or warm precipitation. From 8/17 to 9/17, the mean ST increases while the air temperature decreases. Mean discharge also starts to decrease with air temperature at this time, indicating that there is less water in the stream to warm throughout the day (Figure 28). This results in an overall increasing trend and greater diurnal variance in ST as both Q and AT increase. After the first annual snowfall in early October (onset of Interval 2), there is a small peak in Q and stabilized ST near freezing temperatures, suggesting extensive snow melt, which was observed in the field in mid-October.

Interval 5 appears to encompass a period when most winter snow in the cirque has melted and the summer baseflow regime has resumed (Figures 26 and 29). During this interval, discharge is most tightly tied to air temperature, and not as much with temperatures in the debris of the rock glacier (Table 10). Stream temperature has a stronger relationship with both surface and subsurface temperatures than discharge for this interval, suggesting that there may be active melting of internal ice. Because most of the snow cover is already gone during Interval 5, an open network of rubble that is also strongly correlated with air temperature (Tables 8-9) allows warm air to inundate

void spaces and potentially melt internal ice via conduction or air pumping. In contrast to Interval 1, Q has a positive correlation with ST during interval 5, indicating that greater amounts of water in the stream are associated with warmer water temperatures. This suggests that warm air temperatures during Interval 5 may be causing warm precipitation that is affecting ST (rather than snowmelt) when discharge is high. Warmer days show a greater increase in ST during precipitation events, either due to the fact that rain on these days is actually warmer, or that the rocks in the cirque were warmed throughout the day, resulting in overall warmer water moving through the matrix of the landforms. There were not many precipitation events recorded at Goethe during Interval 5, however short thunderstorms could have occurred elsewhere in the cirque (not at the weather station), thereby contributing to streamflow.

By comparing Interval 1 and Interval 5, it is apparent that different processes dominate their respective runoff regimes; Interval 1 is dominated by snowmelt and Interval 5 is dominated by precipitation. Discharge has the strongest correlations with AT for both intervals relative to any other parameter, however ST has a much stronger correlation with AT during Interval 5 than Interval 1 (Table 10). These findings suggest that melting of snow is not the dominant process at work during Interval 5, which is to be expected as most snow was melted off in late May according to Goethe and Bishop Pass records, and field observations in July (Figure 26). Stream temperature and discharge relationships with average GRG surface and subsurface temperatures also support this hypothesis. During Interval 5, ST has a best-fit second-order polynomial relationship with subsurface temperatures, where ST increases as subsurface temperatures increase. When subsurface temperatures reach 4° C, ST begins to decrease (Figure 30). This threshold might indicate the melting of internal ice as subsurface temperatures reach this temperature. More data is necessary to make any conclusive interpretations.

Another rather speculative hypothesis for the relationship between ST and subsurface temperatures during Interval 5 involves an unusual peak streamflow event that

occurred on July 5th (day 324 on Figure 29). Discharge rapidly increased to nearly 5 times that of previous days then rapidly declined back to baseflow levels over the course of 36 hours, without a significant rain event. Stream temperature also shows a gradual decline to 1° C over the course of a few days, then a rapid incline back to its background levels established prior to the event. The continued gradual increase in Q and decrease in ST, then rapid decline in Q and increases in ST to background levels, suggests that this event was caused by substantial draining of stored water somewhere in or on the rock glacier (e.g., surficial lakes or cavities in the ice). This event is preceded by a period of increasingly warm AT upwards of 10° C (Figure 29), although AT on the day of the event was only a few degrees above freezing. A surge of stored water within the debris of the rock glacier could have flowed out when a conduit became available with generally increasing AT. Although 3 mm of precipitation was recorded at Bishop Pass (~17 km southeast), no precipitation was recorded at the Goethe weather station. It is unlikely that a highly localized heavy rainstorm occurred at the location of the surge (and not at the weather station), thereby causing mass melting of snow and ice and large peaks in streamflow. It is possible that the precipitation event recorded at Goethe two days prior to the surge (which coincided with warm air temperatures) caused heavy melting of snow and ice that then initiated the event (Figure 29). Stream temperature begins to decline on the day of this warm precipitation event, indicating the beginning of substantial ice-melt. It is not until two days later when Q rapidly increases, that melting was great enough to create a conduit for the surge. Such events have been documented before on Sierra Nevada rock glaciers, where an outburst flood was documented on the Mendel rock glacier, just a few kilometers south of the Goethe rock glacier (Konrad and Clark, 1998).

6.4 Evidence for Ice-Melt Contributions to Streamflow

Though sparse, tritium signatures in the stream are consistent with my interpretations of stream discharge and stream temperature variations during the summer months.

Because of the large amount of uncertainty regarding actual discharge in the stream due to various sources of error, quantities of discharge attributed to ice melt are rough estimates at best. Regardless, general trends are consistent, exhibiting a snowmelt-dominated hydrological regime during Interval 1 (0-5% estimated ice melt), and a precipitation dominated regime during Interval 5 with significant contributions from internal pre-1950 ice-melt (7-19% estimated ice melt). These estimates are also consistent with previous work at the Galena Creek rock glacier, where estimates of ice melt were nil, indicating that the rock debris mantle is very efficient at insulating internal ice thereby preventing direct melting of the core (Cecil et al., 1998). My estimates for Interval 5 are somewhat higher than their estimates for ice contribution, which may reflect the uncertainty in both sets of measurements, or the uncertainty in the source of the water in Cecil et al.'s study.

The tritium signatures display an apparent inversion to what would generally be expected, where late-summer (Interval 1) samples are higher than early summer (Interval 5) samples. However, the excess amount of winter precipitation in 2010-2011 (nearly 120% of normal) was reflected in the stream flow data for the summer of 2011. There was still significant snowpack in the cirque when the sample was collected in mid-summer of 2011, much more than the snow cover in early summer of 2012. One would expect early summer runoff to contain almost entirely snowmelt, yet the winter of 2011-2012 received nearly half the snowfall of winter 2010-2011, which is supported by field observations. The tritium content of runoff in the fall of 2011 was lower than expected possibly because an early snowstorm hit the region one week prior to sample collection, resulting in a higher tritium content and higher perceived percentage of snowmelt in the stream. Field observations indicate that although the stream was covered in snow during this time, it was still flowing, so could have contained some residual melt of internal ice. Temperatures in the debris at this time varied from a few degrees below to a few degrees above freezing, in contrast to air temperature that was -10° C, which could have contributed to some residual internal melting (Figures 9-15).

7.0 Conclusions

Thermal and hydrological conditions in the Goethe cirque indicate a large sensitivity to meteorological conditions that is seasonally moderated by cold internal temperatures within the ice and debris of the landforms. The two contrasting summers during the yearlong study period exhibited different characteristics, particularly in discharge, stream temperature, and relative contribution of runoff source. The summer of 2011 was largely affected by exceptional snowpack from the previous winter, which was expressed by lower mean debris matrix temperatures, strong correlations between discharge and air temperature, and tritium signals that indicate a nearly pure snow-melt source for the outlet stream. The summer of 2012 was characterized by an exceptionally low snowpack compared to the winter of 2011, which was expressed by higher mean matrix temperatures, strong correlations between stream temperature and matrix temperatures, and a tritium signal that indicated a modest amount of ice melt contribution to discharge in the outlet stream.

The spectrum of landforms investigated in this study exhibit similarities and differences depending on the season. Ice-cored landforms (GRG and VRG) have statistically different temperature distributions than the non-ice-cored landform (RPD) in the summer months. Both GRG and VRG have similar temperature distributions, medians and variances, indicating they are closely linked in terms of ground thermal development, and generally exhibit higher gradients and lower surface temperatures than RPD. Medians, distributions and variances of temperature gradients within the rubble are similar between all landforms for fall, winter and spring (Intervals 2, 3, and 4), which is expected because temperatures in the matrix are completely or partially disconnected from the atmosphere depending on snow cover. GRG generally has higher variance and a greater number of outliers due to a larger sample size and a greater variety of morphologic locations. Temperature profiles of GRG and VRG indicate a reasonable

depth to the 0° C isotherm (possible frozen ground) and the lowest annual ground temperatures when averaged. Temperature profiles of RPD indicate unreasonable depths to frozen ground; instead suggesting the minimum ground temperature at depth is above freezing, consistent with the lack of a buried ice core below. Small gradients, high temperature means, and strong correlation of matrix temperature to air temperature also support that RPD is likely non-ice-cored.

The TAL was originally included in the project to serve as a control for matrix temperatures at the GRG, however, further scrutiny of the landform when there was lack of snow cover suggests that the loggers are adjacent to what morphologically looks like a small valley-wall rock glacier with an over steepened front. TAL displayed the lowest average temperatures, smallest depths to the 0° C isotherm, and the largest gradients of any landform studied, which provide more evidence that this landform could be ice-cored or is adjacent to an ice-cored landform. Its topographically high and steep location and proximity to Alpine Col, a mountain pass in the cirque to the other side of the Glacier Divide, may be affecting the microclimate surrounding TAL.

Strong correlations between matrix temperatures and hydrological parameters suggest that the open network of debris that is exposed after surface snow has melted may induce melting of internal ice. Furthermore, strong correlations of matrix temperatures with air temperatures create a relationship favorable for ice-melt if air temperatures continue to increase as observed over the last 30 years. With projected decreases in snow cover in the Sierra Nevada (Stewart et al., 2004; Knowles et al., 2006), mean matrix temperatures could rise to the point that buried ice and rock glaciers, of whatever origin, rapidly decay. The longer the air in the matrix is connected to rising atmospheric temperatures, the greater the potential melting of internal ice of these alpine landforms. Increases in air temperature also would result in an increased percent of rain versus snow of annual precipitation, in turn accelerating the hydrologic response in Sierran rock glaciers, as exhibited during rain events during periods of Interval 1 and 5

when snowcover had melted. Increased temperature of precipitation could also induce melting of internal ice as it flows over buried ice lenses or ice cores. Earlier onset of spring snowmelt will likely change the timing of peak runoff in alpine basins, as well as increase the duration that the rock glacier debris matrix is open to warm air temperatures.

Future work should strive to collect more temperature samples from each respective landform for a greater sample density to make statistical analysis and direct comparison more meaningful. A valuable follow-up study would be to investigate two different cirques: one with a rock glacier, and one that contains a non-ice cored talus with similar aspect and elevation as a control on the rock glacier results. The feasibility of such a project would depend on field conditions, access, and viable field sites. In order for the rating curve to be more accurate, it is crucial to deploy a barometric pressure sensor at the stream gauging site in order to correctly model air pressure at the site and calibrate the levelogger. I would also suggest utilizing a dye-tracer or salt-tracer method for calculations of discharge in the field, as the stream channel is complex causing errors in the flowmate method. Tritium signatures of runoff as a proxy for glacial ice melt could also be validated with a turbidity record, where a larger content of suspended sediment of the stream corresponds to a larger contribution of ice melt. Stream turbidity combined with tritium content and stream temperature trends would better constrain the seasonality of rock glacier ice melt in the stream. Accurately quantifying the thermal regime and discharge relationships in alpine valleys is crucial for understanding the sensitivity of rock glaciers and permafrost to changing climate.

References

Achim Zeileis and Gabor Grothendieck (2005). zoo: S3 Infrastructure for Regular and Irregular Time Series. Journal of Statistical Software, 14(6), 1-27. URL http://www.jstatsoft.org/v14/i06/

Azocar, G.F. and Brenning, A. (2010). Hydrological and geomorphological significance of rock Glaciers in the dry Andes, Chile (27°-33°S). Permaforst and Periglacial Processes 21: 42 53.

Balch, E.S. (1990). Glaciers or Freezing Vaverns. Philadelphia, PA: Allen, Lane, Scott.

Barsch, D. (1996). Rock Glaciers—Indicator for the Present and Former Geoecology in High Mountain Environments. Springer Verlag, Berlin-Stuttgart.

Barsch, D. (1996). Rockglaciers. *Rockglaciers. Series: Springer Series in Physical Environment, ISBN: 978-3-642-80095-5. Springer Berlin Heidelberg (Berlin, Heidelberg), Edited by Dietrich Barsch, vol. 16*, *16*.

Basagic, H. J. (2008). Quantifying twentieth century glacier change in the Sierra Nevada, California. M.S. Thesis, Portland State University, Portland.

Berger, J., Krainer, K., Mostler, W. (2004). Dynamics of an active rock glacier: Oztal Alps, Austria. *Quaternary Research* 62: 233-242.

Berthling, I. (2011). Beyond confusion: Rock glaciers as cryo-conditioned landforms. *Geomorphology*, *131*(3), 98-106.

Burger, K.C., Degenhardt, J. J., Giardino, J.R. (1999). Engineering geomorphology of rock glaciers. *Geomorphology* 31: 93-132.

Brenning, A. (2005). Geomorphological, hydrological and climatic significance of rock glaciers in the Andes of central Chile (33-35 degrees S). *Permafrost and Periglacial Processes*, 16: 231-240.

Calkin, P. E., and Ellis, J. M. (1980). A lichenometric dating curve and its application to Holocene glacier studies in the central Brooks Range, Alaska. *Arctic and Alpine Research*, 245-264.

Cecil, L. D., Green, J., Vogt, S., Michel, R. and Cottrell, G. (1998). Isotopic composition of ice cores and meltwater from Upper Fremont Glacier and Galena Creek rock glacier, Wyoming. Geografiska Annaler: Series A, *Physical Geography* 80: 287-292.

Chamberlin, T. C., and Salisbury, R. D. (1906). *Geology* (Vol. 1). New York: Henry Holt and Company.

Chambers, J. M., Cleveland, W. S., Kleiner, B. and Tukey, P. A., (1983), Graphical Methods for Data Analysis. Wadsworth & Brooks/Cole

Clark, D.H., Clark M.M., and Gillespie, A.R. (1994). Debris-covered glaciers in the Sierra Nevada, California, and their implications for snowline reconstructions. *Quaternary Research* 41 (2): 139-153.

Clark, D. H., & Gillespie, A. R. (1997). Timing and significance of late-glacial and Holocene cirque glaciation in the Sierra Nevada, California. *Quaternary International* 38: 21-38.

Clark, D.H., Steig, E.J., Potter, N., Gillespie, A.R. (1998). Genetic variability of rock glaciers. *Geografiska Annale* 80: 175- 182.

Daly, C., Neilson, R.P., Phillips, D.L. (1994). A statistical-topographic model for mapping climatological precipitation over mountainous terrain. Journal of Applied Meteorology, 33: 140-158.

De Jong, M. G. G., & Kwaduk, J. K. (1988). Fossil rock glaciers in central Vorarlberg, Austria. *Arctic and Alpine Research*: 86-96.

Dettinger, M.D. and Cayan, D.R. (1994). Large-scale atmospheric forcing of recent trends toward early snowmelt runoff in California. *Journal of Climate* 6: 606-623.

Dettinger, M.D., Cayan, D.R., Meyer, M.K., and Jeton, A.E. (2004). Simulated hydrological responses to climate variations and change in the Merced, Carson, and American River Basin, Sierra Nevada, CA, 1900-2099. *Climatic Change* 62: 283-317.

Foster, H. L., & Holmes, G. W. (1965). A large transitional rock glacier in the Johnson River area, Alaska Range. *US Geol. Surv. Prof. Paper*: 112-116.

Giardino, J.R., Vitek, J.D., DeMorett, J.L. (1992). A model of water movement in rock glaciers and associated water characteristics. In Periglacial Geomorphology, Dixon JC, Abrahams AD (eds). John Wiley & Sons: Chichester; 159–184 Haeberli, W. (1985). Creep of mountain permafrost. Mitteilungen der Versuchsanstalt fur Wasserbau, Hydrologie und Glaziologie der ETH Zurich, 77.

Hanson, S., Hoelzle, M. (2004). The thermal regime of the active layer at the Murtel rock glacier based on data from 2002. *Permafrost and Periglacial Processes* 15: 273-282.

Harris, S.A. and Pedersen, D.E. (1998). Thermal regimes beneath coarse blocky material. *Permafrost and Periglacial Processes* 9: 107-120.

Hoelzle, M., Wegmann, M. and Krummenacher, B. (1999). Miniature temperature dataloggers for mapping and monitoring of permafrost in high mountain areas: First experience from the Swiss Alps. *Permafrost and Periglacial Processes* 10: 113-124.

Humlum, O. (1996). Origin of rock glaciers: observations from Mellemfjord, Disko Island, central West Greenland. *Permafrost and Periglacial Processes 7*(4), 361-380.

Humlum, O. (1997). Active layer thermal regime at three rock glaciers in Greenland. *Permafrost and Periglacial Processes,* 8: 383-408.

Humlum, O. (1998). The climatic significance of rock glaciers. *Permafrost and Periglacial Processes*, *9*(4), 375-395.

Ikeda, A., Matsuoka, N., & Kääb, A. (2003). A rapidly moving small rock glacier at the lower limit of the mountain permafrost belt in the Swiss Alps. In *Proceedings of the Eighth International Conference on Permafrost* 1: 455-460.

Ishikawa, M., and Hirakawa, K. (2000). Mountain permafrost distribution based on BTS measurements and DC resistivity soundings in the Daisetsu Mountains, Hokkaido, Japan. *Permafrost and Periglacial Processes* 11(2): 109-123.

Jackli, H. (1957). Gegenwartsgeologie des bündnerischen Rheingebiets.Ein Beitrag zur exogenen Dynamik alpiner Gebirgslandschaften, *Geotechnische Serie* 36. Kümmerle & Frey: Bern.

Jackson, L. E., & MacDonald, G. M. (1980). Movement of an ice-cored rock glacier, Tungsten, NWT, Canada, 1963-1980. *Arctic*, *33*(4), 842-847.

Johnson, B. G., Thackray, G. D., & Van Kirk, R. (2007). The effect of topography, latitude, and lithology on rock glacier distribution in the Lemhi Range, central Idaho, USA. *Geomorphology*, *91*(1), 38-50.

Juliussen, H. & Humlum, O. (2007). Towards a TTOP ground temperature model for mountainous terrain in central-eastern Norway. *Permafrost and Periglacial Processes* 18: 161-184.

Kerschner, H. (1978). Paleoclimatic inferences from Late Würm rock glaciers, eastern central Alps, western Tyrol, Austria. *Arctic and Alpine Research*: 635-644.

Konrad, S.K., and Clark, D.H. (1998). Evidence for an Early Neoglacial glacier advance from rock glaciers and lake sediments in the Sierra Nevada, California, U.S.A. *Arctic and Alpine Research*, 30: 272-284.

Luckman, B., & Kavanagh, T. (2000). Impact of climate fluctuations on mountain environments in the Canadian Rockies. *Ambio: A journal of the human environment*, *29*(7): 371-380.

Maurer, H., & Hauck, C. (2007). Geophysical imaging of alpine rock glaciers. *Journal of Glaciology*, *53*(180): 110-120.

Martin, H. E., & Whalley, W. B. (1987). Rock glaciers part 1: rock glacier morphology: classification and distribution. *Progress in Physical Geography*, *11*(2): 260-282.

Millar, C.I. and Westfall, R.D. (2007). Rock glaciers and related periglacial landforms in the Sierra Nevada, California, U.S.A; inventory, distribution and climatic relationships. Quaternary International, doi:10.1016/j.quaint.2007.06.004.

Millar, C. I., & Westfall, R. D. (2008). Rock glaciers and related periglacial landforms in the Sierra Nevada, CA, USA; inventory, distribution and climatic relationships. *Quaternary International*, *188*(1): 90-104.

Millar, C. I., & Westfall, R. D. (2010). Distribution and climatic relationships of the American pika (Ochotona princeps) in the Sierra Nevada and western Great Basin, USA; periglacial landforms as refugia in warming climates. *Arctic, Antarctic, and Alpine Research*, *42*(1): 76-88.

Millar, C. I., Westfall, R. D., & Delany, D. L. (2012). Thermal and hydrologic attributes of rock glaciers and periglacial talus landforms: Sierra Nevada, California, USA. *Quaternary International*.

Moiseev, P. A., & Shiyatov, S. G. (2003). Vegetation dynamics at the treeline ecotone in the Ural highlands, Russia. In *Alpine biodiversity in Europe* (pp. 423-435). Springer Berlin Heidelberg.

Monnier, S., Camerlynck, C., Rejiba, F., Kinnard, C., Feuillet, T., and Dhemaied, A., (2011). Structure and genesis of the Thabor rock glacier (Northern French Alps) determined from morphological and ground-penetrating radar surveys. *Geomorphology*, 134(3-4): 269-279.

Muller, S.W. (1947). Permafrost, or permanently frozen ground and related engineering problems. Ann Arbor, Michigan: Edward Bros, 231 pp.

Outcalt, S.I., Nelson, F.E., and Hinkel, K.M. (1990). The zero-curtain effect: heat and mass transfer across an isothermal region in freezing soil. *Water Resources Research,* 26: 1509-1516.

Parmesan, C. (2006). Ecological and evolutionary responses to recent climate change. *Annual Review of Ecology, Evolution, and Systematics*: 637-669.

Pauli, H., Gottfried, M., & Grabherr, G. (1996). Effects of climate change on mountain ecosystems–upward shifting of alpine plants. *World Resource Review*, *8*(3): 382-390.

Plummer, L. N., Michel, R. L., Thurman, E. M. and Glynn, P. D. (1993). Environmental tracers for age dating young ground water, in Regional Ground-WaterQ uality,e dited by W. M. Alley, pp. 255-294, Van Nostrand Rei. nhold, New York, 1993.

Plummer, L.N., Böhkle, J.K., and Busenberg, Eurybiades (2003). Approaches for ground water dating *in* Lindsey, B.D., Phillips, S.W., Donnelly, C.A., Speiran, G.K., Plummer, L.N., Böhlke, J.K., Focazio, M.J., Burton, W.C., and Busenberg, Eurybiades, Residence times and nitrate transport in groundwater discharging to streams in the Chesapeake Bay Watershed: *U.S. Geological Survey Water Resources Investigations Report* 03-4035: 12-24.

Portfolio & Risk Advisory Group and Commerzbank Securities (2009). its: Irregular Time Series. R package version 1.1.8. http://CRAN.R-project.org/package=its

Potter, N. (1972). Ice-cored rock glacier, Galena Creek, Northern Absaroka Mountains, Wyoming. *Geological Society of America Bulletin*, 83: 3025-3058.

Potter Jr, N., Steig, E. J., Clark, D. H., Speece, M. A., Clark, G. T., & Updike, A. B. (1998). Galena Creek rock glacier revisited—New observations on an old controversy. *Geografiska Annaler: Series A, Physical Geography*, *80*(3-4), 251-265.

R Core Team (2012). R: A language and environment for statistical computing. R Foundation for Statistical Computing, Vienna, Austria. ISBN 3-900051-07-0, URL http://www.R-project.org/.

Rohn, O. (1900). A reconnaissance of the Chitna River and Skolai Mountains, Alaska. *U.S. Geological Survey 21st Ann Rep. Pt.* 2:399-440.

Santos-Gonzalez, J., Gonzalez-Gutierrez, R., Gomez-Villar, A., Redondo-Vega, J. (2009). Ground thermal regime in the vicinity of relict rock glaciers (Cantabrian Mountains, NW Spain). *Finisterra* XLIV 87:35-44.

Schrott, L. (1996). Some geomorphological-hydrological aspects of rock glaciers in the Andes (San Juan, Argentina). Zeitschrift Fur Geomorphologie: 161-173.

Spencer, A.C. (1900). A peculiar form of talus (abstract). *Science* 11: 188.

Thompson, W.F. (1962). Preliminary notes on the nature and distribution of rock glaciers relative to true glaciers and other effects of climate on the ground in North America. Int. Assoc. Scientific Hydrol. Colloque d'Obergurgl. *Commission of Snow and Ice*, 58: 212-219.

Vick, S. G. (1981). Morphology and the role of landsliding in formation of some rock glaciers in the Mosquito Range, Colorado. *Geological Society of America Bulletin*, *92*(2): 75-84.

Vonder Mühll, D., & Haeberli, W. (1990). Thermal characteristics of the permafrost within an active rock glacier (Murtèl/Corvatsch, Grisons, Swiss Alps). *Journal of Glaciology*, *36*(123), 151-158.

Wahrhaftig, C., & Cox, A. (1959). Rock glaciers in the Alaska Range. *Geological Society of America Bulletin*, *70*(4), 383-436.

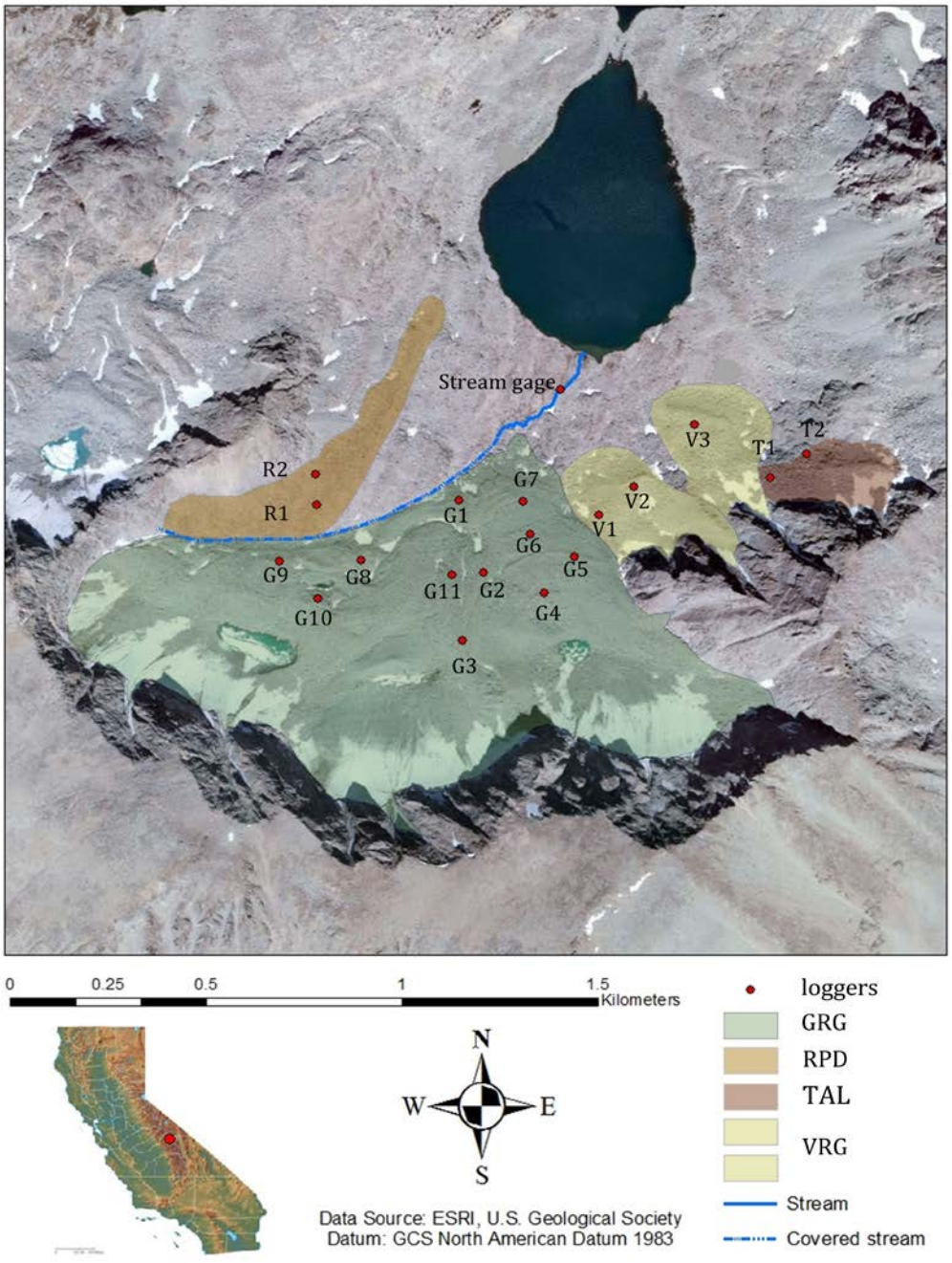

Figure 1. Map of the Goethe rock glacier and surrounding landforms. Red dots indicate temperature logger sites. Morphologically distinct landforms are defined as Goethe Rock Glacier (GRG), Recess Peak debris (RPD), talus (TAL), and two valley-wall rock glaciers (VRG).

Figure 2. Equipment used for datalogging at the field site clockwise from topleft: a) Campbell Scientific custom-made weather station, b) stilling well and transect for collecting stream runoff measurements, c) surface logger deployment, d) Solinst levelogger and iButton temperature logger.

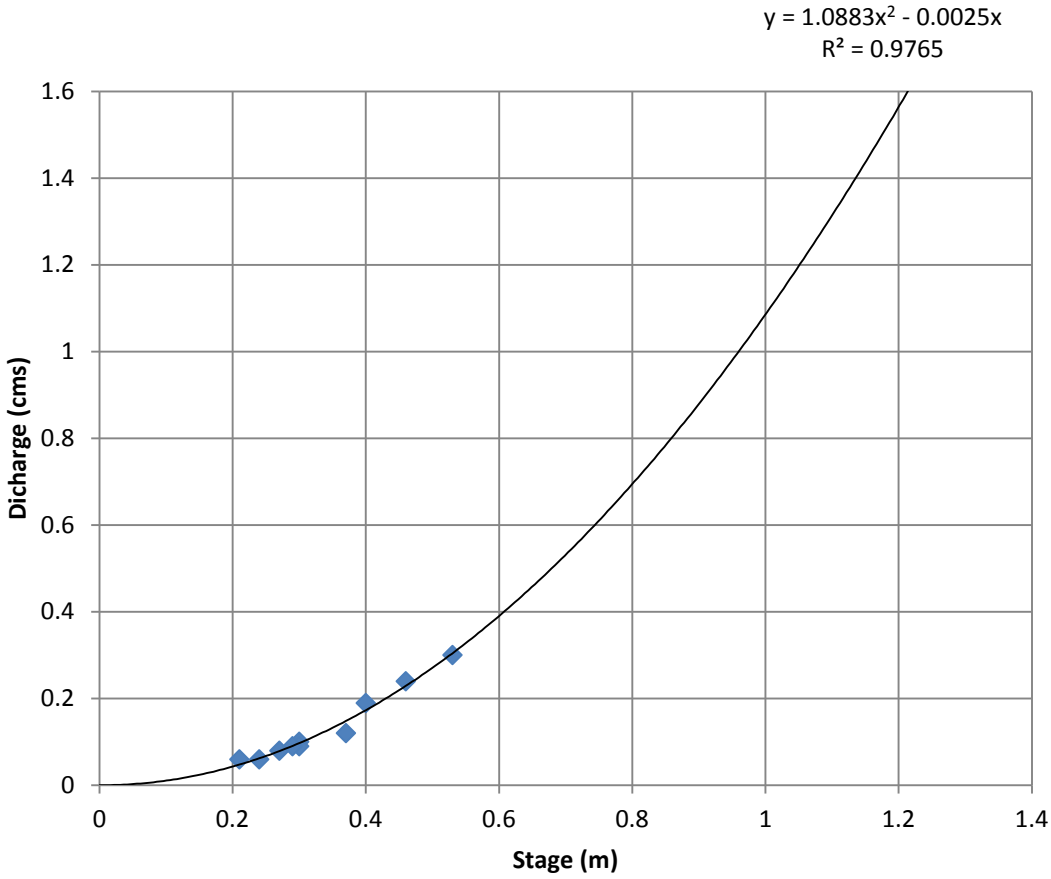

Figure 3. Rating curve of stream stage and discharge observations that were collected in the field. Plot shows the trendline projected to maximum stage height recorded by the levelogger in the outlet stream.

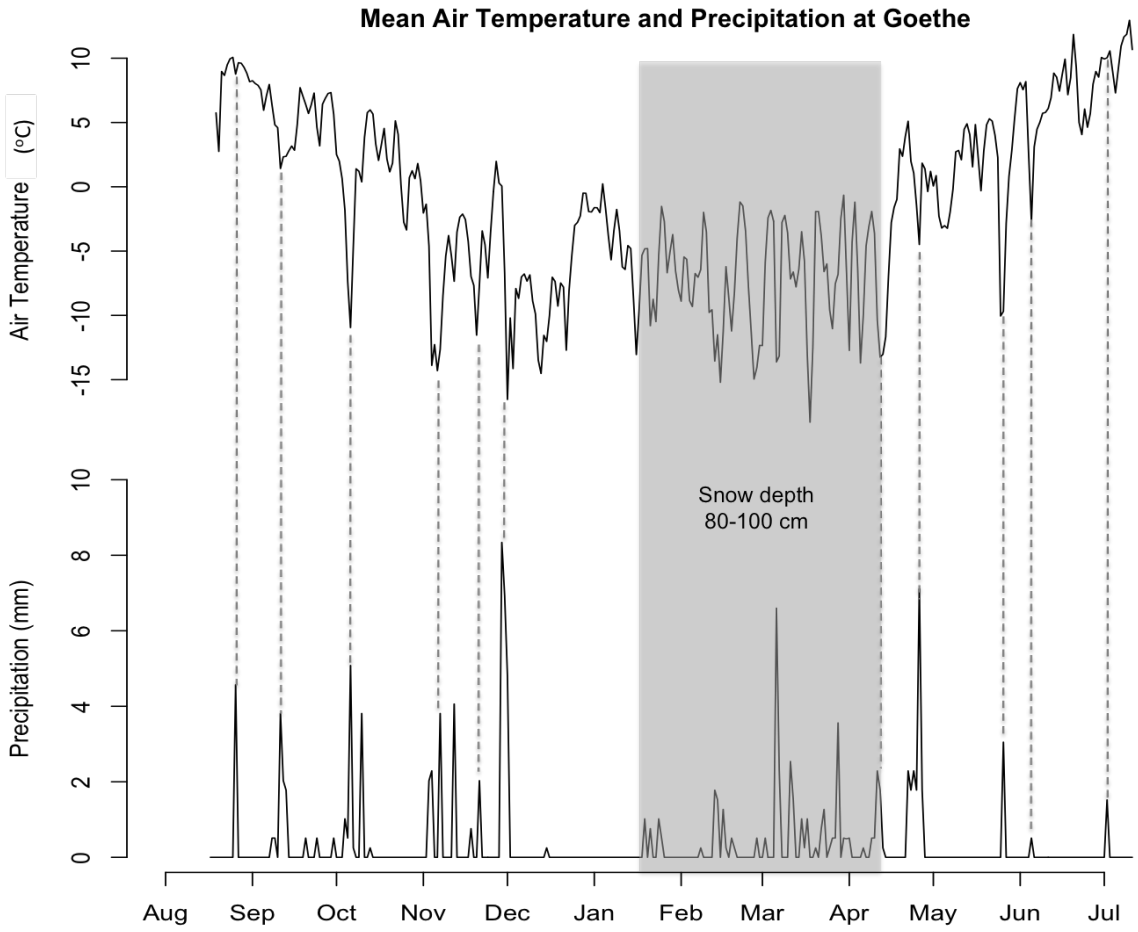

Figure 4. Daily mean air temperature (DMAT) and total precipitation recorded by the Goethe weather station from August 2011-July 2012. During summer, fall and spring months, drops in temperature correspond to precipitation events. The snow depth record was retrieved from the Bishop Pass Geostationary Operational Environmental Satellite (GOES) weather station, operated by NOAA at an elevation of 3482 m (NOHRSC, 2013). Snow depth from 80-100 cm is deep enough for temperature loggers in the debris to become disconnected with atmospheric temperatures.

A)

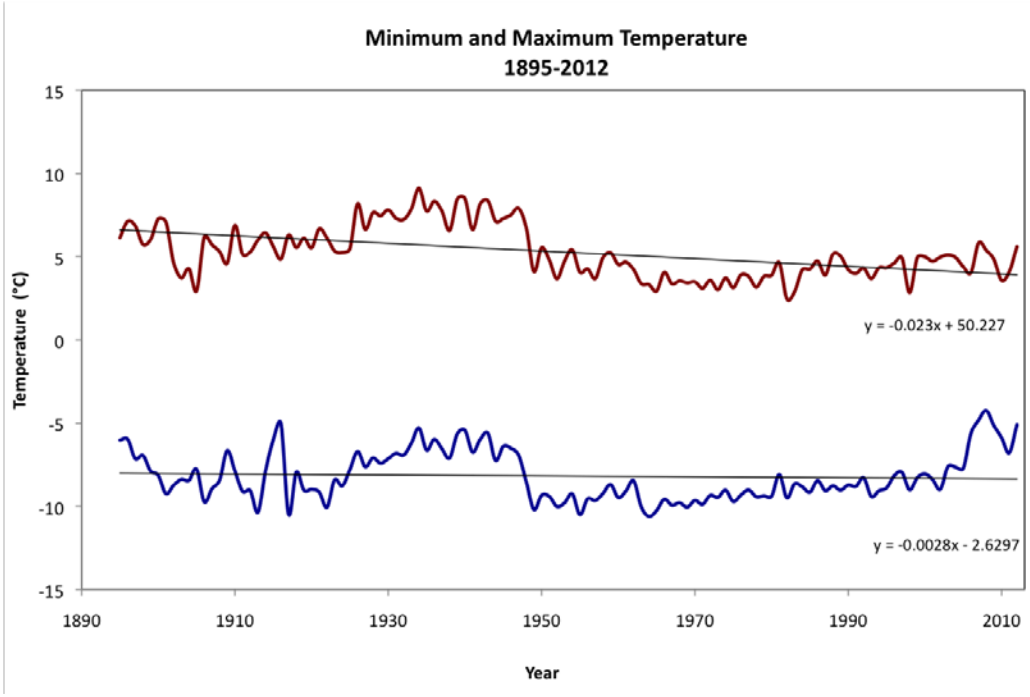

B)

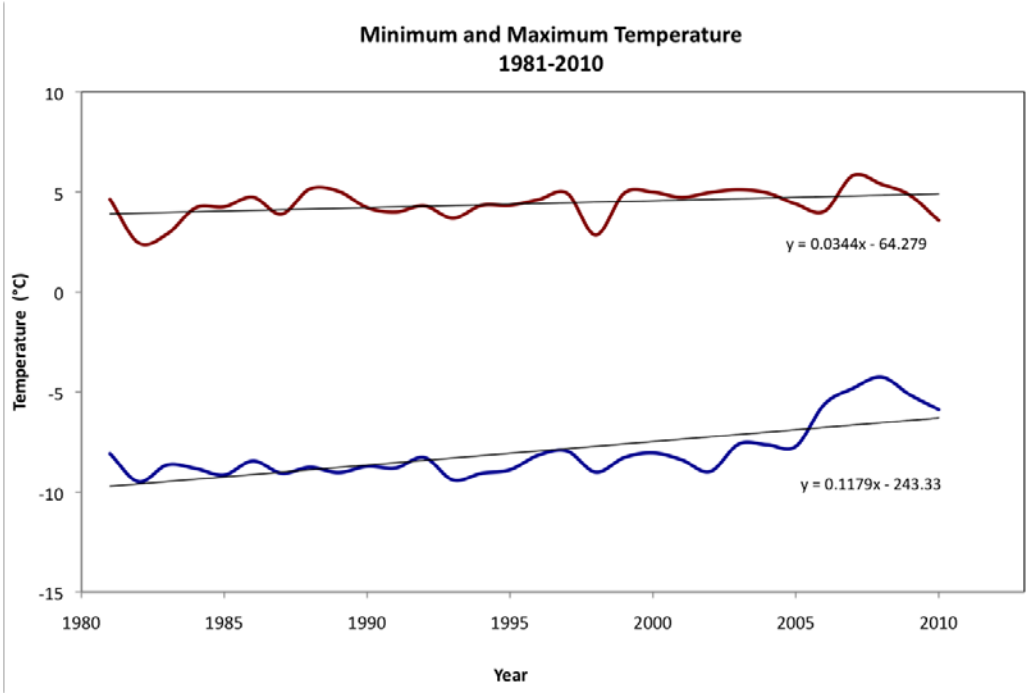

Figure 5. PRISM's minimum (blue) and maximum (red) temperature for the Goethe cirque from 1895 to 2012 (A), and from 1981 to 2010 (B).

A)

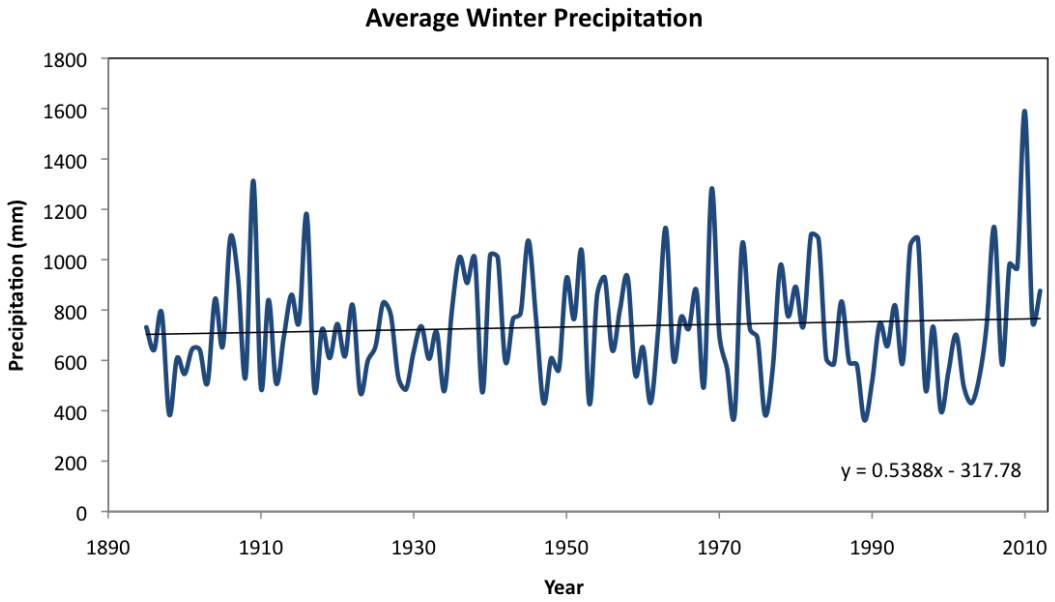

B)

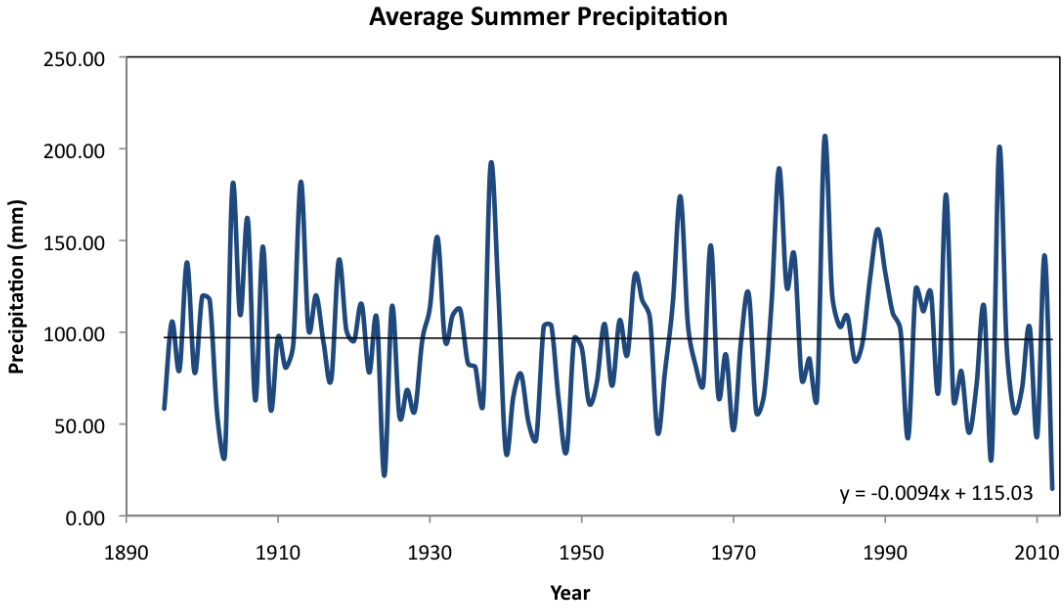

Figure 6. PRISM's winter (A) and summer (B) precipitation for the Goethe cirque from 1985 to 2012. Average winter precipitation is calculated from October to April for each year, and summer precipitation is calculated from May to September.

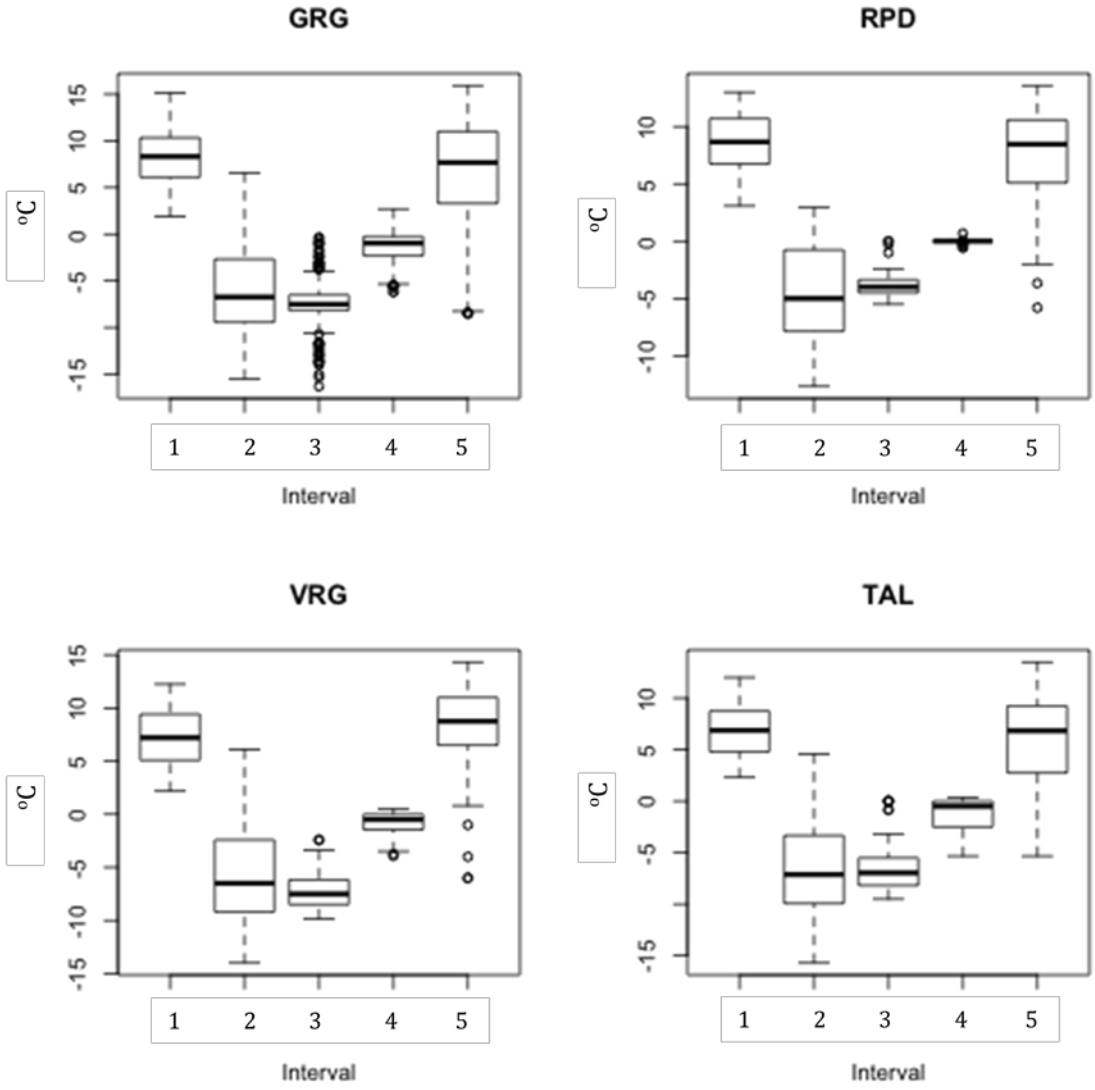

Figure 7. Box plots of surface temperature intervals at each landform. Seasonal intervals were determined based on similar temperature fluctuations and magnitudes (See figures 9-20 for individual Interval parameters).

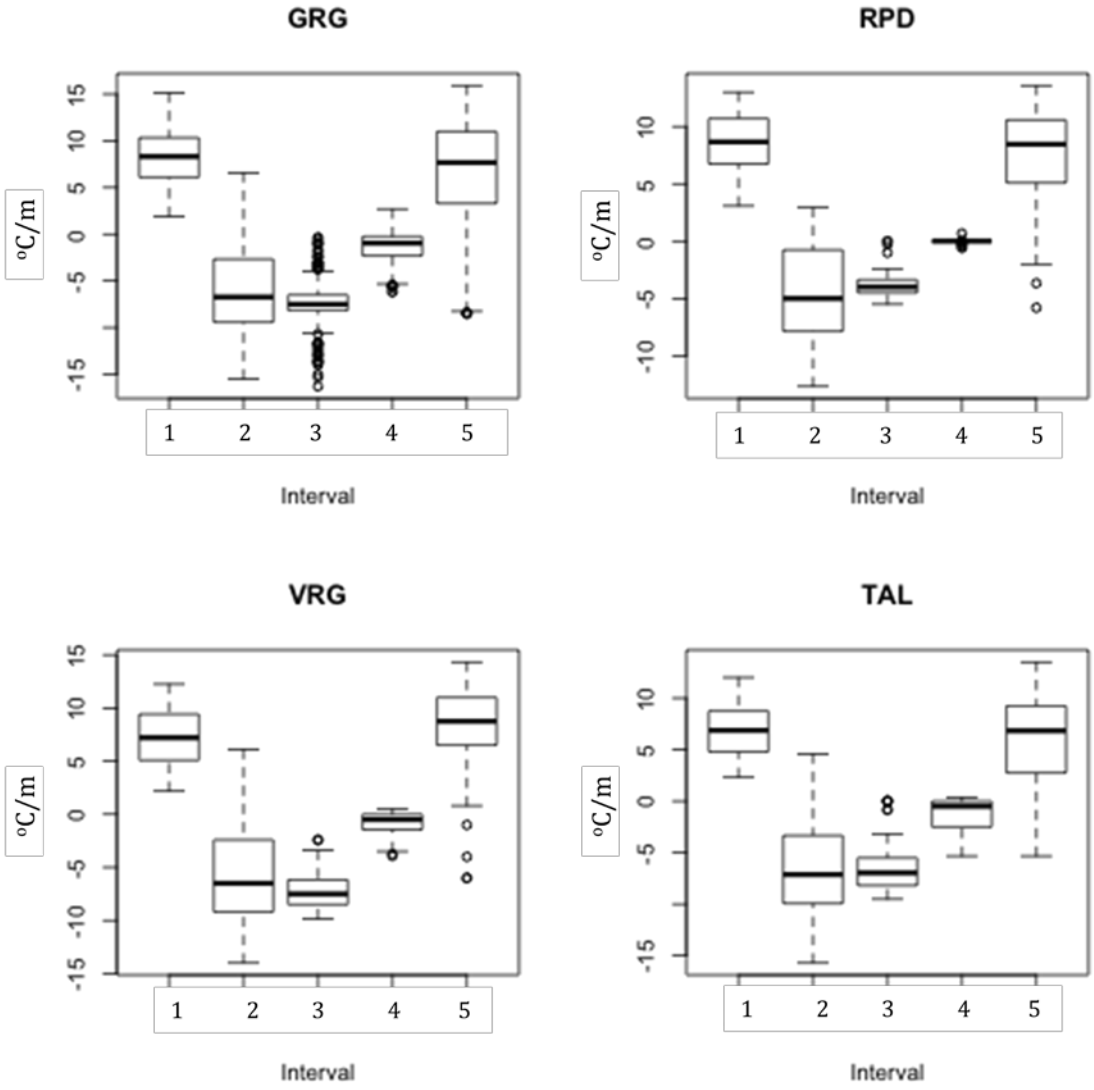

Figure 8. Box plots of temperature gradients (°C/m) within the rock debris of each landform for each interval. Seasonal intervals were determined based on similar temperature fluctuations and magnitudes (See figures 9-20 for individual interval parameters). Gradient intervals are the same as each corresponding surface temperature interval.

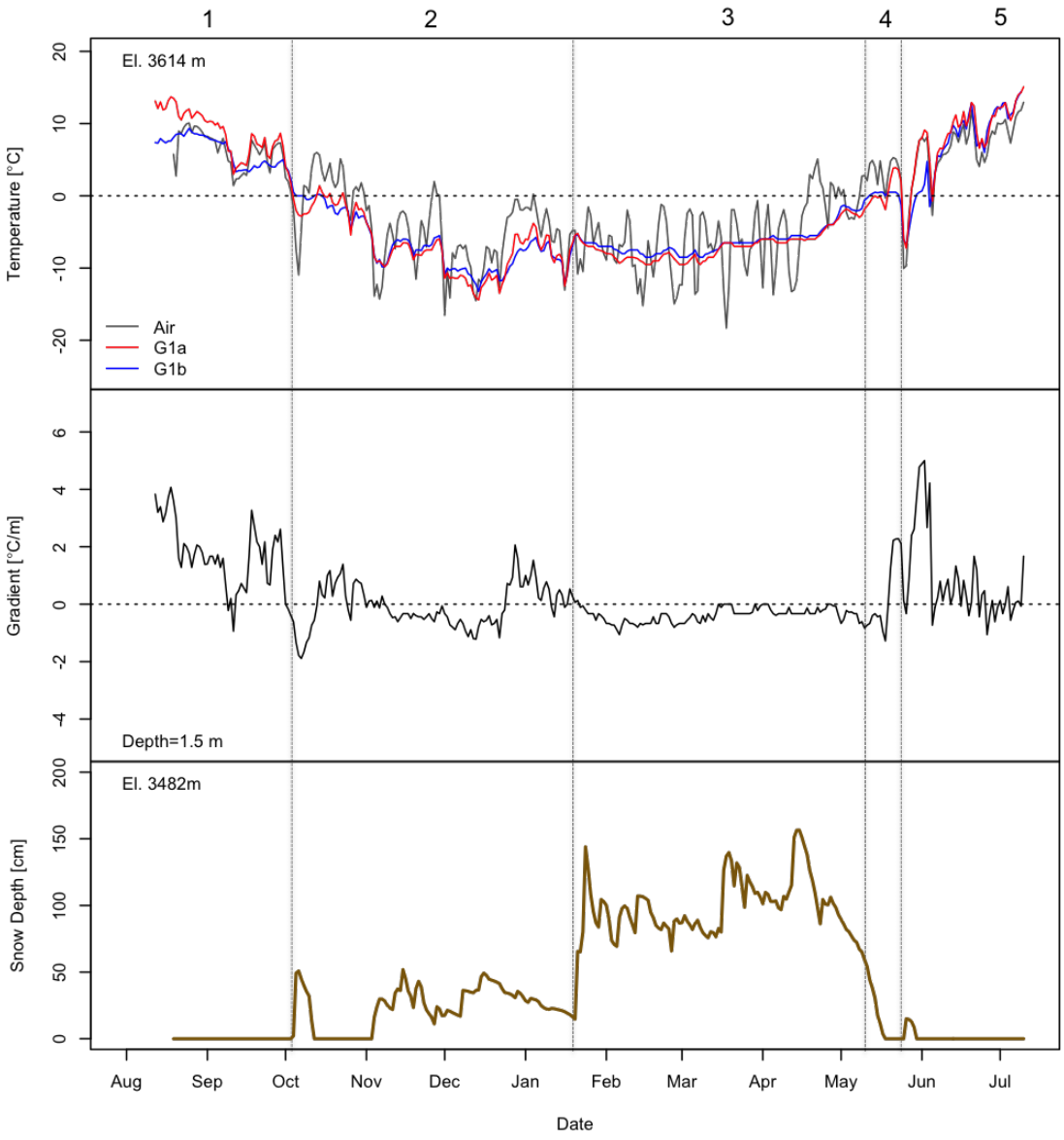

Figure 9. Daily average temperature for logger site G1 for August 12, 2010 - July 11, 2011. Logger G1a (red) is at the surface of the debris at an elevation of 3614 m, and logger G1b (blue) is at a depth of 1.5 m. Interval numbers are shown at the top. The snow depth record is from the Bishop Pass weather station at 3482 m in elevation.

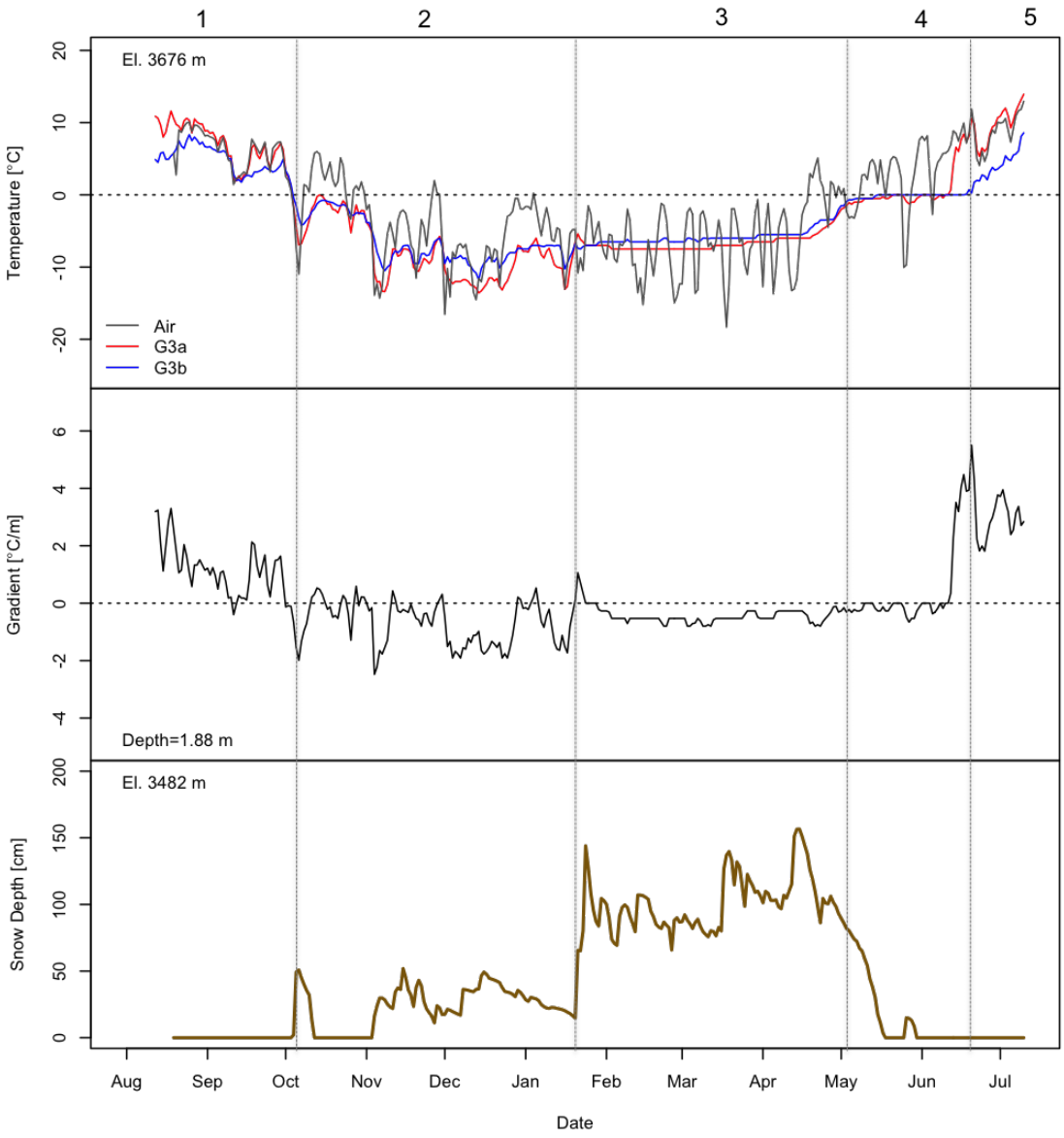

Figure 10. Daily average temperature for logger site G3 for August 12, 2010 - July 11, 2011. Logger G3a (red) is at the surface of the debris at an elevation of 3676 m, and logger G3b (blue) is at a depth of 1.88 m. Interval numbers are shown at the top. The snow depth record is from the Bishop Pass weather station at 3482 m in elevation.

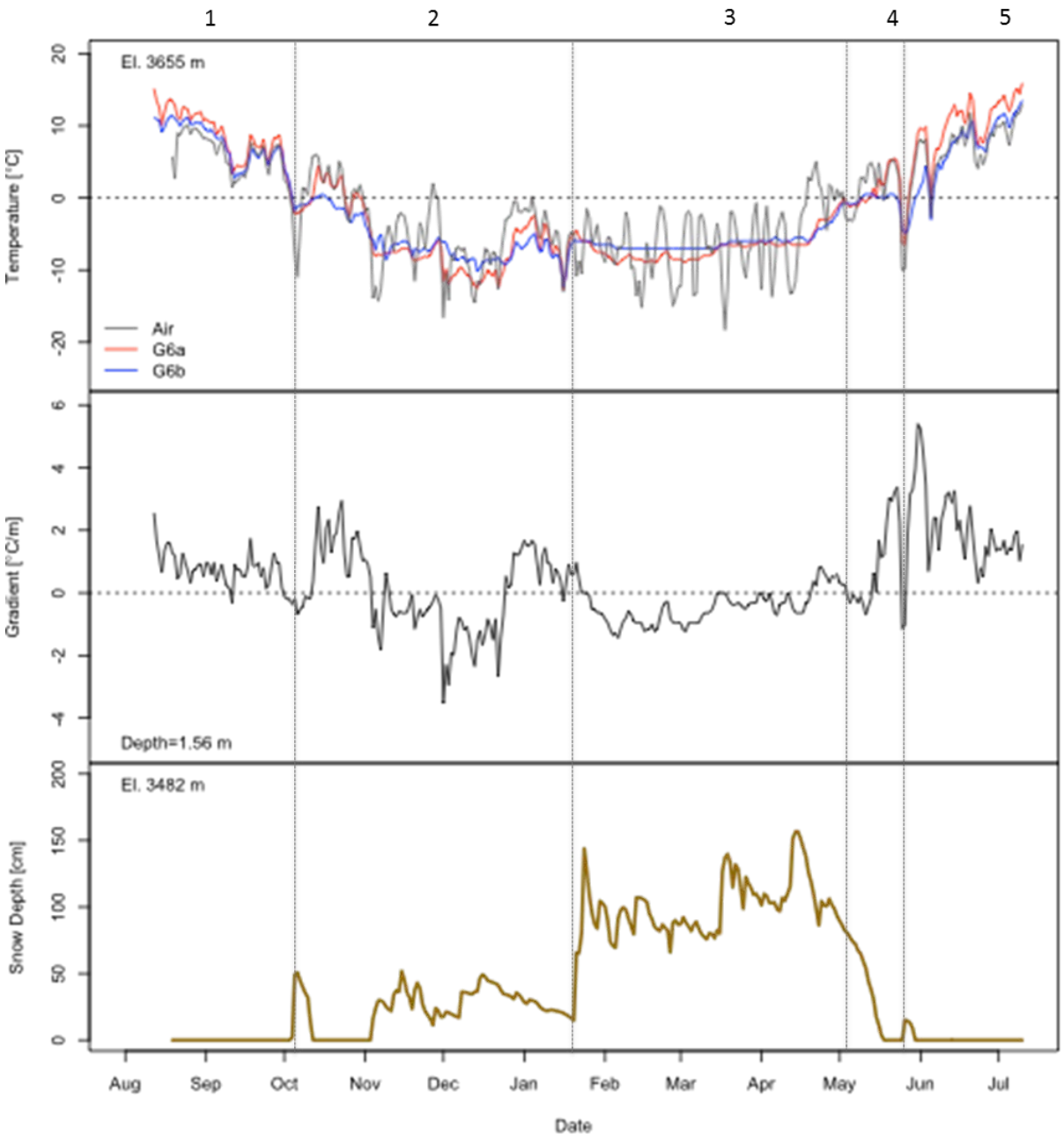

Figure 11. Daily average temperature for logger site G6 for August 12, 2010 - July 11, 2011. Logger G6a (red) is at the surface of the debris at an elevation of 3655 m, and logger G6b (blue) is at a depth of 1.56 m. Interval numbers are shown at the top. The snow depth record is from the Bishop Pass weather station at 3482 m in elevation.

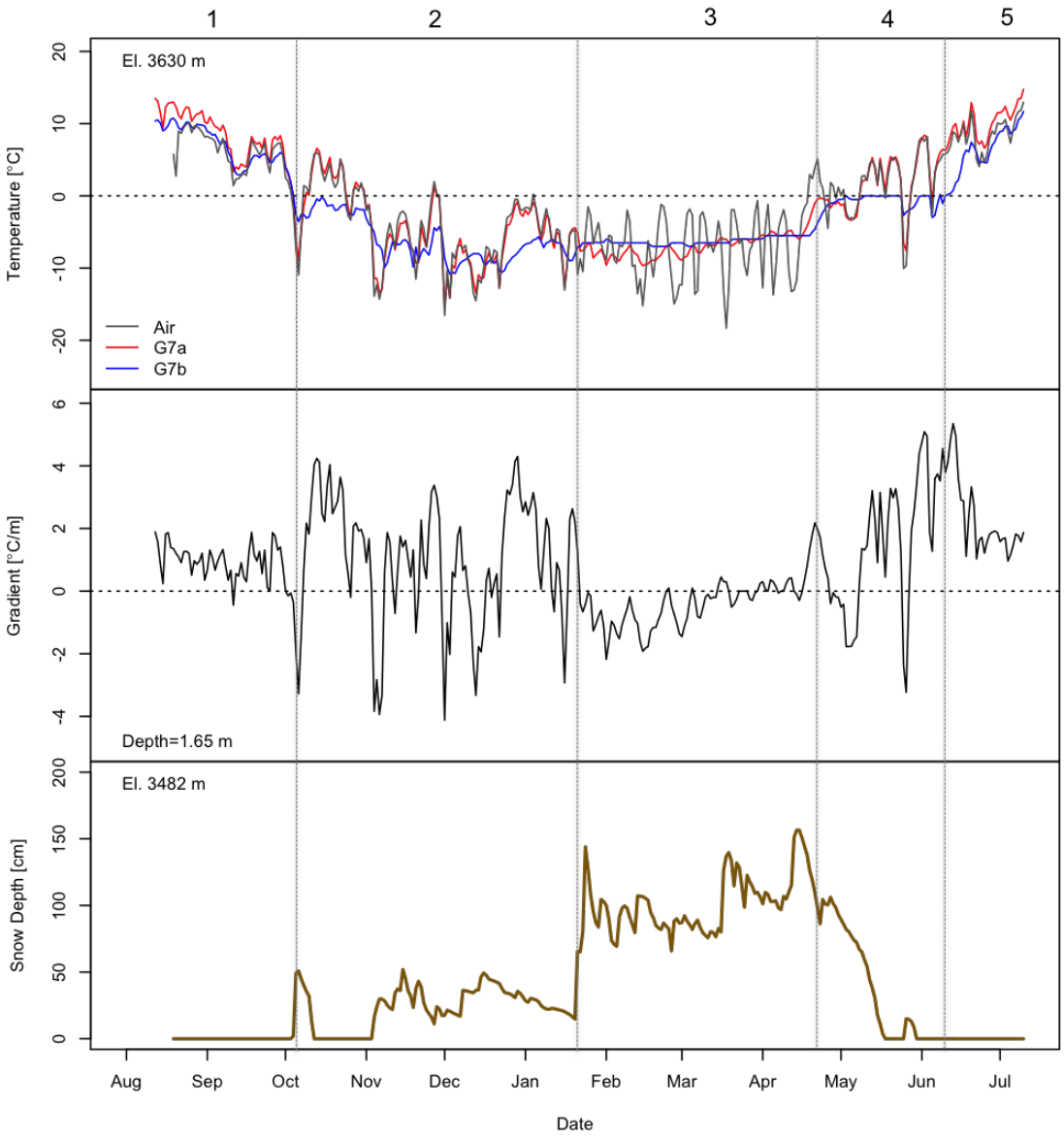

Figure 12. Daily average temperature for logger site G7 for August 12, 2010 - July 11, 2011. Logger G7a (red) is at the surface of the debris at an elevation of 3630 m, and logger G7b (blue) is at a depth of 1.65 m. Interval numbers are shown at the top. The snow depth record is from the Bishop Pass weather station at 3482 m in elevation.

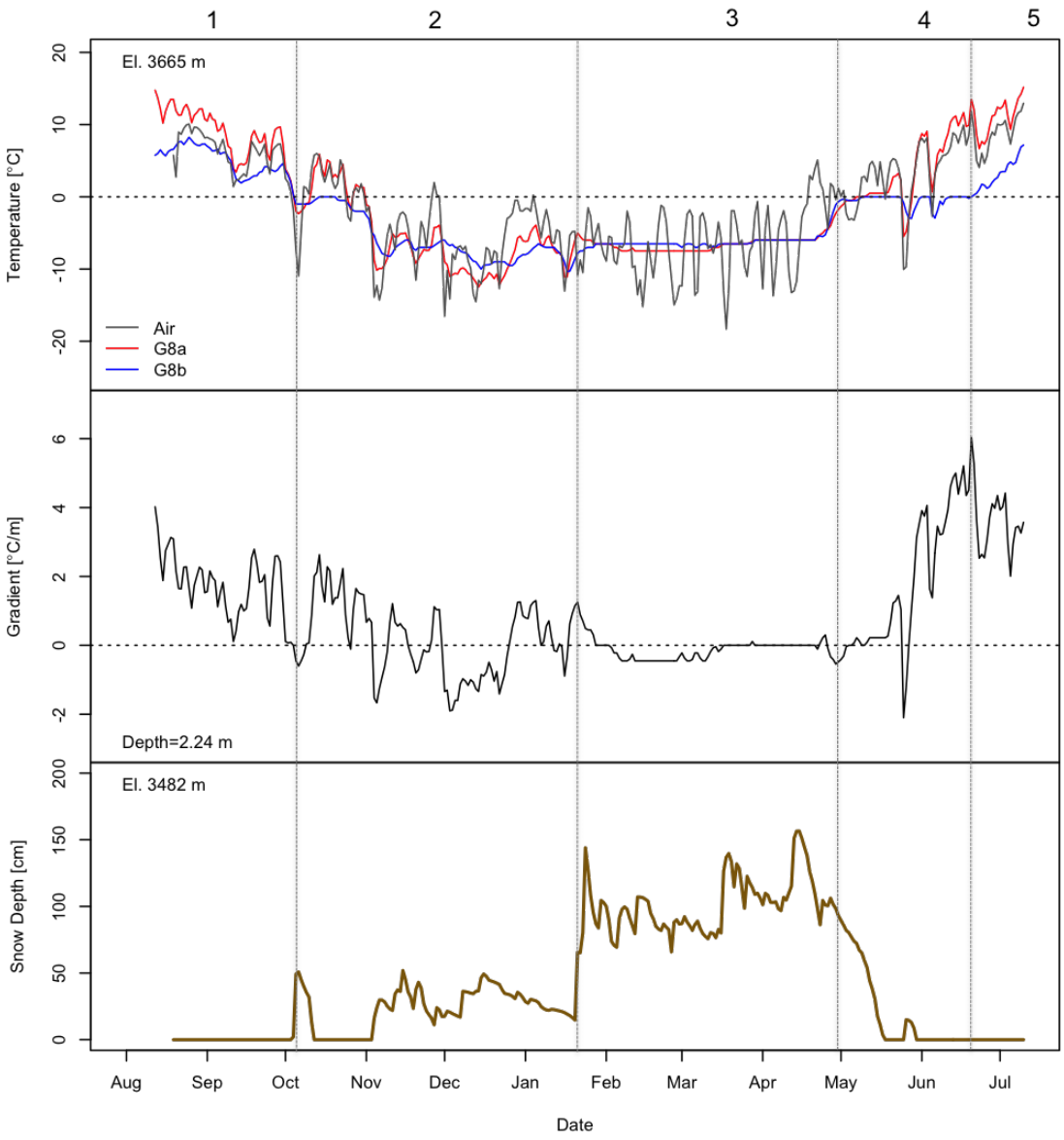

Figure 13. Daily average temperature for logger site G8 for August 12, 2010 - July 11, 2011. Logger G8a (red) is at the surface of the debris at an elevation of 3665 m, and logger G8b (blue) is at a depth of 2.24 m. Interval numbers are shown at the top. The snow depth record is from the Bishop Pass weather station at 3482 m in elevation.

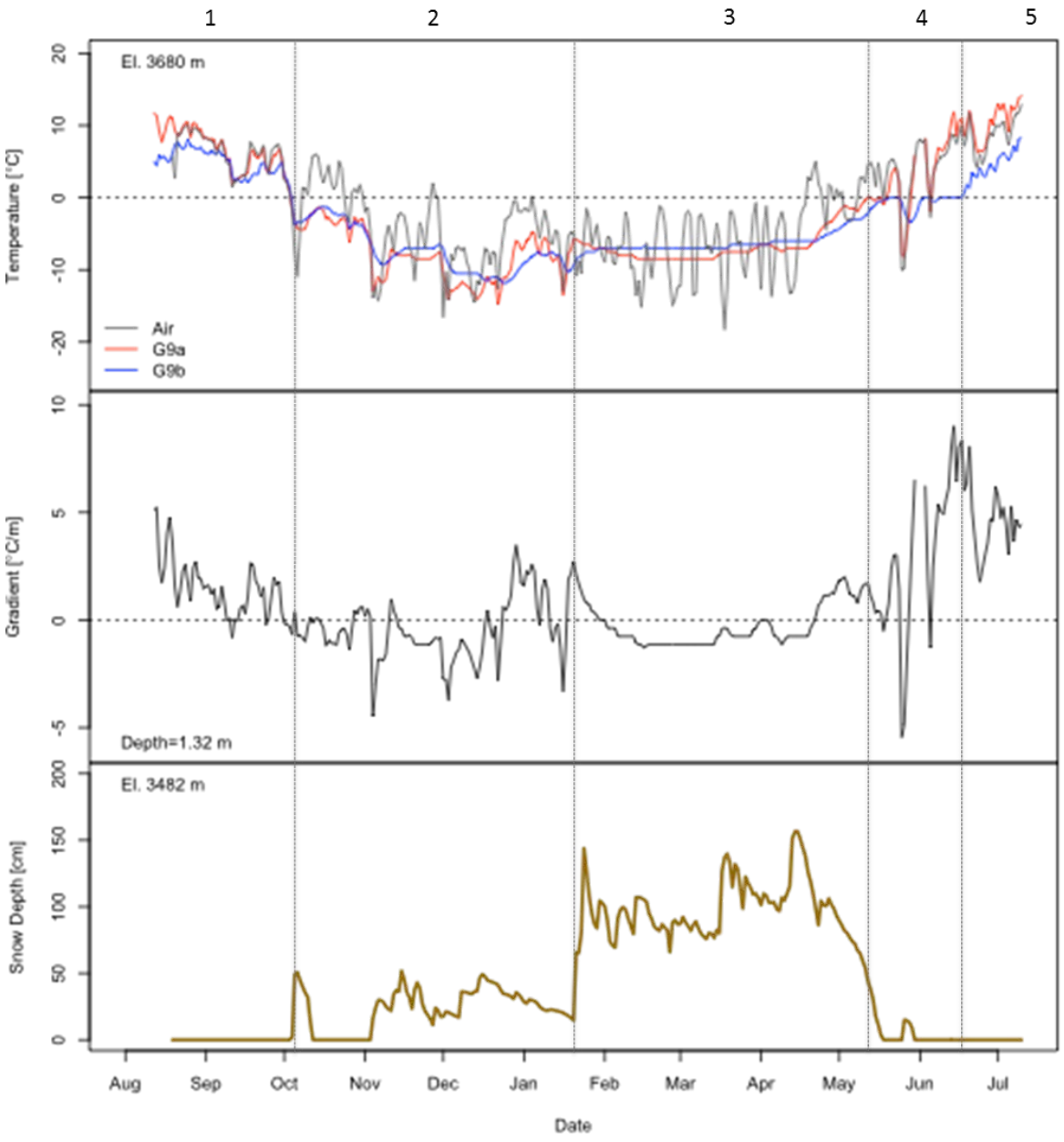

Figure 14. Daily average temperature for logger site G9 for August 12, 2010 - July 11, 2011. Logger G9a (red) is at the surface of the debris at an elevation of 3680 m, and logger G9b (blue) is at a depth of 1.32 m. Interval numbers are shown at the top. The snow depth record is from the Bishop Pass weather station at 3482 m in elevation.

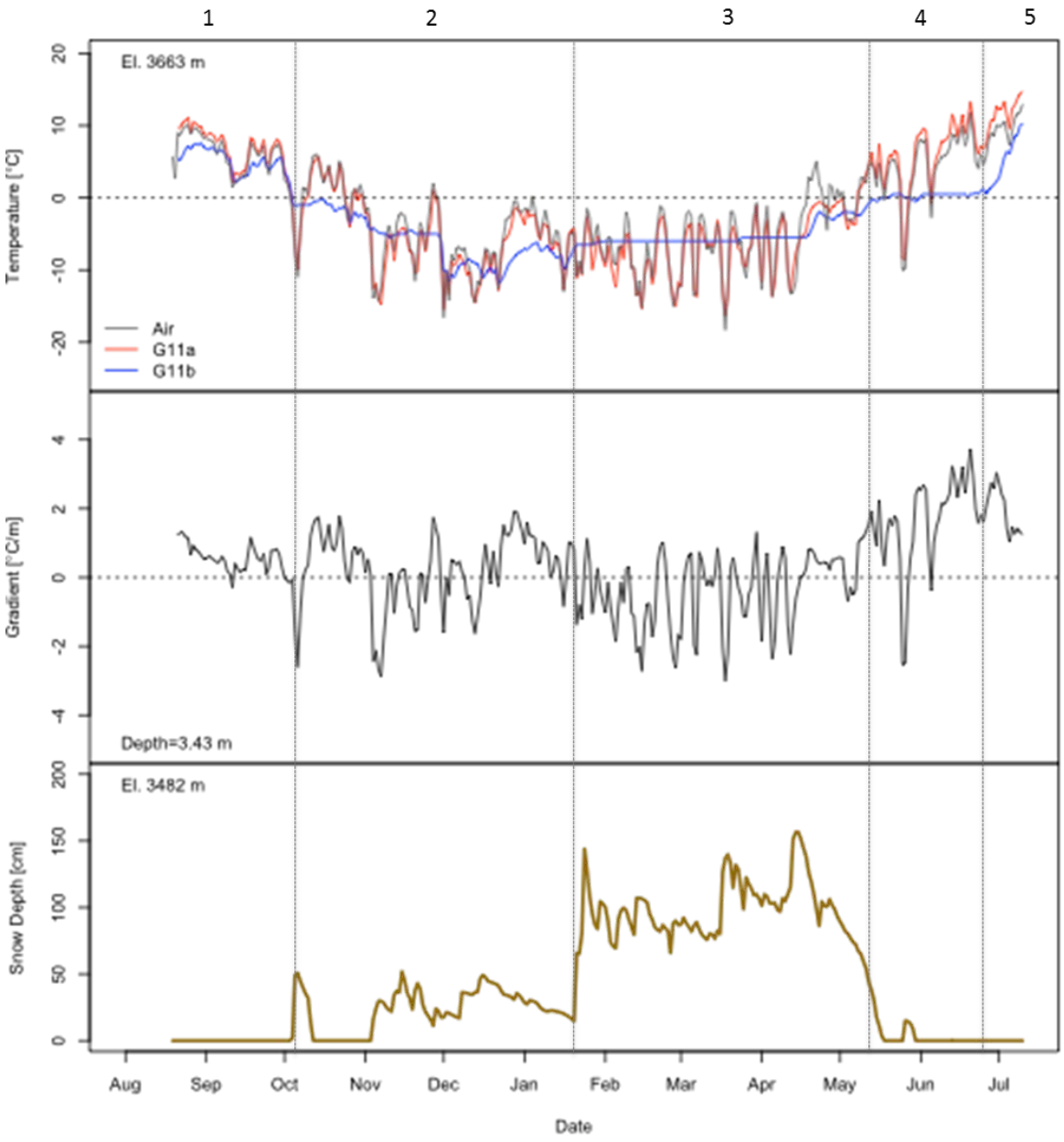

Figure 15. Daily average temperature for logger site G11 for August 12, 2010 - July 11, 2011. Logger G11a (red) is at the surface of the debris at an elevation of 3663 m, and logger G11b (blue) is at a depth of 3.43 m. Interval numbers are shown at the top. The snow depth record is from the Bishop Pass weather station at 3482 m in elevation.

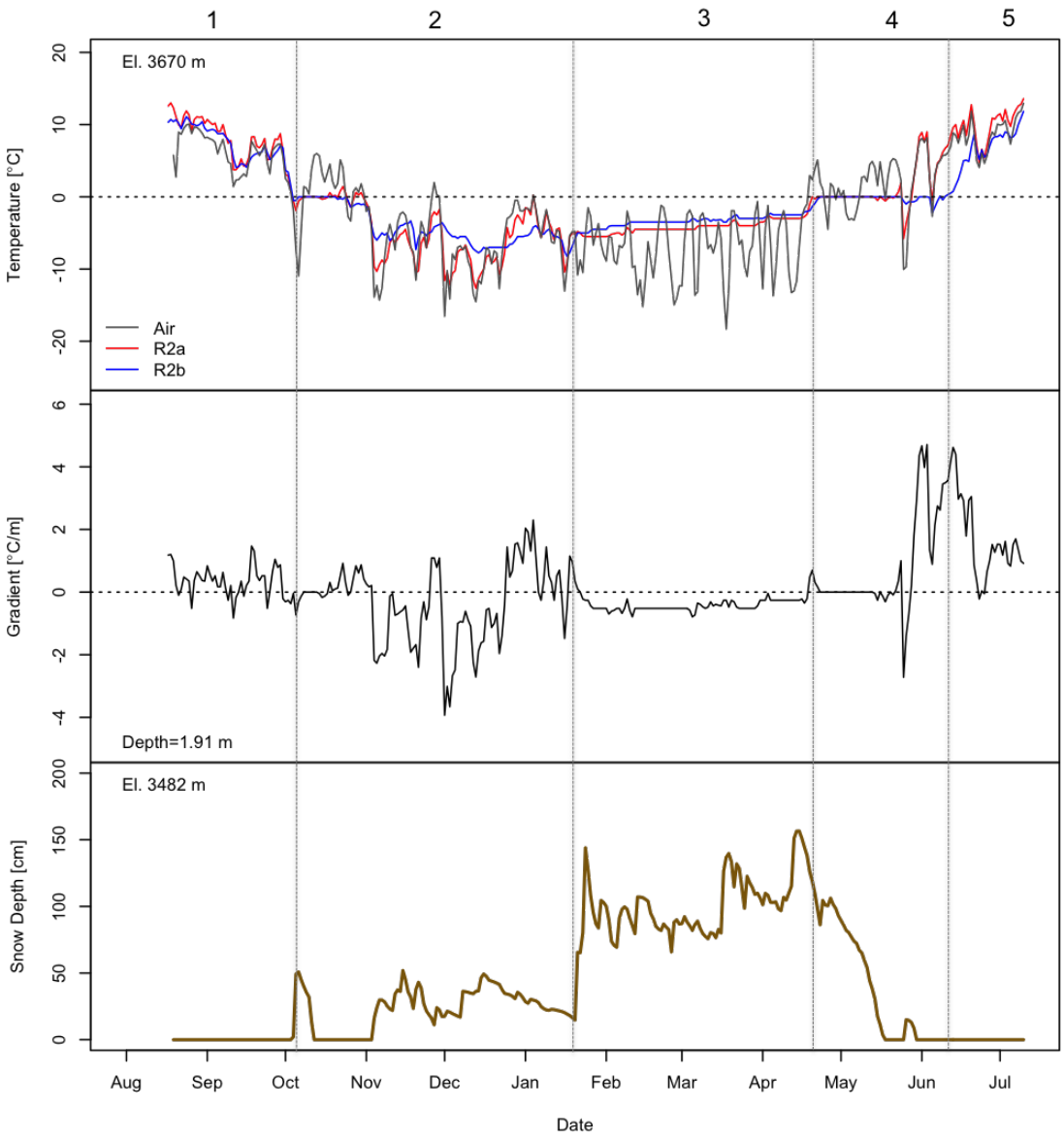

Figure 16. Daily average temperature for logger site R2 for August 12, 2010 - July 11, 2011. Logger R2a (red) is at the surface of the debris at an elevation of 3670 m, and logger R2b (blue) is at a depth of 1.91 m. Interval numbers are shown at the top. The snow depth record is from the Bishop Pass weather station at 3482 m in elevation.

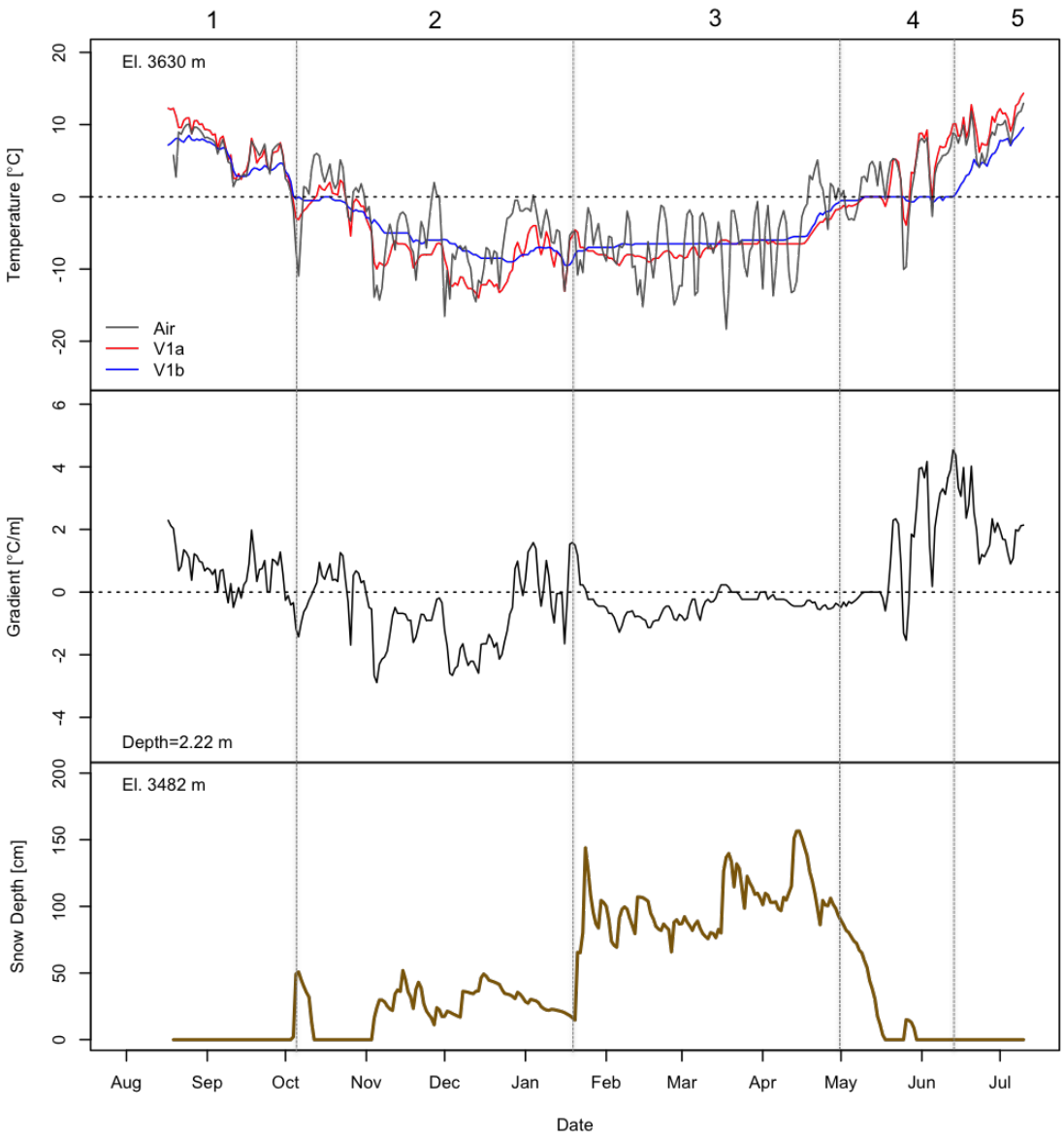

Figure 17. Daily average temperature for logger site V1 for August 12, 2010 - July 11, 2011. Logger V1a (red) is at the surface of the debris at an elevation of 3630 m, and logger V1b (blue) is at a depth of 2.22 m. Interval numbers are shown at the top. The snow depth record is from the Bishop Pass weather station at 3482 m in elevation.

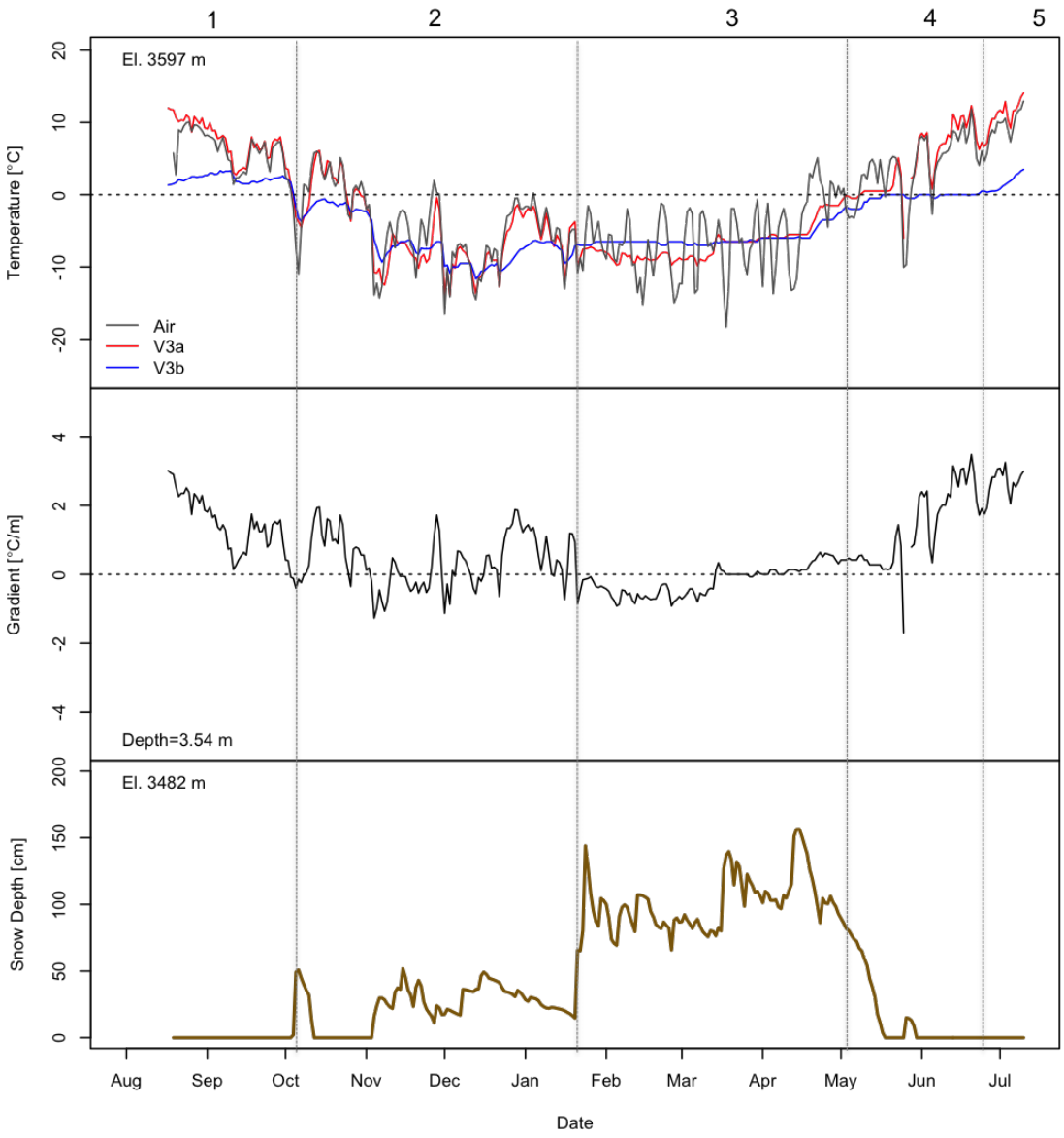

Figure 18. Daily average temperature for logger site V3 for August 12, 2010 - July 11, 2011. Logger V3a (red) is at the surface of the debris at an elevation of 3597 m, and logger V3b (blue) is at a depth of 3.54 m. Interval numbers are shown at the top. The snow depth record is from the Bishop Pass weather station at 3482 m in elevation.

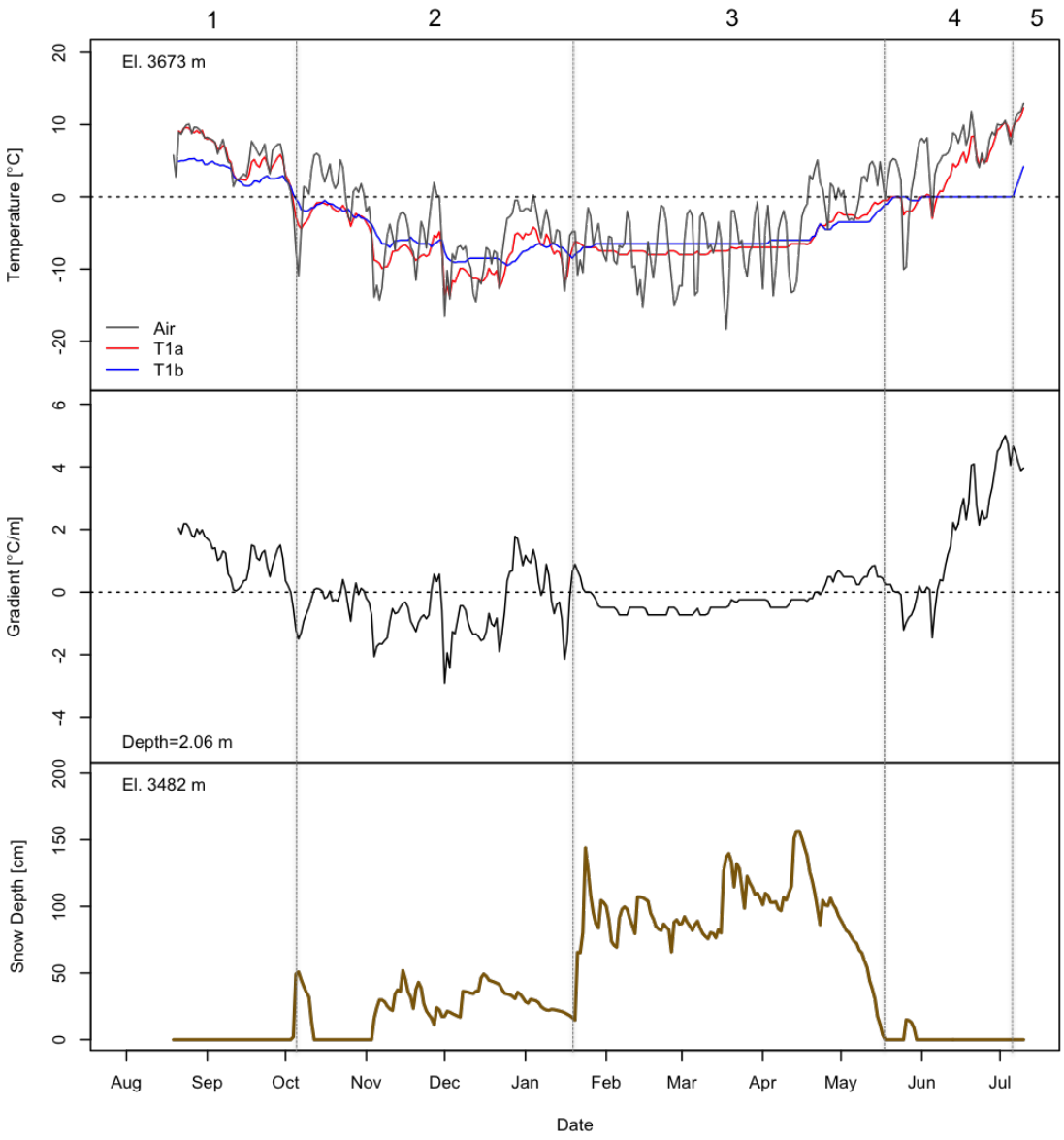

Figure 19. Daily average temperature for logger site T1 for August 12, 2010 - July 11, 2011. Logger T1a (red) is at the surface of the debris at an elevation of 3673 m, and logger T1b (blue) is at a depth of 2.06 m. Interval numbers are shown at the top. The snow depth record is from the Bishop Pass weather station at 3482 m in elevation.

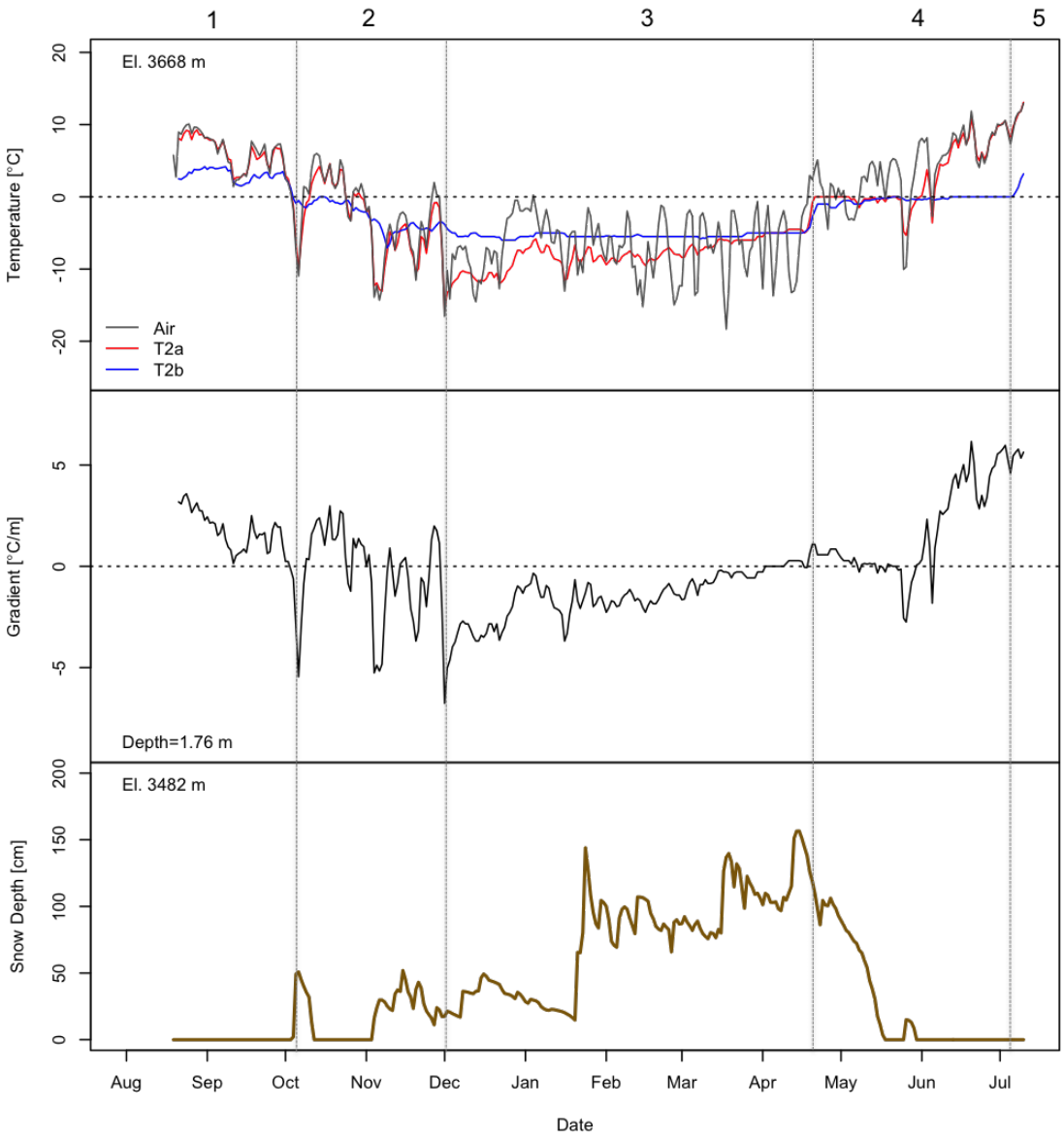

Figure 20. Daily average temperature for logger site T2 for August 12, 2010 - July 11, 2011. Logger T2a (red) is at the surface of the debris at an elevation of 3668 m, and logger T2b (blue) is at a depth of 1.76 m. Interval numbers are shown at the top. The snow depth record is from the Bishop Pass weather station at 3482 m in elevation.

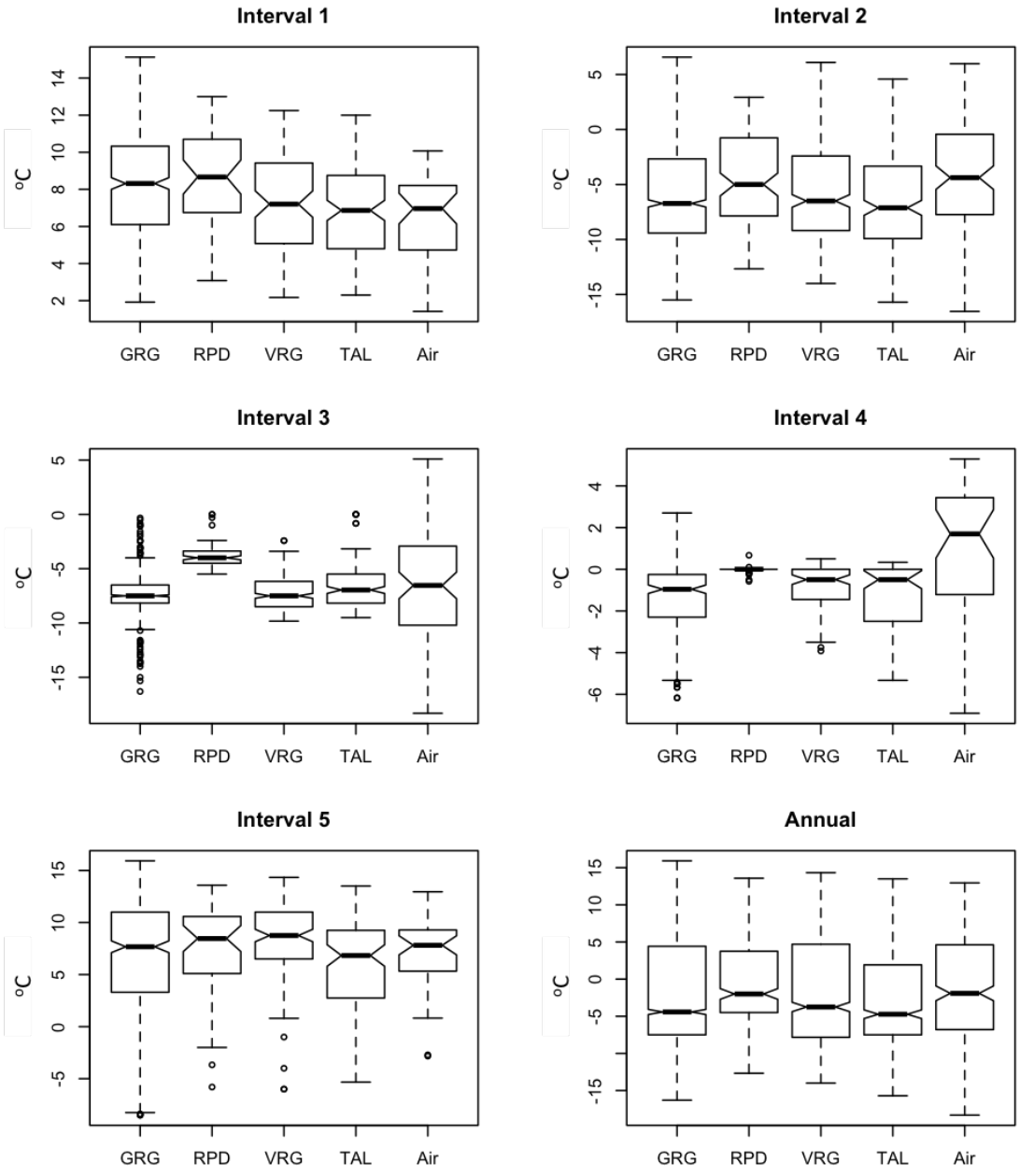

Figure 21. Box plots of surface temperature at each landform for each seasonal interval. Box plots are a visualization of descriptive statistics where the upper bracket represents the maximum value, the lower bracket is the minimum value, the top of the 'box' is the 3rd quartile, the bottom of the 'box' is the 1st quartile, and the middle bar is the median. Any points outside the bracket are outliers. The width of the notches in the box is inversely proportional to sample size. If any two notches do not overlap, this implies a statistically significant difference between the medians of the two populations.

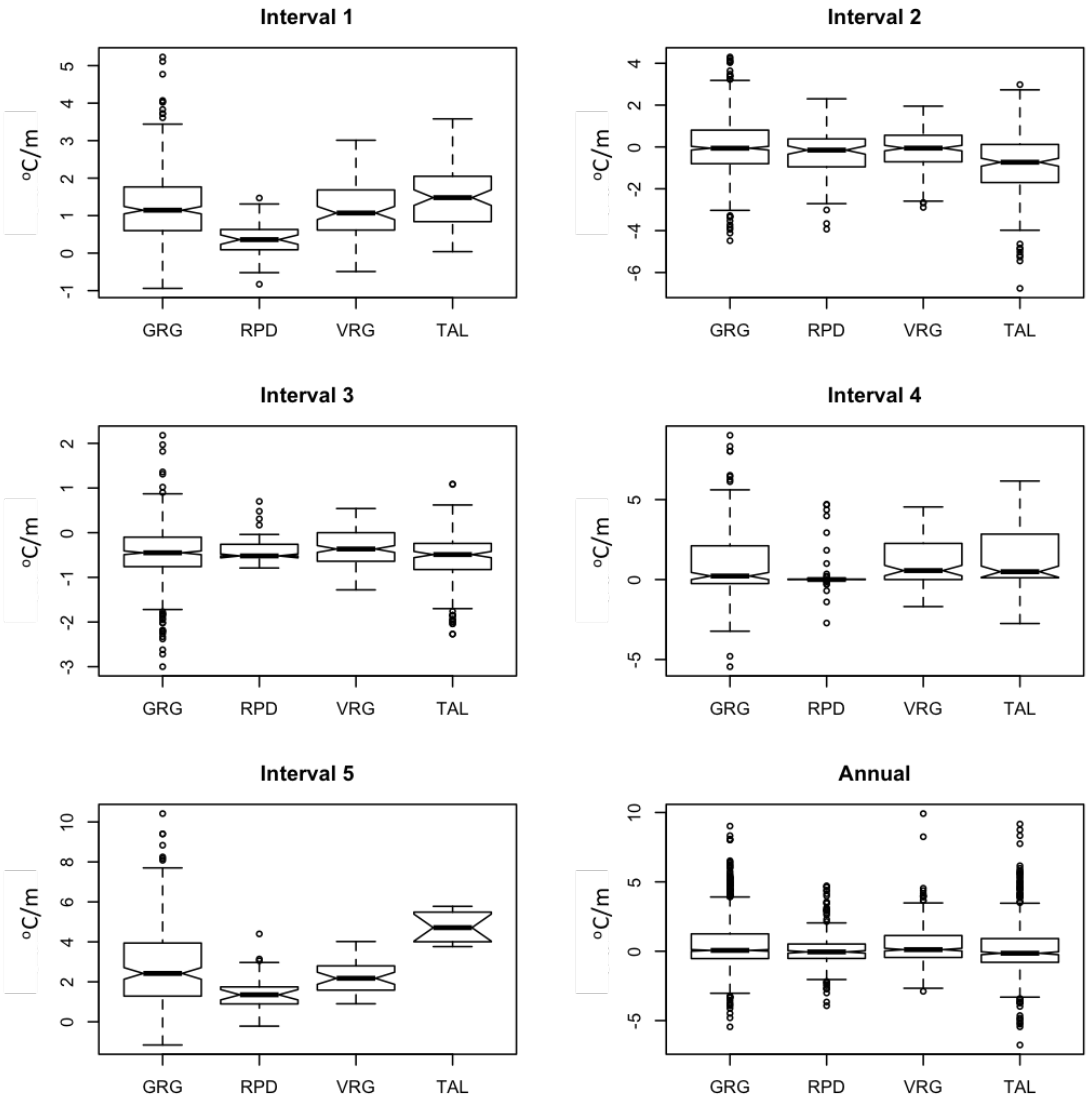

Figure 22. Box plots of the subsurface temperature gradient at each landform for each seasonal interval. Box plots are a visualization of descriptive statistics where the upper bracket represents the maximum value, the lower bracket is the minimum value, the top of the 'box' is the 3rd quartile, the bottom of the 'box' is the 1st quartile, and the middle bar is the median. Any points outside the bracket are outliers. The width of the notches in the box is inversely proportional to sample size. If any two notches do not overlap, this implies a statistically significant difference between the medians of the two populations.

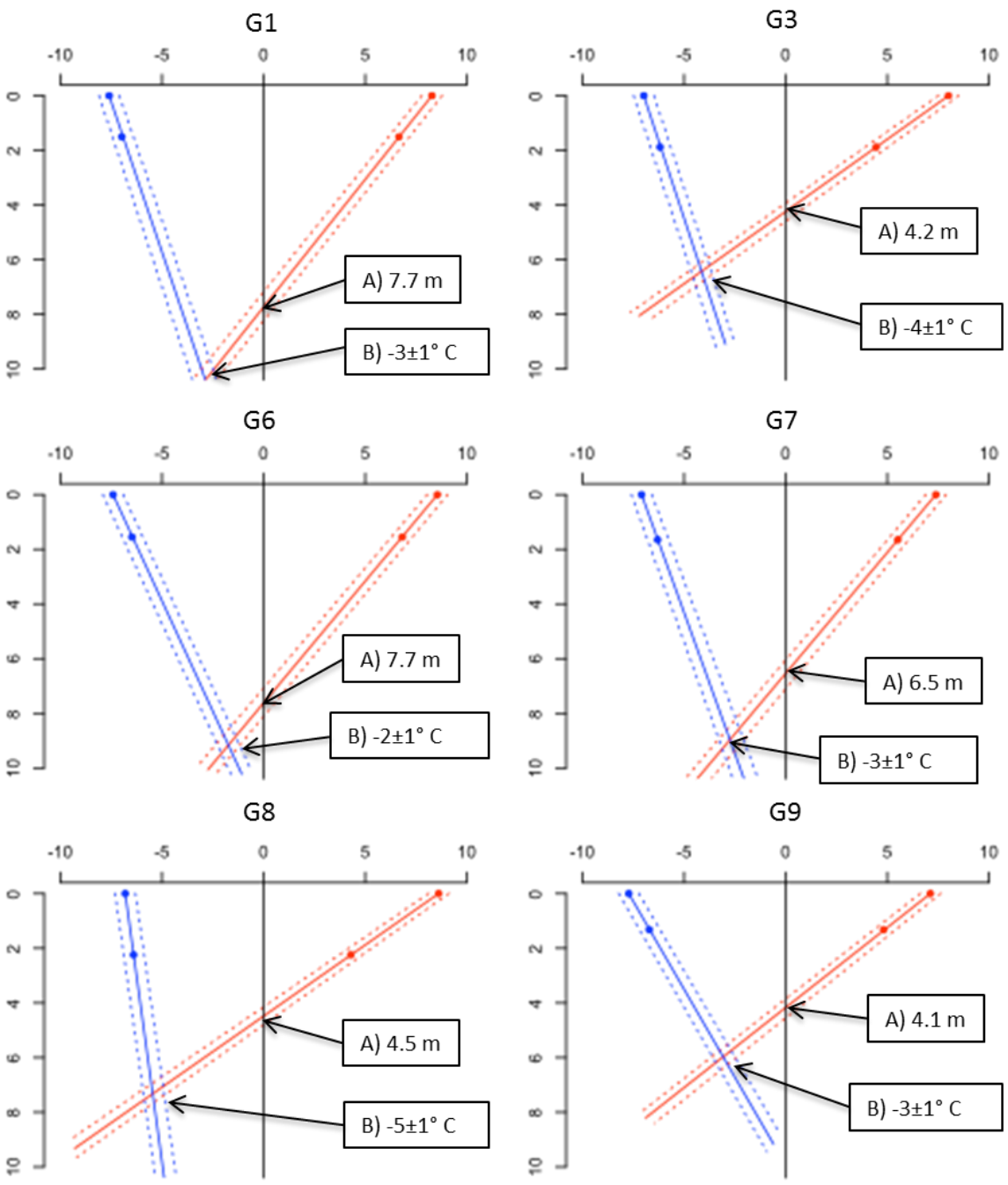

Figure 23. Projected ground thermal profiles at logger sites G1-G9. The y-axis is depth (meters) below the surface logger at each respective site, and the x-axis is temperature (°C). Where the summer profile (red) intersects the 0°C isotherm indicates the depth at which ice can exist in the debris (A). Where the summer and winter profiles intersect each other indicates the average annual ground temperature (B).

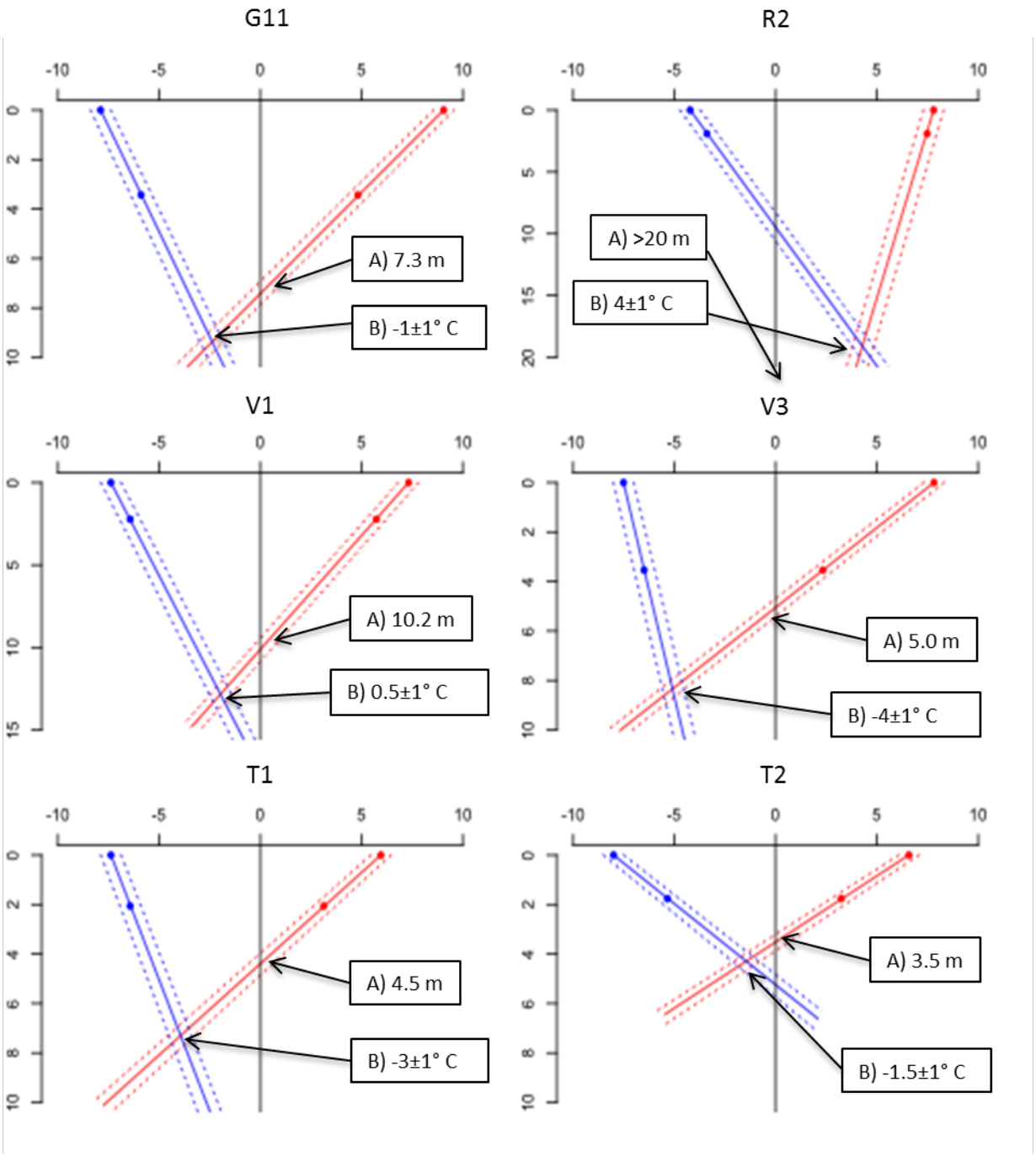

Figure 24. Projected ground thermal profiles at logger sites G11-T2. The y-axis is depth (meters) below the surface logger at each respective site, and the x-axis is temperature (°C). Where the summer profile (red) intersects the 0°C isotherm indicates the depth at which ice can exist in the debris (A). Where the summer and winter profiles intersect each other indicates the average annual ground temperature (B).

A)

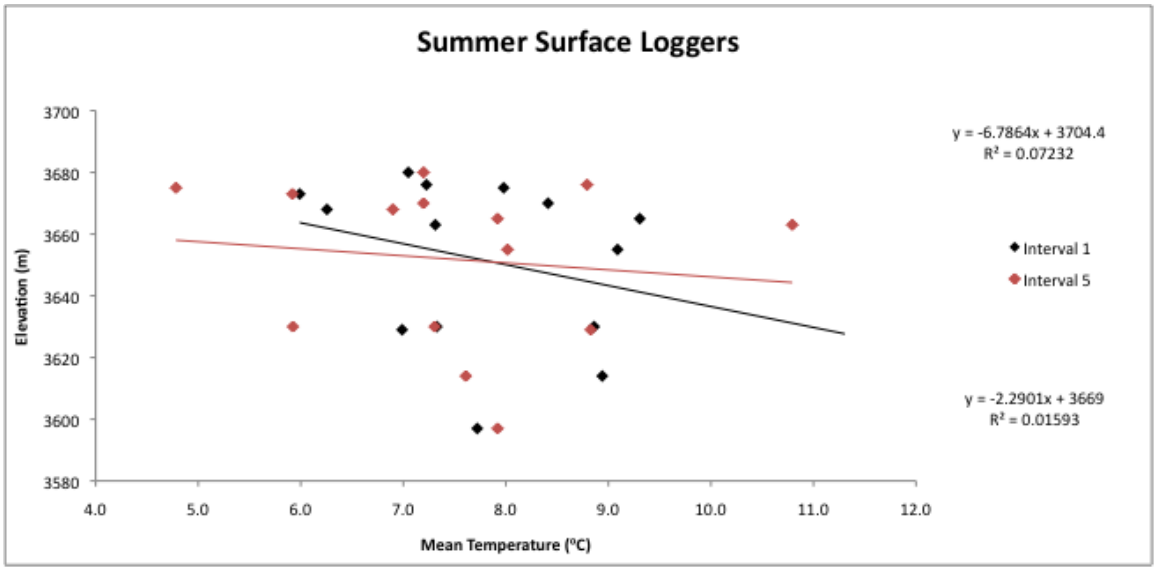

B)

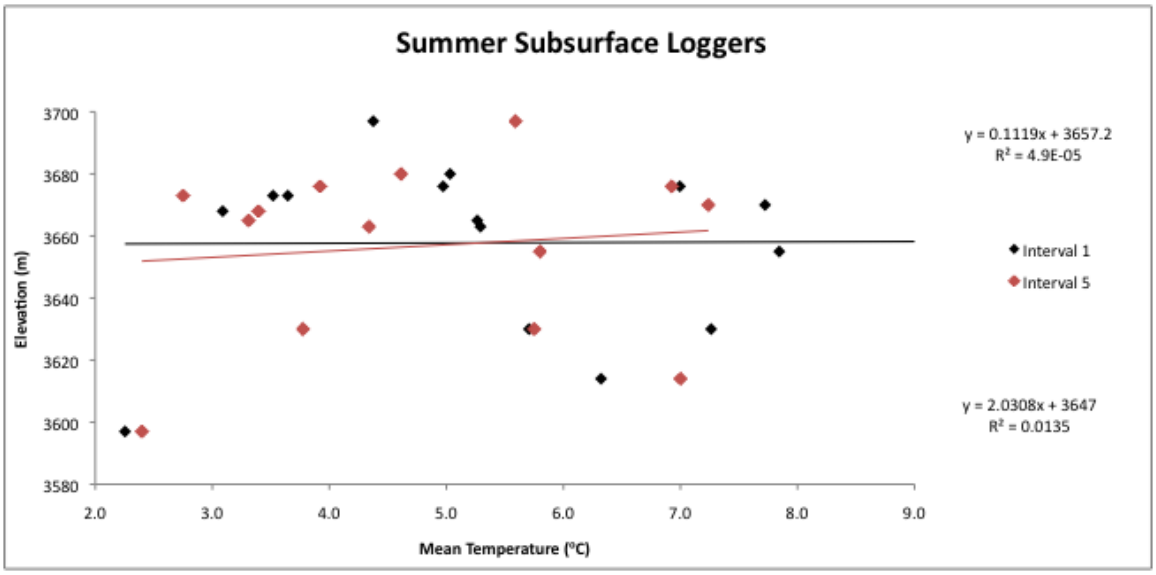

Figure 25. Regressions between surface (A) and subsurface (B) temperatures of all landforms in the cirque and elevation for the summer (Intervals 1 and 5). Equations of trendlines and R^2 values are shown, with the top relating to Interval 1, and the bottom relating to Interval 5.

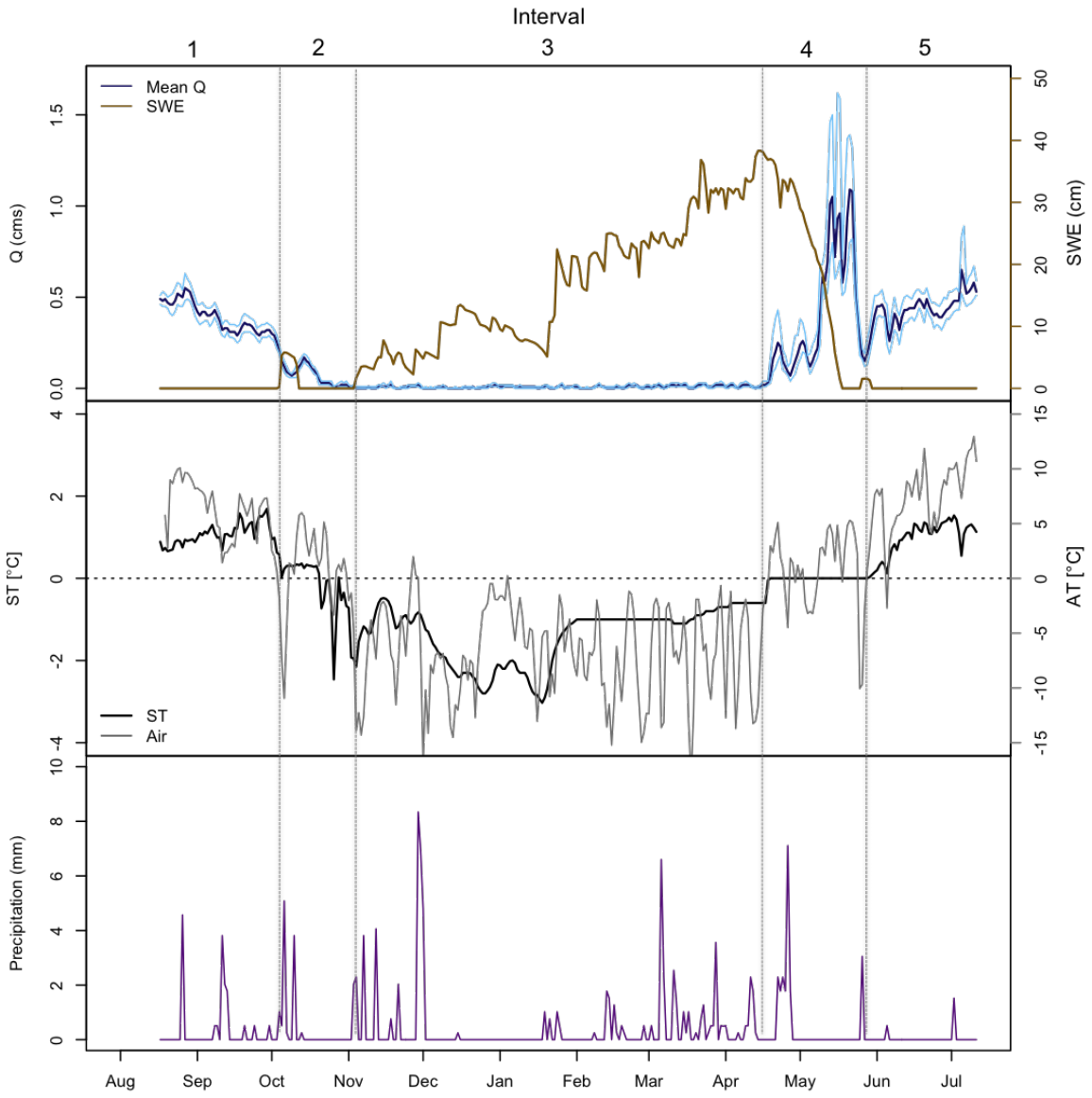

Figure 26. Seasonal intervals for daily mean discharge (Q) and stream temperature (ST) at the Goethe rock glacier outlet stream. Snow water equivalent (SWE) and precipitation records are from the Bishop Pass weather station at 3482 m in elevation. Non-snow precipitation from Goethe (3663 m) is overlaid with Bishop Pass records to show similarities and differences between the weather stations.

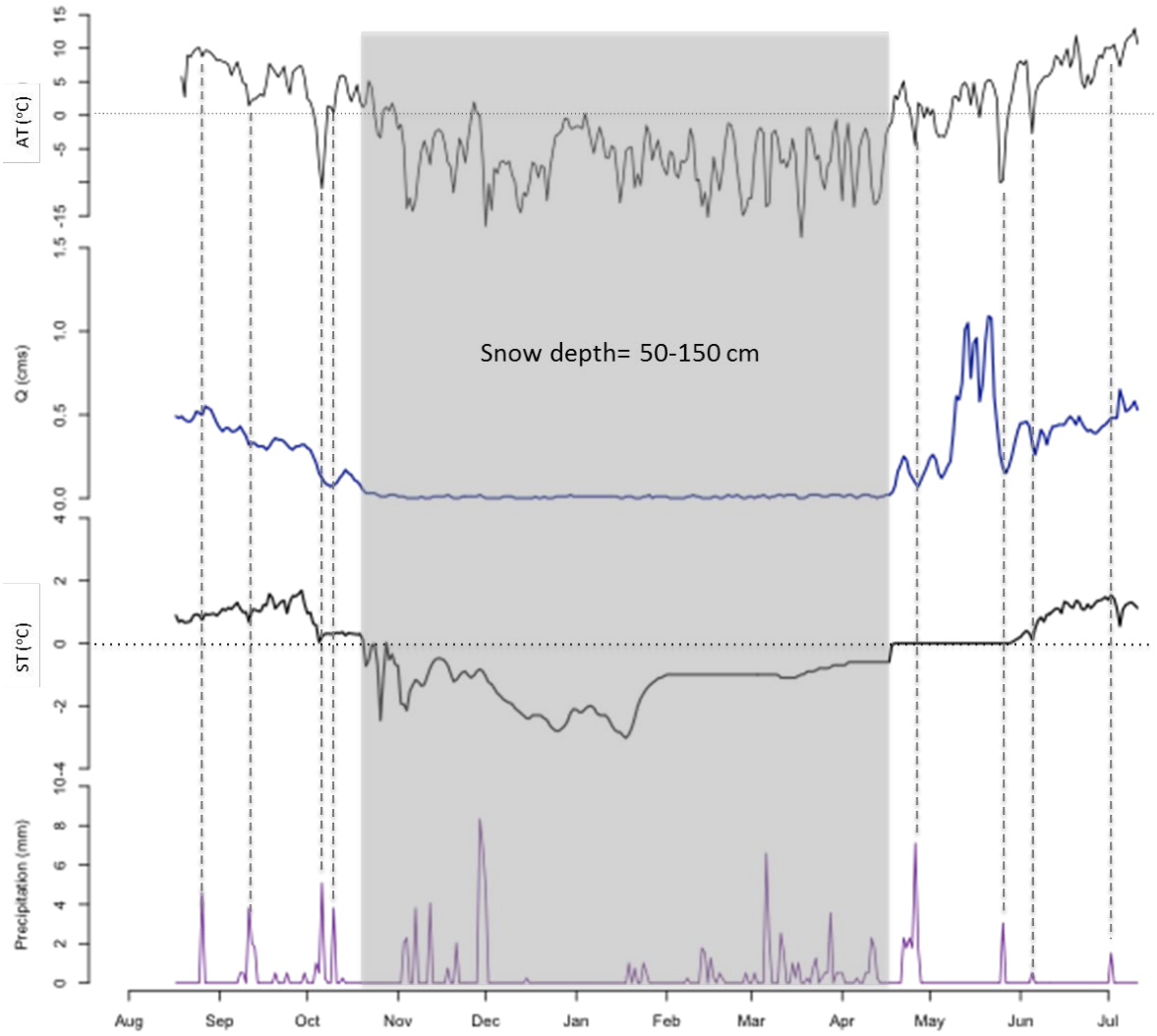

Figure 27. Relationships between average air temperature (AT), discharge (Q), stream temperature (ST), and total precipitation at the Goethe rock glacier outlet stream. Months with snow depth greater than 50 cm is blocked out in grey to indicate when the stream is dry or frozen to the channel bed. Precipitation events directly correspond with decreases in air temperature and stream temperature and lagged increases in discharge by approximately 1-3 days.

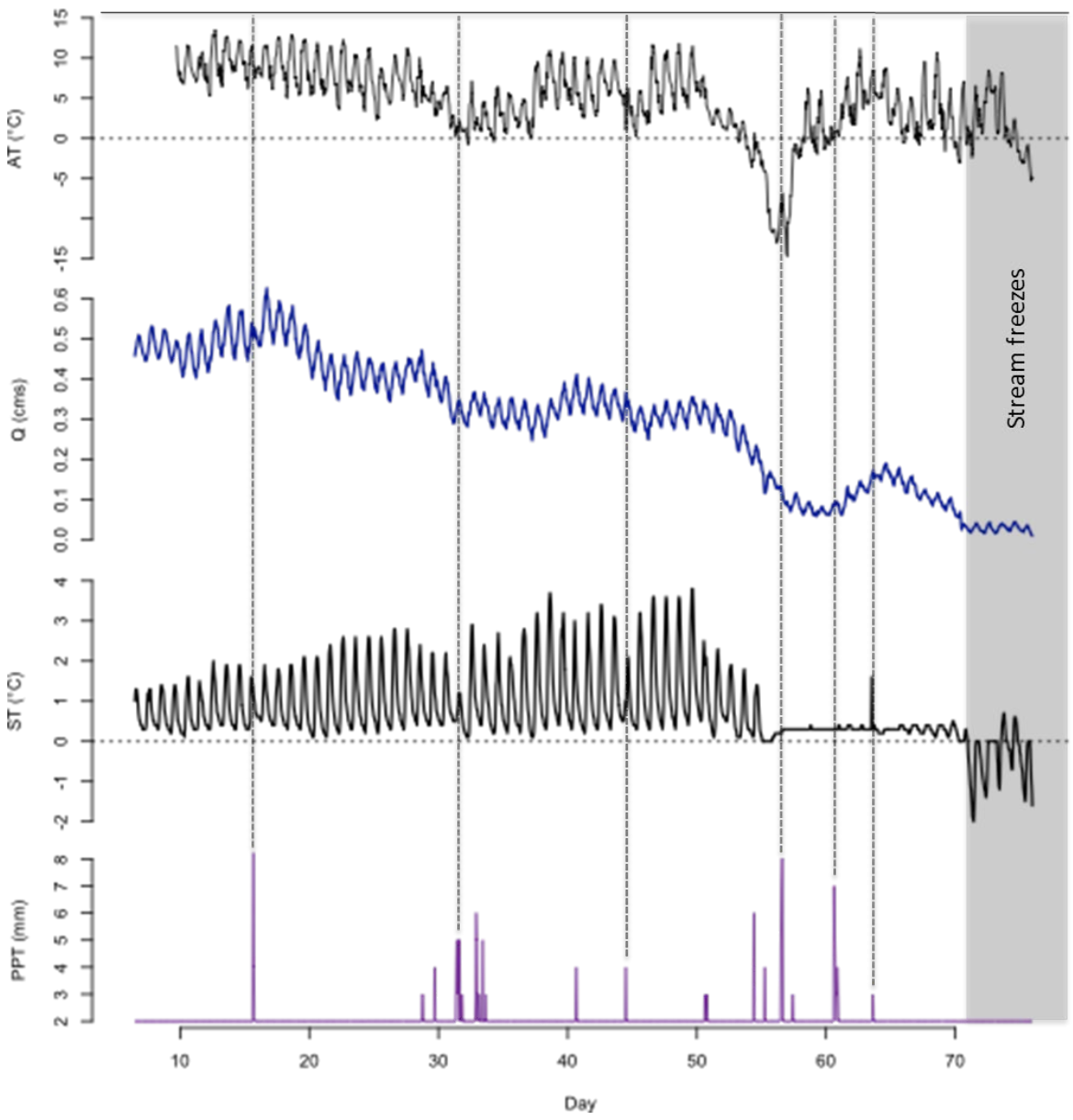

Figure 28. Hourly air temperature (AT), stream discharge (Q), stream temperature (ST), and precipitation (PPT) at the Goethe rock glacier outlet stream from August 17, 2010 to October 31, 2010 (Intervals 1 & 2). Dark purple precipitation events are recorded at Goethe, and pink precipitation events are recorded at Bishop Pass. Each peak in AT, Q, and ST indicates one day. When ST drops below 0°C, it is inferred that the stream is no longer flowing or is frozen to the channel bed.

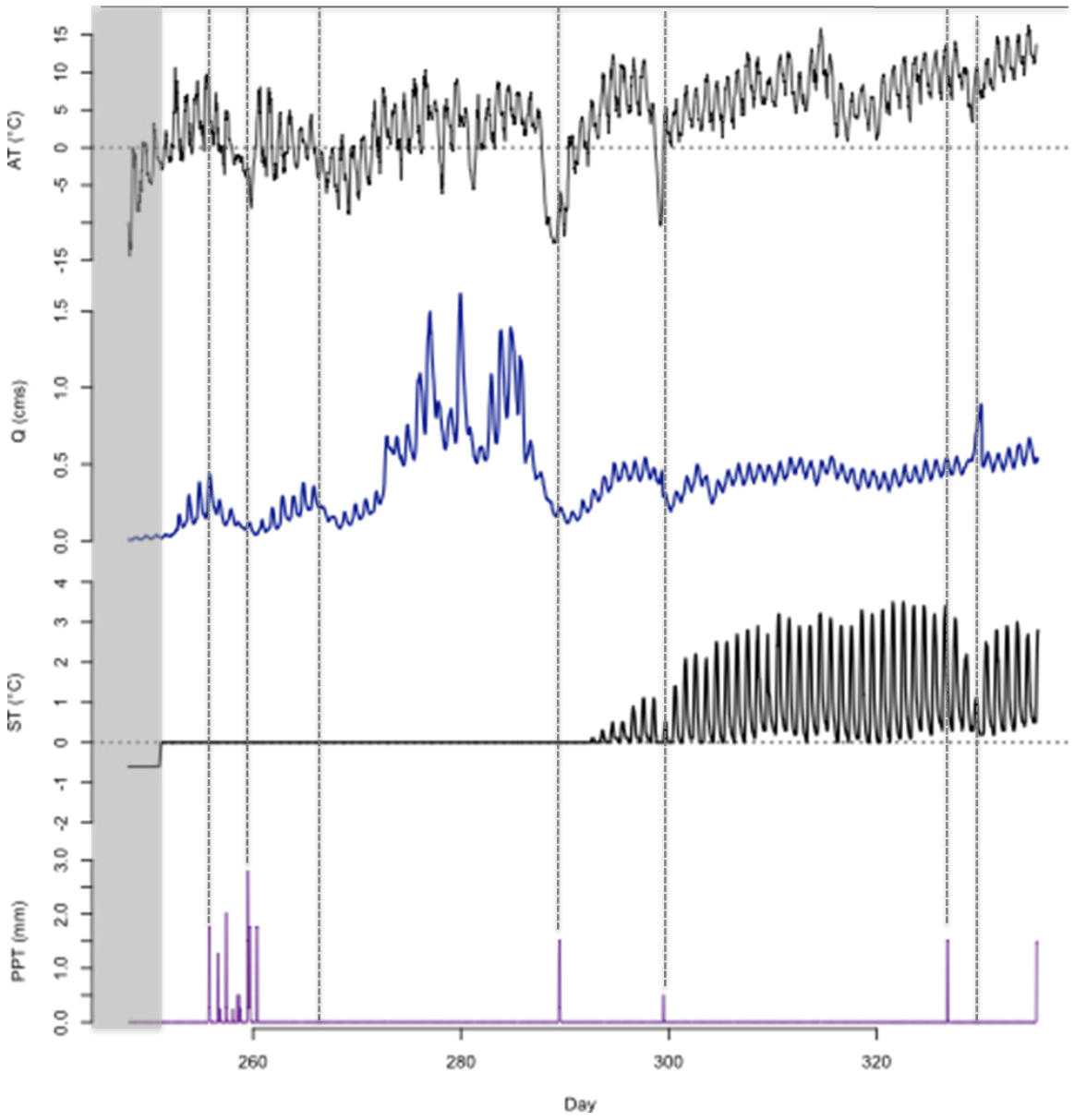

Figure 29. Hourly air temperature (AT), stream discharge (Q), stream temperature (ST), and precipitation (PPT) at the Goethe rock glacier outlet stream from April 15, 2011 to July 11, 2011. Dark purple precipitation events are recorded at Goethe, and pink precipitation events are recorded at Bishop Pass. Each peak in AT, Q, and ST indicates one day.

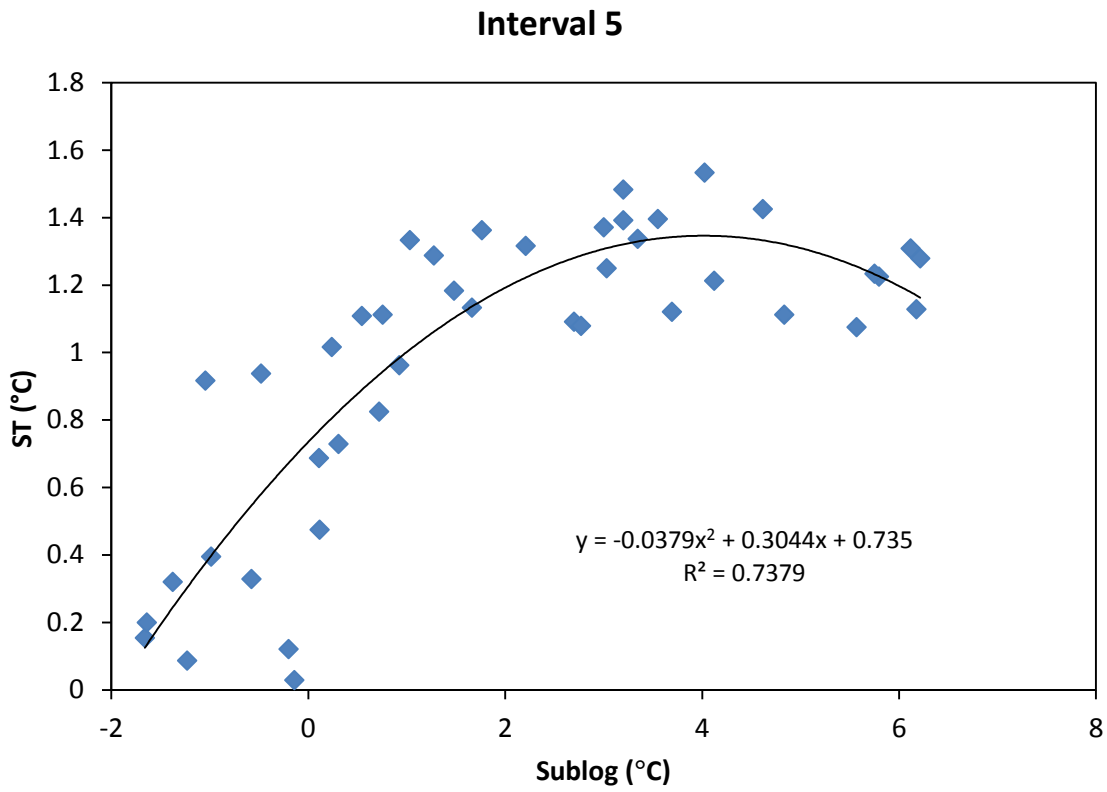

Figure 30. Second-order polynomial regression between stream temperature (ST) and average subsurface temperatures of GRG (Sublog) during Interval 5.

Table 1. Observed stream level (at the stilling well) and corresponding discharge measured at the field site in the summers of 2011 and 2012. Level was first measured in 10ths of a foot, and then converted to meters.

Date & Time	Level (ft)	Q (cfs)	Level (m)	Q (cms)
8/14/11 9:00	0.7	2.14	0.21	0.06
8/15/11 13:00	1	3.43	0.30	0.10
8/15/11 17:00	1.2	4.34	0.37	0.12
8/16/11 10:00	0.8	2.2	0.24	0.06
8/16/11 17:00	0.9	2.81	0.27	0.08
8/19/11 18:30	1	3.27	0.30	0.09
8/20/11 8:30	0.95	3.13	0.29	0.09
7/11/12 15:00	1.5	8.38	0.53	0.30
7/12/12 7:30	1.3	6.55	0.40	0.21

Table 2. Monthly values of precipitation (mm) for the Goethe PRISM, Goethe Weather Station, and Bishop Pass GOES datasets from August 2011-July2012.

Month	Goethe PRISM	Goethe WS	Bishop Pass WS
Aug-11	5	5	10
Sep-11	17	10	46
Oct-11	40	11	68
Nov-11	40	15	88
Dec-11	3	417	8
Jan-12	139	3	106
Feb-12	39	6	45
Mar-12	152	23	111
Apr-12	104	57	100
May-12	0	3	18
Jun-12	9	1	7
Jul-12	2	2	67
TOTAL:	**551**	**553**	**610**

Table 3. Geographic parameters of each logger location in the Goethe cirque. Depth of the subsurface logger is in meters. The mean annual surface temperature (MAST) and mean annual temperature at depth (MADT) are in °C. Blank cells are loggers that malfunctioned when retrieved from the field area.

Logger	Elevation (m)	Depth (m)	MAST	MADT
G1	3614	1.5	-1.92	-2.29
G3	3676	1.88	-2.80	-2.92
G4	3675	---	-1.76	---
G5	3668	1.96	---	-2.19
G6	3655	1.55	-1.15	-1.66
G7	3630	1.65	-0.84	-2.13
G8	3665	2.24	-1.11	-2.84
G9	3680	1.32	-2.68	-3.46
G10	3676	---	-2.72	---
G11	3663	3.43	-1.43	-2.58
R1	3697	1.75	---	-1.78
R2	3670	1.91	-0.45	-0.63
V1	3630	2.22	-2.04	-2.29
V2	3629	---	-1.92	---
V3	3597	3.54	-1.45	-3.67
T1	3673	2.06	-2.87	-3.34
T2	3668	1.76	-2.18	-2.25

Table 4. Mean surface (a) and subsurface (b) temperatures for each landform and daily mean air temperature (DMAT) in °C for each seasonal interval. All temperatures have a ± 0.5°C instrumental error.

	Interval 1	Interval 2	Interval 3	Interval 4	Interval 5
DMAT	**6.4**	**-4.3**	**-6.8**	**2.4**	**8.9**
ALL	6.47	-5.45	-6.58	-1.23	5.96
GRG a	8.22	-5.97	-7.34	-1.45	6.28
GRG b	5.85	-5.71	-6.34	-1.26	4.96
RPD a	8.41	-4.72	-4.22	-0.24	7.20
RPD b	6.05	-3.91	-4.42	-0.52	6.41
VRG a	7.35	-5.75	-7.25	-1.26	8.02
VRG b	3.98	-5.73	-6.46	-0.87	4.07
TAL a	6.12	-4.79	-7.69	-1.39	6.41
TAL b	3.30	-4.10	-5.88	-0.92	3.07

Table 5. Mean temperature for each surface (a) and subsurface (b) logger during each seasonal interval. Intervals are determined by similar temperature characteristics among the loggers.

Logger	Interval 1	Interval 2	Interval 3	Interval 4	Interval 5
G1a	8.94	-6.61	-7.60	-2.54	7.61
G1b	6.32	-6.46	-6.98	-1.54	7.00
G3a	7.23	-7.74	-6.98	-1.36	8.79
G3b	4.97	-6.44	-6.18	-0.99	3.92
G4a	7.98	-5.50	-7.24	-1.42	4.78
G5b	3.65	-1.68	-4.57	---	---
G6a	9.09	-5.57	-7.41	-1.90	8.02
G6b	7.84	-5.61	-6.48	-1.36	5.80
G7a	8.86	-4.40	-7.09	-1.42	5.92
G7b	7.26	-5.98	-6.30	-1.07	3.77
G8a	9.31	-5.40	-6.81	-1.19	7.92
G8b	5.26	-5.78	-6.40	-0.97	3.31
G9a	7.05	-7.58	-7.72	-1.75	7.20
G9b	5.03	-7.13	-6.71	-1.92	4.61
G10b	6.99	-6.62	-7.53	-1.45	6.93
G11a	7.31	-4.97	-7.89	3.33	10.79
G11b	5.29	-5.67	-5.89	-0.78	4.34

Logger	Interval 1	Interval 2	Interval 3	Interval 4	Interval 5
R1b	4.38	-3.76	-5.46	-0.77	5.59
R2a	8.41	-4.72	-4.22	-0.23	7.20
R2b	7.72	-4.05	-3.39	-0.27	7.24
V1a	7.33	-6.52	-7.38	-2.12	7.31
V1b	5.71	-5.17	-6.43	-0.85	5.75
V2a	6.99	-5.74	-6.86	-1.00	8.83
V3a	7.72	-4.99	-7.51	-0.68	7.92
V3b	2.25	-6.28	-6.49	-0.89	2.40
T1a	5.99	-6.62	-7.38	-2.03	5.92
T1b	3.52	-5.72	-6.43	-1.37	2.75
T2a	6.26	-2.97	-8.00	-0.76	6.90
T2b	3.09	-2.48	-5.34	-0.48	3.39

Table 6. Average gradients between surface and subsurface loggers for each landform during seasonal intervals. Interval 4 gradients are determined based on Interval 4 bounds for subsurface gradients, as most surface loggers have shorter Interval 4 bounds.

Interval	GRG	RPD	VRG	TAL
1	1.23	0.36	1.14	1.50
2	0.02	-0.34	-0.12	-0.88
3	-0.45	-0.40	-0.35	-0.63
4	0.95	0.43	1.11	1.43
5	2.59	1.48	2.41	4.77

Table 7. Average seasonal and annual gradients (°C/m) for each logger site containing both surface and subsurface loggers.

Logger	Interval1	Interval 2	Interval 3	Interval 4	Interval 5	Annual
G1	1.75	-0.09	-0.41	-0.03	0.87	0.23
G3	1.20	-0.68	-0.47	0.33	3.10	0.70
G6	0.80	0.03	-0.59	0.15	1.99	0.33
G7	0.97	0.95	-0.36	1.59	2.35	0.79
G8	1.80	0.16	-0.14	1.44	3.47	0.77
G9	1.53	-0.40	-0.66	2.22	4.46	0.61
G11	0.59	0.19	-0.52	1.19	1.88	0.34
R2	0.36	-0.34	-0.40	0.43	1.48	0.09
V1	0.73	-0.60	-0.43	0.90	2.10	0.11
V3	1.54	0.36	-0.26	1.27	2.73	0.63
T1	1.20	-0.44	-0.44	1.19	4.19	0.22
T2	1.80	-1.33	-0.82	1.66	5.35	0.03

Table 8. Correlation coefficients (r) between air temperature and surface temperatures in the debris of the landforms for each interval.

Logger	Elevation	1	2	3	4	5
G1	3614	0.79	0.81	0.22	0.13	0.89
G3	3676	0.85	0.79	0.30	0.15	0.88
G4	3675	0.83	0.91	0.44	0.20	0.93
G5	3673	---	---	---	---	---
G6	3655	0.82	0.81	0.30	0.10	0.92
G7	3630	0.82	0.97	0.41	0.26	0.92
G8	3665	0.85	0.82	0.24	0.14	0.85
G9	3680	0.84	0.79	0.26	0.17	0.86
G10	3676	0.86	0.69	0.32	0.10	0.87
G11	3663	0.99	0.98	0.95	0.25	0.83
R1	3697	---	---	---	---	---
R2	3670	0.83	0.88	0.40	0.31	0.89
V1	3630	0.81	0.79	0.32	0.33	0.82
V2	3629	0.83	0.89	0.00	0.21	0.80
V3	3597	0.84	0.91	0.35	0.34	0.78
T1	3673	0.92	0.84	0.32	0.28	0.82
T2	3668	0.98	0.89	0.41	0.26	0.88

Table 9. Correlation coefficients (r) between air temperature and subsurface temperatures in the debris of the landforms for each interval.

Logger	Elevation	1	2	3	4	5
G1	3614	0.69	0.74	0.20	0.15	0.63
G3	3676	0.75	0.75	0.45	0.25	0.65
G4	3675	---	---	---	---	---
G5	3673	0.67	0.52	0.36	0.16	0.65
G6	3655	0.80	0.67	0.30	0.20	0.78
G7	3630	0.76	0.70	0.30	0.22	0.73
G8	3665	0.71	0.63	0.32	0.12	0.69
G9	3680	0.71	0.64	0.24	0.15	0.68
G10	3676	---	---	---	---	---
G11	3663	0.86	0.65	0.40	0.10	0.81
R1	3697	0.75	0.55	0.36	0.06	0.71
R2	3670	0.75	0.69	0.36	0.08	0.70
V1	3630	0.72	0.55	0.39	0.19	0.69
V2	3629	---	---	---	---	---
V3	3597	0.31	0.73	0.20	0.02	0.28
T1	3673	0.73	0.60	0.33	0.03	0.70
T2	3668	0.61	0.55	0.44	0.04	0.51

Table 10. Correlation coefficients (r) between stream temperature (ST), air temperature (AT), discharge (Q), average GRG surface temperatures, and average GRG subsurface temperatures.

	Interval 1	Interval 5
ST & AT	0.18	0.63
ST & surface	-0.47	0.71
ST & subsurface	-0.36	0.82
Q & ST	-0.52	0.54
Q & AT	0.75	0.78
Q & surface	0.74	0.57
Q & subsurface	0.73	0.66

Table 11. Tritium content for three stream samples and one snow sample (TU± e TU) and the corresponding discharge in the outlet stream at time of sample collection (Q). The percent of snowmelt was calculated with the ratio of the average stream water TU to the average snow sample TU.

Goethe stream	TU	eTU	Q (cms)	% Snowmelt
8/19/11	4.03	0.14	0.45	**100%**
10/13/11	3.72	0.14	0.16	**95%**
7/11/12	3.41	0.11	0.54	**87%**
Snow Sample				
8/20/11	3.91	0.16		

Appendix A: Outlier removal for surface temperature loggers

i) In order to assess the true temperatures of the surface loggers that were in direct sun, I first categorized the time series into intervals that were defined based on similar characteristics of lapse rates between the loggers and the Goethe weather station.

Interval 1: Days 1-43, (8/12/11—9/23/11) summer
Interval 2: Days 43-60, (9/24/11—10/10/11) equinox to first winter storm
Interval 3: Days 61-100, (10/11/11—11/19/11) after first storm
Interval 4: Days 101-280, (11/20/11—5/17/12) Winter until Snow depth=0
Interval 5: Days 281-335, (5/18/12—7/12/12) summer

ii) Based on the intervals defined in section i, I selected cloudy days with low solar radiance from the weather station data to serve as control days. This helped me define "normal" temperature differences between each respective logger and the weather station air temperature.

Date	Day	Interval
8/26/11	15	1
9/11/11	31	1
10/2/11	52	2
10/10/11	60	2
11/5/11	86	3
11/6/11	87	3
11/11/11	92	3
11/20/11	101	4
12/28/11	139	4
5/25/12	288	5
6/15/12	309	5
7/4/12	328	5

iii) I then defined the maximum possible time periods for outlier loggers to be in direct sun during each interval. The elevation is the difference in elevation between the logger and the Goethe weather station (3663 m). The top box in each cell is the calculated temperature difference from the weather station ambient air temperature according to the control days and the bottom cell is the actual timeframe that the logger was in direct sun.

Logger ID	Elevation	Interval 1	Interval 2	Interval 3	Interval 4	Interval 5
G1a	-49 m	+1.50	---	---	---	+1.25
		8:00-17:00				6:00-18:30
G3a	+13 m	+0.55	-2.25	---	---	+1.00
		8:00-17:30	8:15-16:45			6:30-18:30
G6a	-8 m	+2.00	+0.75	-1.00	-2.50	+3.00
		8:00-17:30	9:00-16:30	9:30-15:30	10:30-14:00	6:30-18:30
G7a	-33 m	+2.00	+0.50	---	---	+1.00
		8:00-17:00	9:00-16:30			6:30-18:30
G8a	+2 m	+2.00	+1.50	---	---	+0.75
		6:30-16:00	10:00-15:30			6:00-17:30
G9a	+17 m	---	---	---	---	+2.50
						6:00-17:30
G11a (20)	0 m	+0.50	-0.50	---	---	+0.50
		7:00-17:00	8:00-16:00			6:00-17:30
R2a (13)	+7 m	+1.50	+0.50	---	---	+0.50
		5:30-16:30	7:00-16:00			6:00-17:00
V1a (14)	-33 m	+1.00	+0.5	---	---	?
		7:30-17:30	8:30-16:30			7:00-18:00
V2a (15)	-34 m	+1.00	-1.00	-2.00	---	+1.00
		7:30-17:30	8:15-16:30	9:00-16:30		7:00-18:30
V3a (16)	-66 m	+1.50	-0.50	-1.00	---	+0.50
		8:30-18:30	9:30-18:00	10:30-17:30		7:30-18:30

Appendix B: interpolation of hourly temperature data

1) Install the “its” and “zoo” packages

```
require(its)
require(zoo)
```

2) Read in master file of irregularly spaced timeseries

```
hourly <- read.csv(file="hourly_master.csv", header=T)
```

3) Format dates in csv to read mm/dd/yyyy.

```
dates <- c(as.character(hourly$Date))
times <- c(as.character(hourly$Time))
x <- paste (dates, times)
time <- as.POSIXct(strptime(x, "%m/%d/%Y %H:%M:%S", tz=""))
```

4) Define the variable to be interpolated and convert to zoo object as a matrix

```
degC<- (hourly[c(1:1892), c(4:32)])
foo <- its(as.matrix(degC),time)
```

5) This designates the timeframe desired (hourly) from T1 to T2

```
t1 <- ISOdate(2011,8,12, tz="")
t2 <- ISOdate(2012,7,11, tz="")
inc <- 1*60*60
bar <- newIts(start=t1,end=t2,by=inc)
```

6) Merge the two time series as irregular time series (example)

```
bam1y <- union(foo,bar)[,1]
bam1y <- as.zoo(bam1y)
bam1y.spline <- na.spline(bam1y)
```

Appendix C: Pressure Sensor Calibration

i) Barometric air pressure model

In order to accurately model the actual water level in the Goethe outlet stream, I needed to first model the air pressure that was above the water column, then subtract that value from the recorded value on the Levelogger Junior. In this case a barometric sensor would come in handy, however, there was not one for the project. I first downloaded air pressure and air temperature record from the Bishop Airport (station pressure), then calculated a unique lapse rate between the airport and my field site. All calculated and standard parameters were input into the barometric formula.

$$p = p_0 \cdot \left(1 - \frac{L \cdot h}{T_0}\right)^{\frac{g \cdot M}{R \cdot L}}$$

where:

Variable	Parameter	Value
p	Modeled air pressure at Goethe	≈645-680 mbar
P_0	Station pressure at Bishop Airport	≈850-890 mbar
L	Temperature lapse rate	(Calculated hourly in °C)
h	Elevation change	2260 m
T_o	Sea level standard temperature?	288.15 K
g	Gravitational acceleration	9.8 m/s^2
M	Molar mass of dry air	0.0289644 kg/mol
R	Universal gas constant	8.31447 J/(mol K)

ii) Zero-point offset

The zero-point offset is 9.5 m (31.17 ft) of water column less an altitude correction. This value is the lowest expected barometric pressure at mean sea level. The lowest barometric pressure decreases as elevation increases at a rate of approximately 1/1000 meters of elevation. The Levelogger's altitude is at 3535 m.

1) The levelogger's elevation-corrected barometric pressure offset value (***Z)*** is:

- $\boldsymbol{Z} = (9.5 - 3535/1000)$

2) The calculated value is then subtracted from the barometric sensor record (in this case the modeled air pressure from Appendix C, section i) to obtain the amount of pressure the Levelogger is sensing ($\boldsymbol{B_p}$***)***:

- $\boldsymbol{B_p} = \boldsymbol{P - (Z)}$

3) The amount of barometric pressure that was influencing the Levelogger can vary each day, or even every hour, so these values were extrapolated for each hour of the Levelogger's record. Finally, $\boldsymbol{B_p}$ was subtracted from the total level ***(*** $\boldsymbol{L_T}$***)*** that the sensor recorded to obtain the actual water level ***(L)*** above the sensor:

- $\boldsymbol{L = L_t - B_p}$

Appendix D: Seasonal Intervals

Seasonal intervals that characterize general temperature trends for each logger string. Not every logger has the same interval due to aspect, elevation, snow cover, or depth in the debris matrix.

GRG1

Interval	Days	# of days	Dates
1	1-51	51	8/12-10/1
2	52-163	111	10/1-1/21
3	164-254	90	1/22-4/21
4	(s) 255-281, (d) 255-287	26, 32	4/22-5/18, 4/22-5/24
5	(s)282-336, (d) 288-336	54, 48	5/19-7/11, 5/25-7/11

GRG3

Interval	Days	# of days	Dates
1	1-51	51	8/12-10/1
2	52-163	111	10/2-1/21
3	(s) 164-252, (d) 164-249	88, 85	1/22-4/19, 4/16
4	(s) 253-305, (d) 250-312	52, 62	4/20-6/11, 4/17-6/18
5	(s)306-336, (d) 313-336	30, 23	6/12-7/12, 6/19-7/12

GRG 4s

Interval	Days	# of days	Dates
1	1-51	51	8/12/11-10/1/11
2	52-163	111	10/2-1/21
3	164-250	86	1/22-4/17
4	251-275	24	4/18-5/12
5	276-336	60	5/13-7/12

GRG 5d

Interval	Days	# of days	Dates
1	1-51	51	8/12/11-10/1/11
2	52-114	62	10/2-12/3
3	115-252	137	12/4-4/19
4	NA	--	--
5	NA	--	--

GRG6

Interval	Days	# of days	Dates
1	1-51	51	8/12/11-10/1/11
2	52-163	111	10/2-1/21
3	164-252	88	1/22-4/19
4	(s) 253-275, (d) 253-287	22, 34	4/20-5/12, 4/20-5/24
5	(s)276-336, (d) 288-336	60, 48	5/13-7/12, 5/25-7/12

GRG 7

Interval	Days	# of days	Dates
1	1-51	51	8/12/11-10/1/11
2	52-163	111	10/2-1/21
3	164-250	86	1/22-4/17
4	(s) 251-266, (d) 251-287	15, 36	4/18-5/3, 5/24
5	(s)267-336, (d) 288-336	69, 48	5/4-7/12, 5/25-7/12

GRG 8

Interval	Days	# of days	Dates
1	1-51	51	8/12/11-10/1/11
2	52-170	118	10/2-1/28
3	171-254	83	1/29-4/21
4	(s) 255-283, (d) 255-314	28, 59	4/22-5/20, 6/20
5	(s)284-336, (d) 315-336	52, 21	5/21-7/12, 6/21-7/12

GRG 9

Interval	Days	# of days	Dates
1	1-51	51	8/12/11-10/1/11
2	52-170	118	10/2-1/28
3	171-254	83	1/29-4/21
4	(s) 255-283, (d) 255-311	28, 56	4/22-5/20, 6/17
5	(s)284-336, (d) 312-336	52, 24	5/21-7/12, 6/18-7/12

GRG 10d

Interval	Days	# of days	Dates
1	1-51	51	8/12/11-10/1/11
2	52-163	111	10/2-1/21

3	164-254	90	1/22-4/21
4	255-301	46	4/22-6/16
5	302-336	34	6/17-7/12

GRG 11

Interval	Days	# of days	Dates
1	1-51	51	8/12/11-10/1/11
2	52-163,	111	10/2-1/21
3	164-251	87	1/22-4/18
4	252-315	63	4/19-6/21
5	316-336	20	6/22-7/12

R1b

Interval	Days	# of days	Dates
1	1-51	51	8/12/11-10/1/11
2	52-163	111	10/2-1/21
3	164-252	88	1/22-4/19
4	253-306	53	4/20-6/12
5	307-336	29	6/13-7/12

R2

Interval	Days	# of days	Dates
1	1-51	51	8/12/11-10/1/11
2	52-163	111	10/2-1/21
3	164-249	85	1/22-4/16
4	(s) 250-284, (d) 250-307	34,57	4/17-5/21, 6/13
5	(s) 285-336, (d) 308-336	51, 28	5/22-7/12, 6/14-7/12

V1

Interval	Days	# of days	Dates
1	1-51	51	8/12/11-10/1/11
2	52-163	111	10/2-1/21
3	164-249	85	1/22-4/16
4	(s) 250-279, (d) 250-307	29, 57	4/17-5/16, 6/13
5	(s) 280-336, (d) 308-336	56, 28	5/17-7/12, 6/14-7/12

V2a

Interval	Days	# of days	Dates
1	1-51	51	8/12/11-10/1/11
2	52-163	111	10/2-1/21
3	164-248	84	1/22-4/15
4	249-299	50	4/16-6/5
5	300-336	36	6/6-7/12

V3

Interval	Days	# of days	Dates
1	1-51	51	8/12/11-10/1/11
2	52-163	111	10/2-1/21
3	164-252	88	1/22-4/19
4	(s) 253-282, (d) 253-324	29, 71	4/20-5/19, 6/29
5	(s) 283-336, (d) 325-336	53, 11	5/20-7/12, 6/30-7/12

T1

Interval	Days	# of days	Dates
1	1-51	51	8/12/11-10/1/11
2	52-165	113	10/2-1/23
3	166-252	86	1/24-4/19
4	(s) 253-296, (d) 253-329	43, 76	4/20-6/2, 7/5
5	(s) 297-336 , (d) 330-336	39, 6	6/3-7/12, 7/6-7/12

T2

Interval	Days	# of days	Dates
1	1-51	51	8/12/11-10/1/11
2	52-110	58	10/2-11/28
3	111-250	139	11/29-4/17
4	(s) 251-293, (d) 251-332	42, 81	4/18-5/30, 7/8
5	(s) 294-336, (d)333-336	42, 3	5/31-7/12, 7/9-7/12